Computation of direction selectivity in retinal starburst amacrine cell dendrites – studied using electrophysiological recordings and two-photon imaging

Dissertation

zur Erlangung des Grades
"Doktor der Naturwissenschaften"

Am Fachbereich Biologie
Der Johannes Gutenberg-Universität Mainz

Susanne Hausselt

Mainz, 2006

Dekan:
1. Berichterstatter:
2. Berichterstatter:

Tag der mündlichen Prüfung: 30. Oktober, 2006

Diese Dissertation wurde am Max Planck Institut für medizinische Forschung in Heidelberg in der Abteilung Biomedizinische Optik in der Retinagruppe durchgeführt. Ich habe die vorgelegte Arbeit selbst angefertigt und alle benutzten Hilfsmittel (Literatur, Apparaturen, Material) angegeben.

This thesis work was carried out at the Max Planck Institute for Medical Research in Heidelberg, Germany, in the department of Biomedical Optics in the retina group. I have conducted the experiments and prepared the dissertation myself; all of the resources used (literature, equipment, material) are specified.

Zusammenfassung

Neuronale Schaltkreise in der Netzhaut zerlegen das Bild der Umwelt nach qualitativen Aspekten, wie z.B. Farbe oder Bewegung, bevor die Informationen an höhere Gehirnregionen weitergeleitet werden. Ein Beispiel, an dem seit über 40 Jahren geforscht wird, ist die Verarbeitung von Richtungsinformation in sogenannten ‘richtungsselektiven’ Neuronen, die besonders stark auf eine bestimmte Richtung von Bewegung reagieren. In den letzten Jahren hat sich ein Typ von Interneuron in der Netzhaut als wichtiges Schaltkreiselement bei der Erkennung der Richtung visueller Bewegung herauskristallisiert: die "Starburst" Amakrinzelle. In dieser Arbeit wurden mit Hilfe von elektrophysiologischen Ableitungen und Kalzium-Messungen mittels Zwei-Photonen-Mikroskopie die Mechanismen untersucht, die den richtungs-selektiven Kalziumsignalen in den Dendriten der "Starburst"-Zellen zugrunde liegen. Die Analyse der elektrischen Zellantworten auf visuelle Stimulation, in Verbindung mit Pharmakologie, deutet darauf hin, dass das richtungsselektive Signal (i) nicht präsynaptisch zu der "Starburst"-Zelle entsteht und nicht durch inhibitorische Interaktionen im retinalen Netzwerk hervorgerufen wird. Es kommt vielmehr durch eine ‚zell-interne’ Berechnung zustande, die (ii) von einer spezifischen, d.h. richtungsselektiven Aktivierung spannungsgesteuerter Kanäle abhängt. Messungen der dendritischen Kalziumsignale in Abhängigkeit von der Spannung am Zellkörper weisen (iii) auf einen Unterschied im Ruhepotential zwischen Zellkörper und Dendriten hin. Es wird daher vorgeschlagen, dass der Berechnung der Richtungs-information ein Mechanismus zugrunde liegt, der auf intrinsischen Eigenschaften der "Starburst"-Zellen beruht, genauer auf der Wechselwirkung von zeitlich strukturierten synaptischen Eingängen mit spannungsgesteuerten Kanälen und deren richtungs-spezifischer Aktivierung durch einen dendritischen Spannungsgradienten.

Summary

Neuronal circuits in the retina analyze images according to qualitative aspects such as color or motion, before the information is transmitted to higher visual areas of the brain. One example, studied for over the last four decades, is the detection of motion direction in ‘direction selective’ neurons. Recently, the starburst amacrine cell, one type of retinal interneuron, has emerged as an essential player in the computation of direction selectivity. In this study the mechanisms underlying the computation of direction selective calcium signals in starburst cell dendrites were investigated using whole-cell electrical recordings and two-photon calcium imaging. Analysis of the somatic electrical responses to visual stimulation and pharmacological agents indicated that the directional signal (i) is not computed presynaptically to starburst cells or by inhibitory network interactions. It is thus computed via a cell-intrinsic mechanism, which (ii) depends upon the differential, i.e. direction selective, activation of voltage-gated channels. Optically measuring dendritic calcium signals as a function of somatic voltage suggests (iii) a difference in resting membrane potential between the starburst cell’s soma and its distal dendrites. In conclusion, it is proposed that the mechanism underlying direction selectivity in starburst cell dendrites relies on intrinsic properties of the cell, particularly on the interaction of spatio-temporally structured synaptic inputs with voltage-gated channels, and their differential activation due to a somato-dendritic difference in membrane potential.

Die Größte Sehenswürdigkeit, die es gibt, ist die Welt – sieh sie dir an.

Kurt Tucholsky

Preface

This thesis is divided into an introduction, methods, results and a discussion followed by the bibliography. The introduction attempts to provide some information not only about the retina and direction selectivity in retinal neurons, but also about the techniques used in this study. Especially the application of two-photon microscopy in the retina is noteworthy, as it opens new possibilities in combining functional imaging with visual stimulation.
The appendix contains numbers not mentioned in the results part, several equations underlying paragraphs in the discussion and the description of a biophysical model.

Remains to say: I hope the reading will be informative as well as enjoyable.

❋

Abbreviations

ACh	Acetylcholine
AP	Action potential
CCD	Charge-coupled device
CNS	Central nervous system
DIC	Differential inter-phase contrast
DS	Direction selective/selectivity
DSGC	Direction selective ganglion cell
GABA	Gamma-amino butyric acid
IR	Infrared
LED	Light-emitting diode
ON cell	Retinal neuron depolarizing to light on
OFF cell	Retinal neuron depolarizing to light off
SAC	Starburst amacrine cell
VGC	Voltage-gated channel
VGCC	Voltage-gated calcium channel

Chemical elements and ions

Ag	Silver
Ca^{2+}	Calcium
Cl^{-}	Chloride
Cs^{+}	Cesium
K^{+}	Potassium
Na^{+}	Sodium
Mg^{2+}	Magnesium

Units

A	Ampere	G	Giga (10^{9})
deg	Degree	M	Mega (10^{6})
F	Farad	k	Kilo (10^{3})
Hz	Hertz (1/sec)	m	Milli (10^{-3})
l	Liter	µ	Micro (10^{-6})
M	Molar (mol/liter)	n	Nano (10^{-9})
Ω	Ohm	p	Pico (10^{-12})
sec	Second	f	Femto (10^{-15})
S	Siemens		
V	Volts		

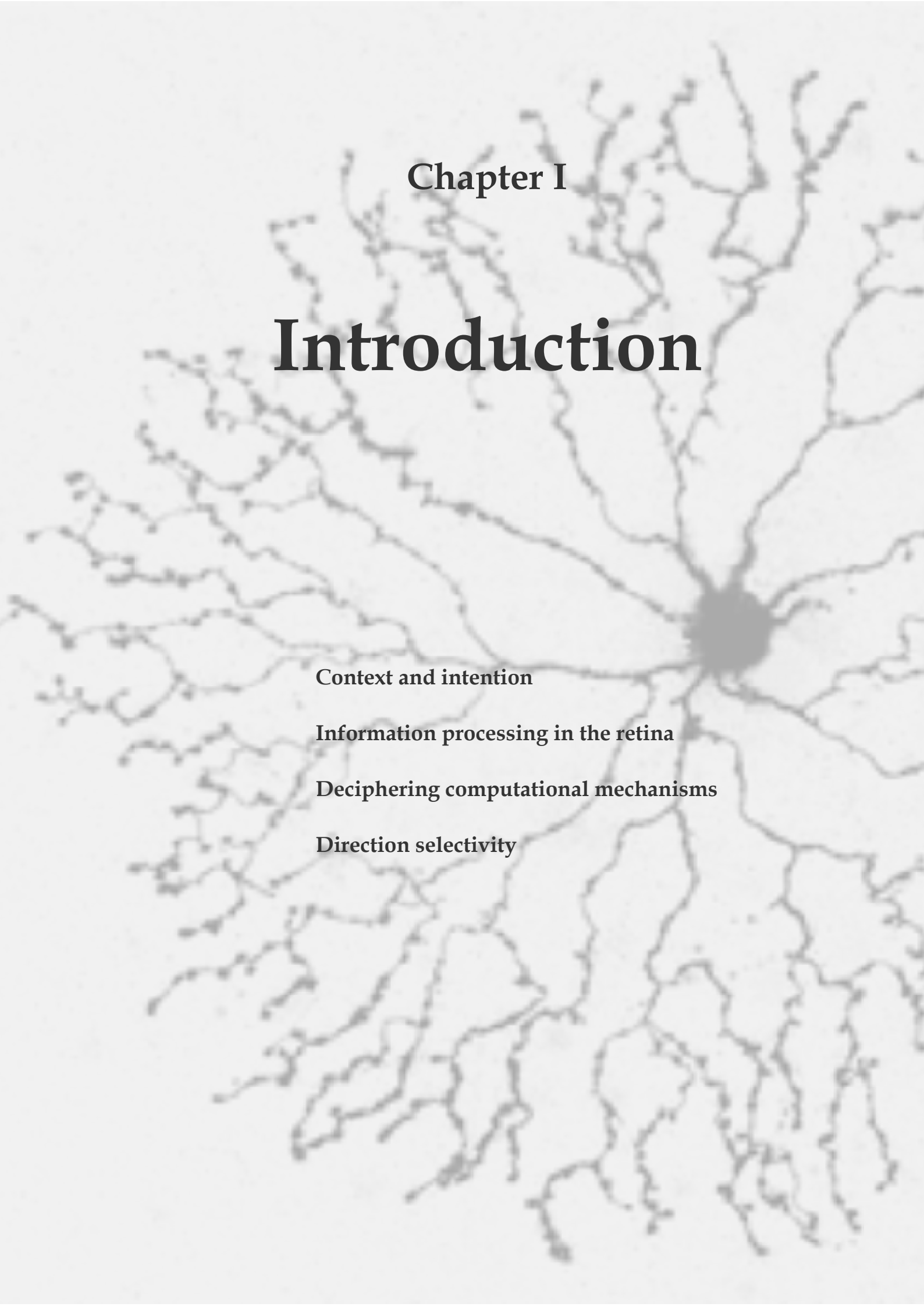

Chapter I

Introduction

Context and intention

Information processing in the retina

Deciphering computational mechanisms

Direction selectivity

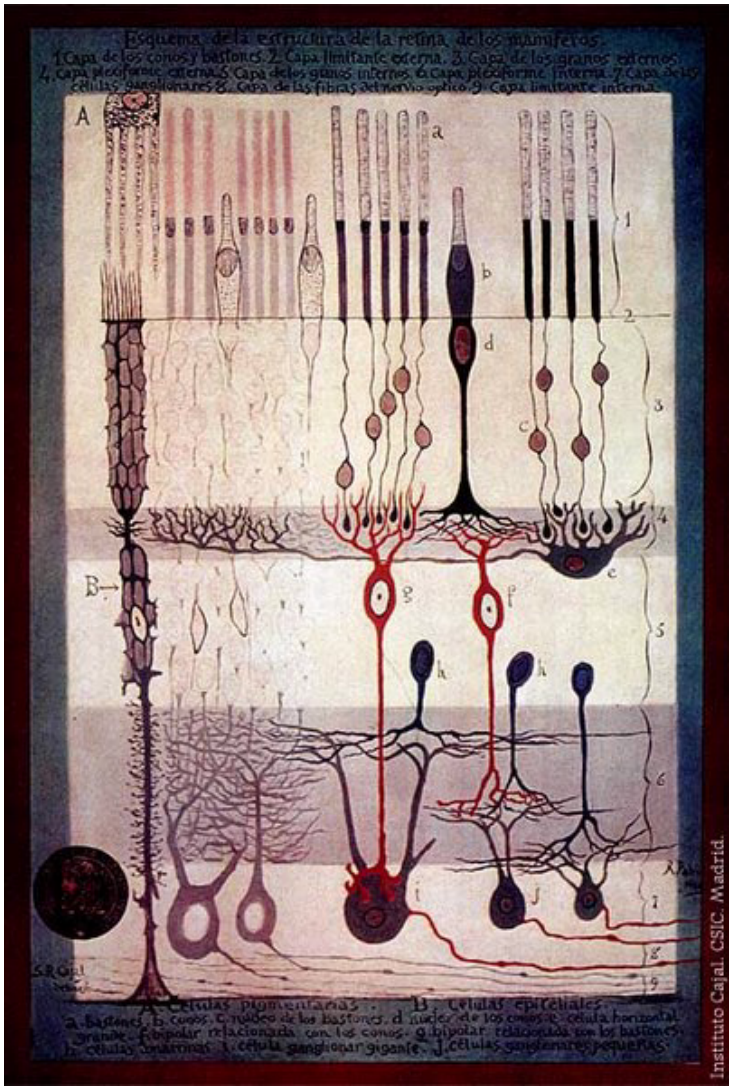

Fig. 1 Retina overview (circa 1900; Ramón y Cajal; *copyright expired, wikipedia.com*).

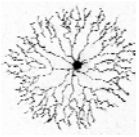

1.1 Context and intention

> Finally, the functional complexity of the retina had been underestimated.
>
> **Masland and Raviola, 2000**

The detection of motion and its direction are essential features of the visual system. Most animals vitally rely on fast perception of moving objects in their environment as these can represent danger, but also food or social contact. Further, visual control of head and body movements is fundamental for orientation in space and for body stability. The first stage of information processing in our visual system, the retina, already features cells which specifically respond to motion in distinct directions. Although these neurons, the direction selective ganglion cells, were described over 40 years ago (Barlow and Hill, 1963), the computational steps underlying their specific response behavior have still not been completely understood. Recent results have shown, that direction selectivity is generated upstream of direction selective ganglion cells and essentially involves a particular type of interneuron, the so-called 'starburst' amacrine cell, which exhibits direction selective responses within its dendrites (for review see Taylor and Vaney, 2003). This study aimed to uncover the role of processing within the starburst cell – and found that an intrinsic mechanism, relying on a gradient in dendritic membrane potential and the differential activation of voltage-gated channels, underlies the directionality in the starburst amacrine cell dendrite.

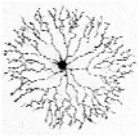

1.2 Information processing in the retina

> We have shown that the function of the retina […] is not to transmit information about the point-to-point pattern of distribution of light and dark in the image formed on it. On the contrary, we find that its function is mainly to analyze this image at every point in terms of […] qualitative contexts […]
>
> **Maturana, Lettvin, McCulloch and Pitts, 1960**

Vision is our dominant sense and thus, out of 'subjective' interest as well as from a medical point of view, scientists have tried to decipher the function of the visual system ever since instruments and techniques arose with which its structures could be studied (Chalupa and Werner, 2003). The retina (Figs. 1, 2), as the visual system's first processing stage, is one of the cardinal model systems for neurobiological research.

As a consequence of its long career in neuroscience, many types of neurons in the retina have been well characterized concerning their morphology, their molecular environment and their physiology (Wässle and Boycott, 1991; Masland, 2001a; Wässle, 2004). Methods of exploration range from single cell recordings (Kuffler, 1953) to behavioral measurements after retinal manipulation (e.g. Yoshida et al., 2001; Mora-Ferrer et al., 2005) and from electron microscopy (Polyak, 1941; Dowling and Boycott, 1966) to labeling of whole groups of cells with genetically encoded indicators (e.g. Dübel et al., 2006).

One crucial advantage of the retina, compared to other brain structures, is the simplicity of measuring its functional output to its 'natural', i.e. physiological, input: The natural stimulus for the retina – an image – can easily be projected either onto the isolated tissue or onto an intact eyecup preparation, while measuring the responses of the output-neurons to the brain, the ganglion cells, in the form of trains of action potentials. Thus, the functional property of a certain type of ganglion cell can be characterized by its responses to visual stimuli with different properties (motion, form, color, contrast, etc.), and the mechanisms, cells and circuits involved in the respective processing can be analyzed.

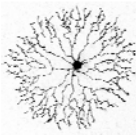

1.2.1 Structure of the retina

With the advent of improved compound microscopes in the middle of the 19th century (La Berge, 1999), descriptions of retinal cells (Treviranus, 1837; as cited in Wade, 1999) and of the conspicuous layered structure of the retina emerged (Schultze, 1866; as cited in Glickstein, 2003). Just like the rest of the central nervous system the retina was believed to consist of continuous elements, which exhibited swellings in some layers and were thinner in others. Owing to the achievements of Santiago Ramón y Cajal, who used Golgi staining (Golgi, 1883; cited from Pannese, 1999) to study the cells of the retina (Ramón y Cajal, 1893; cited from Boycott and Wässle, 1999; e.g. Fig. 1), it was finally accepted that the alternating nuclear and plexiform strata comprise the somata and the neurites of cells, respectively (Fig. 2). As the vertebrate retina features an inverted morphology, light first traverses the whole tissue before being absorbed by the photo-transducible 11-cis retinal embedded in the opsin-molecule (in combination: rhodopsin) sitting in the membranes of the photoreceptor outer segments. Photoreceptors are divided into rods, for dim-light vision, and cones, which are less light-sensitive and exist in up to three types in mammals (Wässle and Boycott, 1991) and up to four types in other vertebrates (Neumeyer, 1989) with different wavelength absorption spectra, determined by the specific opsins they

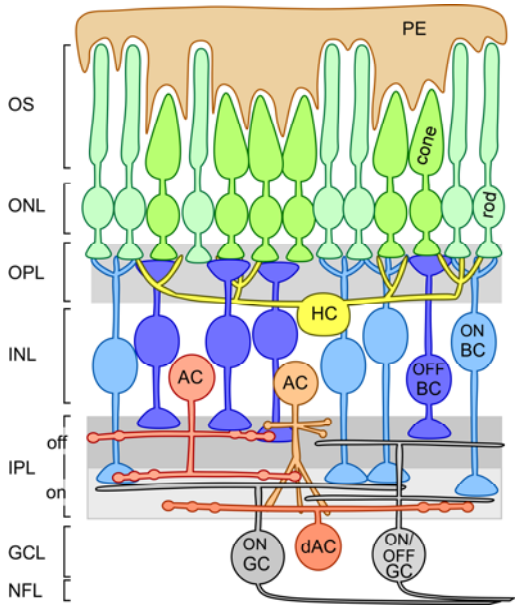

Fig. 2 Vertebrate retina (schematic). Depicted are the different layers of the vertebrate retina: The pigment epithelium (PE) engulfs the outer segments (OS) of the photoreceptors (rods and cones); ONL – the outer nuclear layer with the somata of the photoreceptors (PRs); OPL – the outer plexiform layer, with synapses between PRs, horizontal cells (HCs) and bipolar cells (BCs); INL – the inner nuclear layer consisting of the BC, HC and most amacrine cell (AC) somata; IPL – the inner plexiform layer, divided into an OFF and an ON sublamina, in which OFF and ON BCs and ganglion cells (GCs), respectively, contact each other and diverse ACs; GCL – the ganglion cell layer with somata of all GCs and some displaced ACs (dAC). The nerve fiber layer (NFL) contains the axons of GCs.

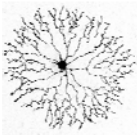

express. When photons are absorbed, a signal transduction cascade is initiated, which eventually leads to depolarization of the photoreceptor membrane and the subsequent release of the excitatory neurotransmitter glutamate. From the photoreceptors the direct path of signal transmission continues via bipolar to ganglion cells, which code their responses in trains of action potentials, but horizontal and amacrine cells are also essentially involved in the computation leading to specific ganglion cell responses (Fig. 2). The optic nerve, formed by ganglion cell axons, transfers the signals to the various visual areas of the brain (for review see e.g. Kandel et al., 2000).

Other than proposed in early studies the information transmitted from the retina to the brain is mostly not a point-to-point image of the visual environment[1] (e.g. Maturana et al., 1960). On the contrary, the different types of ganglion cells (10 to 15, see Fig. 3) relay diverse features of the perceived scene as for instance lightness, contrast, motion and color (Masland, 2001a; b). The computation of these properties involves all of the mentioned neuronal types: photoreceptors, up to 12 types of bipolar cells (Ghosh et al., 2004; MacNeil et al., 2004), one to three types of horizontal cells, at least 29 types of amacrine cells and the ganglion cells themselves (Figs. 2, 3; MacNeil and Masland, 1998; Masland, 2001a; Wässle, 2004). The textbook version of retinal neurotransmission simplifies photoreceptors and bipolar cells as excitatory neurons, i.e. glutamatergic, and horizontal and amacrine cells as mainly inhibitory neurons, i.e. releasing γ-amino-butyric acid (GABA) and GABA or glycine, respectively. The picture is incomplete though without mentioning that there are many more neurotransmitters and neuro-active substances released by retinal, especially amacrine, cells, as e.g. acetylcholine (ACh), serotonin, dopamine and many neuropeptides (Kalloniatis and Tomisich, 1999). In addition, exceptions exist even within seemingly ‘homogenous’ retinal cell classes, for example there is evidence for GABAergic bipolar cells (Kao et al., 2004). The large variety of different receptors for each neurotransmitter (Koulen, 1999; Masland, 1986) yields different transmitter functions on different neurons – excitatory, inhibitory or modulatory. Further, electrical synapses composed of different types of gap junctions also play a role in processing (Söhl et al., 2005; Massey et al., 2003; Vaney and Weiler, 2000). This large array of variables already suggests multiple signaling pathways within the retinal network[2].

[1] In fact, the midget ganglion cells in the fovea centralis of the primate retina do receive input from single cones via single midget bipolar cells providing high spatial resolution (for review see Rodieck, 1998).
[2] This large variability of ‘computational components’ may as well be present in most brain regions.

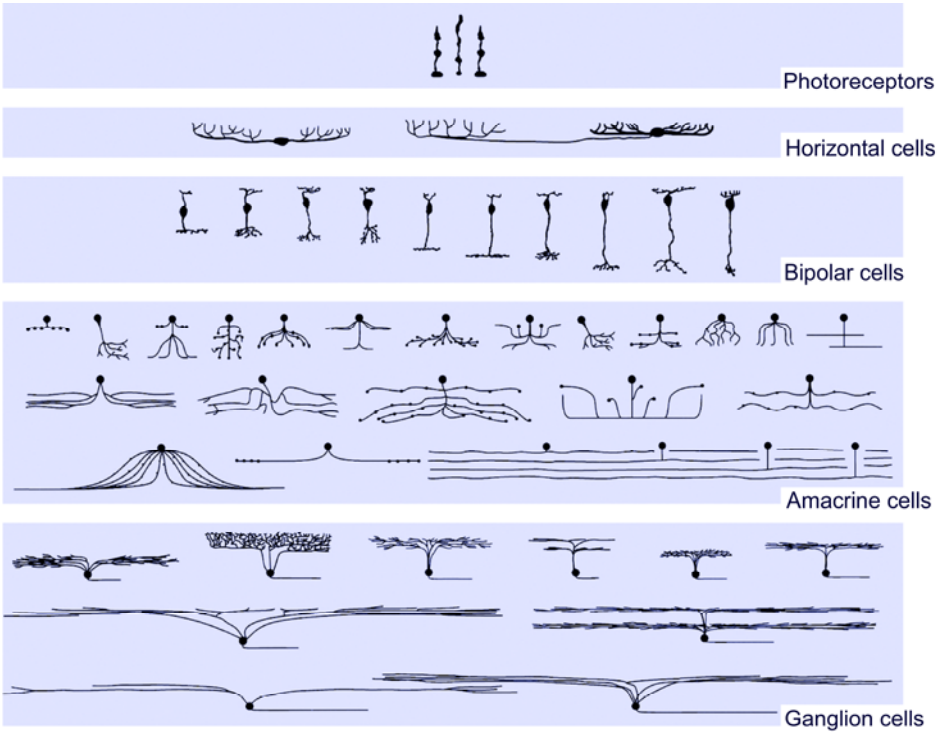

Fig. 3 Different types of retinal neurons.
Examples for each class of retinal neuron are shown (*modified from* Masland, 2001a).

The computational possibilities are further increased by the morphological characteristics of the cells, such as the pattern and diameter of their dendrites, but also by intracellular substructures and by the distribution of transmembrane molecules, such as receptors, ion-transporters or voltage-gated channels. The combination of these factors can cause for example compartmentalization (e.g. Borst and Single, 2000) or intrinsic ion gradients (e.g. Dübel et al., 2006) and defines the response properties of a cell.

In this context it is important to mention that the majority of retinal cells, apart from ganglion cells and some types of amacrine cells, such as for example the polyaxonal types (Stafford and Dacey, 1997; Völgyi et al., 2001), do not obey the function of the 'canonical' vertebrate neuron[3]. Such a 'textbook' neuron integrates dendritic input at the soma, and initiates axonal action potentials (APs) if a certain threshold has been reached, leading ultimately to spike-frequency dependent neurotransmitter release. Most retinal neurons however do not fire trains of APs, but rely on graded potentials.

[3] In many other areas of the brain numerous neurons have been described that do not simply follow the idea of dendritic input and axonal output, there are e.g. dendro-dendritic as well as dendro-axonic synapses in cortical neurons (for review see e.g. Kandel et al., 2000), and new studies continuously soften the rigid idea of the canonical neuron.

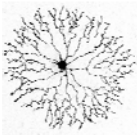

Further, horizontal cells as well as the majority of amacrine cells do not feature a specific output compartment (Fig. 3) but distribute input and output synapses throughout their dendritic tree. Such structures support local processing, which is of particular use in the retina, where space is limited and parallel signaling pathways require neuronal circuits to be efficiently packed. Thus, the retina does not only offer a multitude of intriguing questions to answer, but is also a convenient model system for studying dendritic processing.

1.3 Deciphering computational mechanisms

> The brain computes! […] What is meant here is that any brain takes the incoming sensory data, encodes them into various biophysical variables […] and subsequently performs a large number of ill-specified operations, frequently termed computations […]
>
> **Christoph Koch, 1999**

Although many details of the morphology and physiology of retinal neurons are known, the computational processes leading to a specific response pattern of a ganglion cell have not been completely elucidated (Masland, 2001a; Wässle, 2004). Apart from the fact that the discipline of neuroscience is still in its youth and new principles are discovered constantly, this is partially due to the great demands made on technologies for the analysis of compartmental computation. Classical electrical recordings are immensely helpful in studying neurons, particularly so the whole-cell patch-clamp technique (Sakmann and Neher, 1984; Hamill et al., 1981), which can also be used to measure dendritic events – as long as the dendrite is accessible by the electrode – as well as graded responses at the soma, as done in this study.

The dendrites (and somata) of many retinal neurons are, however, only accessible in a slice preparation, if at all, but not in the flat mounted tissue or an intact eyecup, the only preparations to which complex visual stimuli can be applied. Luckily, new methods of light microscopy and functional imaging developed during the last two decades have begun to overcome these limitations.

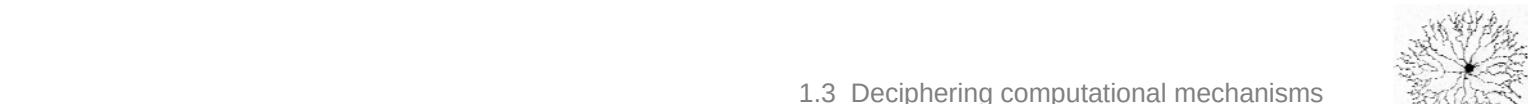

1.3.1 Two photon microscopy

During the last two centuries the development of light microscopic techniques has accelerated continuously – from the advent of aberration-corrected and commercially available compound microscopes around 1830 (La Berge, 1999) up to the plenitude of approaches today, among them total internal reflection fluorescence (TIRF) microscopy, wide-field or confocal laser scanning microscopy, just to name a few. The development of imaging methods was accompanied by new forms of tissue visualization, ranging from cell compartment markers and labeled antibodies, for virtually any target in a specimen, to functional molecules that respond to ion concentrations or pH (for imaging techniques in the retina see e.g. Morgan et al.,

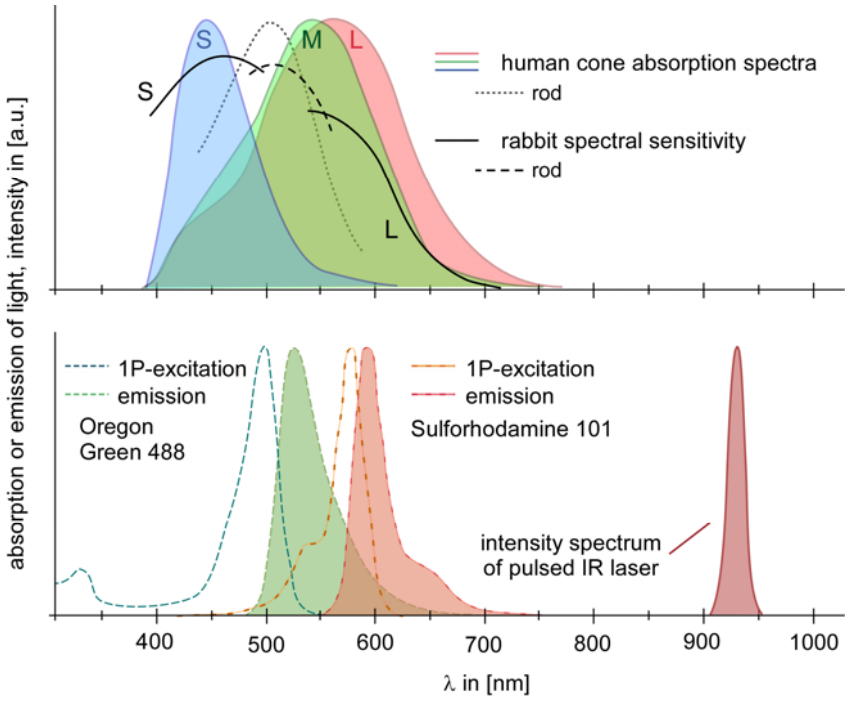

Fig. 4 Comparison of absorption and emission spectra.
Upper panel: Absorption spectra of the three human cone pigments (from Nathans, 1999) and the rod photoreceptor pigment (from Dartnall et al., 1983) and a spectral sensitivity curve derived from ganglion cell responses of rabbit retina (from Armington and Adolph, 1994). *S - Short, M – middle, L – long wavelength cones. Lower panel:* The one-photon (1P) excitation as well as the emission spectra of two commonly used fluorescent indicators (Bio-Rad cellscience online fluorescence database ©2004) overlap with the absorption spectra of the photoreceptors, whereas the light emitted by the mode-locked (pulsed) infrared (IR) laser does not. *Intensities of the different spectra are not to scale.*

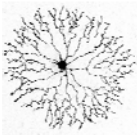

2005). Many of these substances rely on fluorescence, i.e. they absorb light of a certain wavelength and emit light of a different wavelength, normally of longer wavelength, i.e. lower-energy photons (Fig. 5 A). This generally allows, with appropriate filters, to measure the fluorescence of fluorescent dye-labeled cells or sub-cellular structures (for review see Lichtman and Conchello, 2005), e.g. with an ion-sensitive (indicator) dye injected into single neurons. A Ca^{2+}-sensitive indicator dye, for instance, can be used as a proxy for electrical signals from small dendrites, as the intracellular Ca^{2+} concentration ($[Ca^{2+}]$) of a neuron is usually (but see 1.3.2) closely correlated with the membrane potential. Hence, the questions of cellular computation in the retina could be addressed, were it not for one major drawback: the retina is light sensitive. Most commercially available fluorescent dyes absorb and emit light in the visible range (Fig. 4). As such, (i) the strong light sources, e.g. lasers, needed to excite the dye molecules, as well as (ii) the emitted light from the dye would strongly activate or even bleach photoreceptors and would thus prevent simultaneous visual stimulation of the tissue (Fig. 4).

Fortunately for retinal research, W. Denk and coworkers developed a technique (Denk et al., 1990), which solves both issues at once: multi-photon microscopy (MPM). Multi-photon imaging (for review see Zipfel et al., 2003) makes use of the fact that a fluorophor can not only be excited with one photon of higher energy, but also with two nearly simultaneously absorbed photons of approximately half the energy (Göppert-Mayer, 1931), i.e. the double wavelength of the excitation light (Fig. 5). To achieve simultaneous (within $\sim 10^{-6}$ s) absorption of two photons by a single fluorescent molecule the number of photons passing through a unit area per time (the intensity) has to be very high. Large intensities are reached at the focus, and currently technically accomplished with high-power (up to ~ 3 W) titanium sapphire (Ti:S) pulsed infrared lasers as excitation sources. As the pulses of such a 'mode-locked' laser are very short (full-width half-maximum, FWHM, of ~ 100 fs) and its repetition rate is fairly low (~ 80 MHz), the average power that impinges on the tissue is small enough not to damage it thermally. Due to the long wavelength of the laser there is also less scattering in the tissue and good resolution can be achieved even deep in the tissue (Theer et al., 2003). In the retina, the infrared laser greatly reduces the activation of photoreceptors: if tuned to wavelengths above 900 nm the laser light is only absorbed minimally by rods and cones, which thus remain functional for light-stimulation (Fig. 4; Denk and Detwiler, 1999).

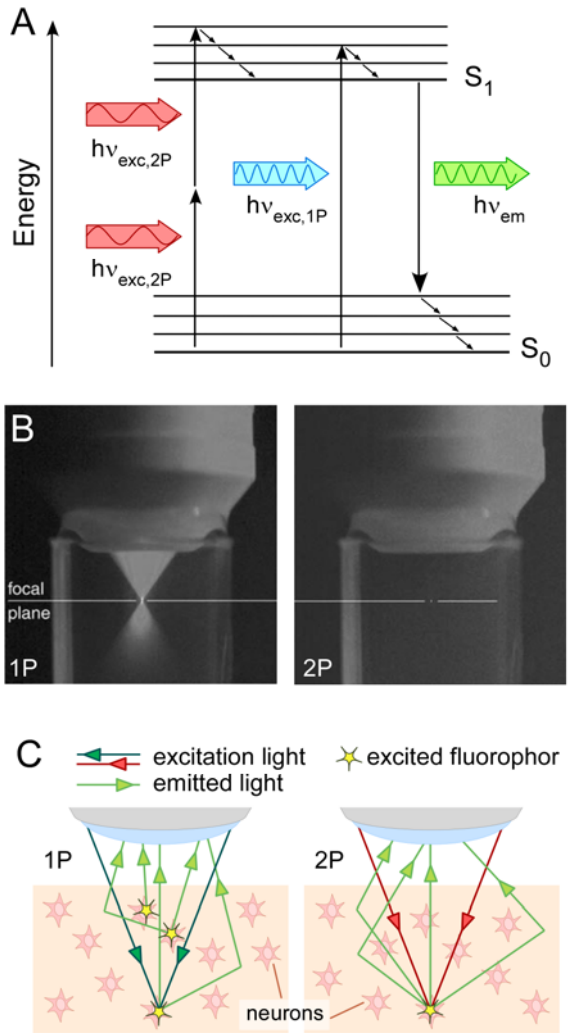

Fig. 5 Two-photon imaging.

A. Jablonski diagram showing the excitation of a fluorophor from the ground state (S_0) to a higher vibrational level of the excited state (S_1) either by two photons of lower energy ($h\nu_{exc,2P}$, *two-photon excitation*), i.e. longer wavelength, or by one photon of higher energy ($h\nu_{exc,1P}$, *single-photon excitation*). The fluorophor relaxes to the lowest level of S_1 (*internal conversion*) before emitting a photon ($h\nu_{em}$) via deactivation back to a vibrational level of the ground state.
In general $2 \cdot h\nu_{exc,2P} > h\nu_{em}$ and $h\nu_{exc,1P} > h\nu_{em}$

B. Photograph of fluorescence emission within a cuvette filled with a fluorescent dye solution (modified from Theer et al., 2005). The left panel shows single-photon excitation: all of the fluorophores within the cone of incident light are excited. In the two-photon case (right panel) the intensity of excitation light is only high enough in the focus. Thus only the fluorophores within the focal volume are excited and emit light.

C. Drawing illustrating that with single-photon excitation multiply scattered photons originating in the focus cannot be distinguished from photons from outside of the focus. (*The pinhole that is in practice used to collect only photons from the focus is omitted.*) With two-photon excitation all photons originate in the focus, allowing the use of light from backscattered photons for detection. Note that the excitation light (*dark green and red arrows*) illuminates the whole focal cone, this is omitted for clarity.

Other benefits of multi-photon excitation arise from the fact that here the fluorescence of a chromophor requires the absorption of two photons, thus depending quadratically, not linearly, on the light intensity. Accordingly, the probability of two-photon absorption also drops non-linearly with the intensity, and effective excitation is only possible within a small focal volume (Fig. 5 B, C). As a consequence, all emitted photons come only from the focus and not from 'accidentally' excited fluorophores outside the focus, as in conventional confocal laser scanning microscopy ('out-of-focus' fluorescence; Fig. 5 B, C). This has several advantages. First, resolution is intrinsically three-dimensional (Figs. 5 B, 6), i.e. no pinhole is needed to eliminate photons originating outside the focal plane. Second, all of the emitted photons, including those scattered on the way back to the microscope objective, can be used, yielding higher excitation efficiency. Third, in the case of the retina, visible

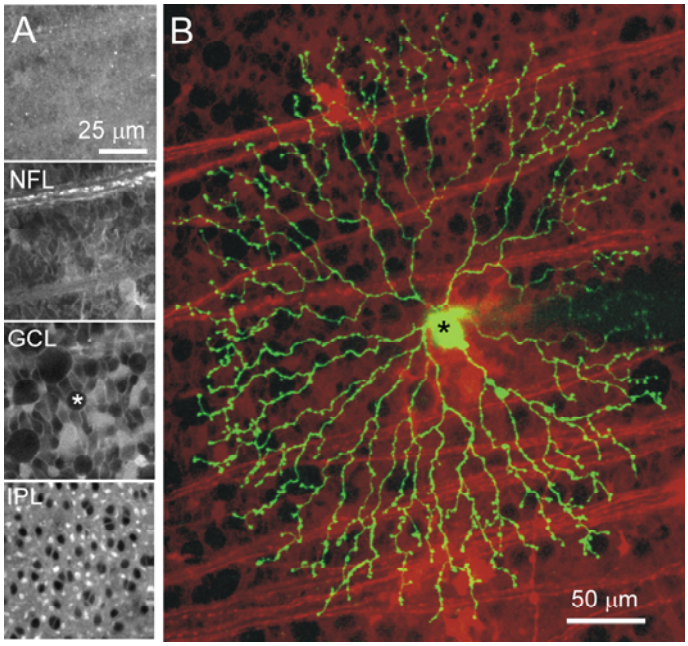

Fig. 6 Two-photon micrographs. **A.** Images of a retinal whole mount at different focal depths, stained with sulforhodamine 101 to visualize the intracellular space. *First panel*: retinal surface, followed by nerve fiber layer (NFL, *second panel*), ganglion cell layer (GCL, *third panel*) and inner plexiform layer (IPL, *fourth panel*). The asterisk denotes the soma of the starburst amacrine cell in B. **B.** Overlay of sulforhodamine images (*red*) and of a starburst amacrine cell (*green*) filled with the Ca^{2+} indicator Oregon green 488 Bapta-1 via a patch-pipette (the shadow of the pipette can be seen on the right). Both pictures are a collapsed series of images.

fluorescence is thus restricted to such a small volume that it usually does not activate photoreceptors, finally making functional imaging applicable to this system.

1.3.2 Electrophysiology

Some limitations of functional imaging can unfortunately, at the present developmental stage, not be avoided. Indicators that allow measurements with high or at least moderate signal-to-noise ratios are at present only available for calcium (Ca^{2+}) and chloride (Cl^-). To draw conclusions towards a cell's overall electrical activity, i.e. its membrane potential, [Ca^{2+}] changes can be monitored[4]. A large spectrum of [Ca^{2+}] indicators with different properties exists, but [Ca^{2+}] signals must be carefully interpreted: Calcium concentrations are not always directly related to the membrane potential, as there are Ca^{2+} release and uptake by intracellular stores, Ca^{2+} extrusion mechanisms and Ca^{2+} influx through receptor- as well as voltage-gated channels. Other ion-dyes available, e.g. for sodium [Na^+] or magnesium [Mg^{2+}] produce only

[4] The chloride (Cl^-) indicators available (e.g. Kuner and Augustine, 2000) yield valuable results for specific questions (mainly concerning inhibitory transmission, e.g. Dübel et al., 2006), but cannot be used to deduce general neuronal activity.

very small signals. Important results have been obtained in population studies with voltage-sensitive dyes (e.g. Petersen et al., 2003), but their application to single cells in whole tissue preparations is tedious and their signal-to-noise ratio usually so low that small responses from single cells can only be detected when averaging numerous trials. To study the trans-membrane voltage of a cell, electrical recordings are yet the method of choice.

The whole-cell patch clamp technique (Hamill et al., 1981) yields a good signal-to-noise ratio, allows controlling the cell's voltage and defining its intracellular ionic milieu. Here, a fine glass capillary (electrode) filled with a solution with similar ionic concentration as in the cell is attached to the membrane of the cell and a connection between the cytosol and the electrode solution is achieved (Fig. 7 B). As the resistance between the electrode wall and the membrane is very high (~ 1-5 GΩ) compared to the resistance between the electrode solution and the inside of the cell (few MΩ) currents flowing between membrane and glass can be neglected and the currents over the cell membrane can be measured (see Fig. 7 for details). With the aid of a sensitive feedback amplifier the voltage over the cell membrane can be controlled (voltage clamp mode; Cole and Curtis, 1939) and currents measured, or currents can be set to a certain value (usually 0 pA) and the membrane voltage recorded (current clamp mode). Owing to the GΩ-resistance between membrane and electrode and the speed of electrical current patch-clamp recordings exhibit very low noise and extremely good

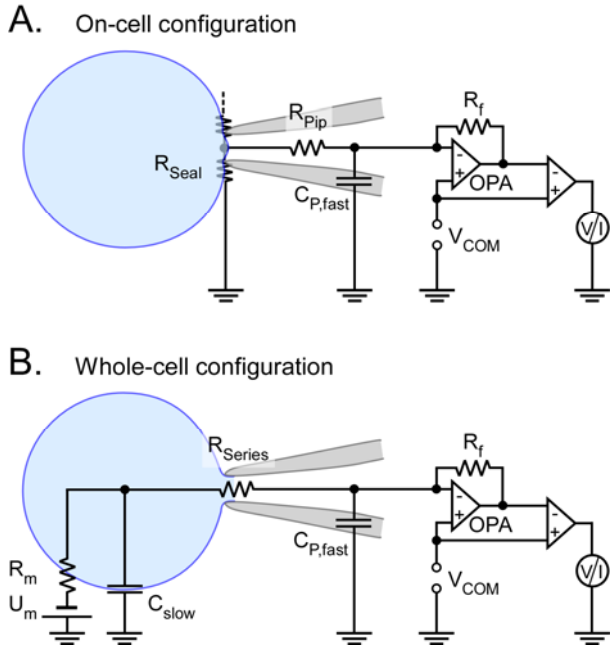

Fig. 7 Patch-Clamp circuit .
Circuit diagrams of the 'whole-cell patch-clamp' technique, illustrated for voltage-clamp mode: **A.** Before breaking into the cell $C_{P,fast}$ (the capacitance of the glass pipette) is measured and compensated **B.** After break-in. Using an operational amplifier (OPA), exactly the current which is needed to compensate for the difference between command voltage (V_{COM}) and voltage over the cell membrane (U_m) is fed back to the cell via a feedback resistance (R_f). Simultaneously this current is recorded. This measurement is based on the fact that there is minimal current flow between cell membrane and patch pipette, i.e. a high seal resistance (R_{Seal}) of several GΩ (A.). To define the membrane resistance R_m, R_{Series} (R_{pip} and the resistance caused by membrane fragments etc.) needs to be reasonably low. C_{slow} is the membrane capacitance of the cell.

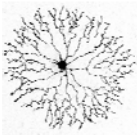

temporal properties, respectively (Hamill et al., 1981). For larger cells with a complex morphology (e.g. extensive dendritic arborization), however, potentials as well as currents that are generated remote from the recording site (e.g. in a distal dendrite) are attenuated, entailing bad voltage-control of these cell compartments (the space-clamp issue; for review see e.g. Numberger and Draguhn, 1996).
Ultimately, both functional imaging and electrical recordings have their specific advantages for studying computational mechanisms in single neurons. In this study both methods were used to approach the question how direction selectivity is generated in the dendrites of starburst amacrine cells.

1.4 Direction selectivity

> Much remains to be clarified in retinal circuitry – not only complex operations such as the computation of motion […]
>
> **Heinz Wässle, 2004**

Direction selectivity, the ability to respond strongly to a specified direction of motion (the preferred direction), but not or minimally to the opposite (null) direction, was for the first time described more that 40 years ago for retinal ganglion cells in the rabbit (Fig. 8 A; Barlow and Hill, 1963; Barlow et al., 1964; Barlow and Levick, 1965). There are two functional types of direction selective ganglion cells (DSGCs): ON DSGCs, with their dendritic trees ramifying in the ON sublamina of the inner plexiform layer (IPL, see Fig. 2; Buhl and Peichl, 1986; Amthor et al., 1989; He and Masland, 1998), respond to a bright spot moving on dark background. They comprise three subtypes of cells with the preferred directions (i) posterior to anterior, and anterior to posterior (ii) with an upward component or (iii) with a downward component (Fig. 8 B; Oyster and Barlow, 1967). Their dendritic field diameters range from 300 µm closest to the visual streak to 800 µm in more peripheral regions (Buhl and Peichl, 1986; Pu and Amthor, 1990; Famiglietti, 1992b). ON DSGCs respond to velocities within a range from 0.4 to 10 deg/sec (Oyster et al., 1972; Wyatt and Daw, 1975). The other type of DGSC, the ON/OFF DSGC, extends its dendritic arborizations in the ON and OFF sublamina of the IPL (Fig. 2, 8 B; Amthor et al., 1984; 1989; Oyster et al., 1993; Yang and Masland, 1994; Amthor and Oyster, 1995)

and responds to stimuli both brighter and darker than the background. These cells exist as four subtypes with the preferred directions: upwards, downwards, anterior to posterior and posterior to anterior (see Fig. 8; Oyster and Barlow, 1967). Their dendritic fields are two to three times smaller than those of ON-DSGCs, thus ranging from 100 µm to 400 µm (Vaney, 1994; Yang and Masland, 1994). ON/OFF DSGCs prefer higher velocities than ON DSGCs, from 1 to 100 deg/sec (Oyster et al., 1972; Wyatt and Daw, 1975), and respond to a large range of contrasts (Merwine et al., 1998).

The dendritic trees of the seven subtypes of DSGCs tile the retina with little overlap, such that a cell of each preferred direction covers every point of the visual field[5] (Vaney, 1994, Amthor and Oyster, 1995, DeVries and Baylor, 1997; Buhl and Peichl,

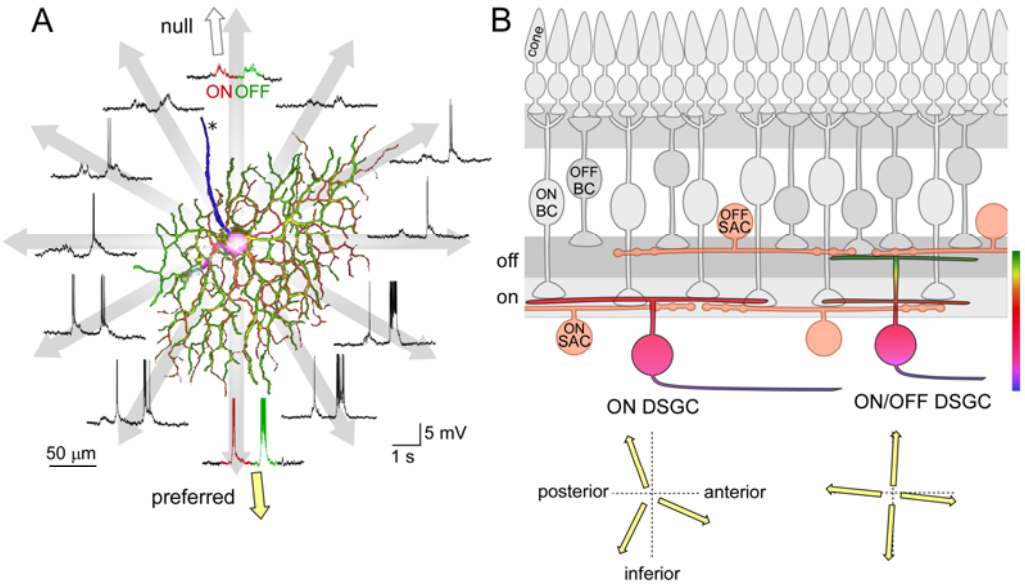

Fig. 8 Directionally selective ganglion cells.
A. Micrograph of an ON/OFF DSGC, color-coded for retinal depth (*see color bar in* B.) overlaid with electrical responses from a whole-cell patch-clamp recording. The cell was stimulated with a bright bar on dark background moving in 12 different directions across the receptive field. The first part of the response in each trace corresponds to the bar entering the receptive field (*ON-signal*), the second to the bar moving out of the receptive field *(OFF-signal)*. The asterisk marks the axon. **B.** Schematic view of the retinal elements known to be involved in the DS circuit: ON and OFF bipolar (BC) as well as starburst amacrine cells (SAC) co-stratify with the dendritic arborizations of ON and ON/OFF DSGCs. Depicted below the respective DSGCs are their preferred directions of motion (in rabbit retina). *Both pictures will appear in a modified form in* (Euler and Hausselt, *in preparation*).

[5] It has been described that ON-DSGCs are only encountered within 40% of the visual streak (Oyster, 1968; Vaney et al., 1981a) or at least that they are not found in very ventral and dorsal regions of the rabbit retina (Vaney et al., 2001). Nevertheless, in these regions of the retina they seem to tile it.

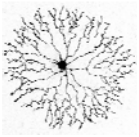

1986). Importantly, until today no correlation between a DSGC's morphology and its preferred direction has been found (Amthor et al., 1984; Oyster et al., 1993; Yang and Masland, 1994). As most of the studies on retinal DS have been carried out on ON/OFF DSGCs in the rabbit, in the following sections the term DSGC is used for these cells; ON DSGCs will be referenced explicitly.

1.4.1 Physiology of direction selective ganglion cells

Many important characteristics of DSGC responses were already described in the original publications and in the extensive work of the following years. Barlow and Levick found that the cells respond in a directionally dependent manner to spots as small as 50 μm when these are displaced over a distance of only 50 μm (or even less, cf. Grzywacz et al., 1994) almost anywhere within the receptive field[6] (Barlow and Levick, 1965). The immediate consequence is that direction selectivity (DS) cannot simply be generated by an excitatory zone adjacent to an inhibitory zone within the DSGC's receptive field (Fig. 9 C), but some mechanism on a smaller scale must account for these DS 'subunits' (Barlow and Levick, 1965). Further experiments showed that a small stimulus moving across the receptive field elicits an asymmetrical wave of inhibition with a constant displacement towards the null-direction relative to the stimulus (Wyatt and Daw, 1975). As DS, but not light-responsiveness, in DSGCs is completely abolished by ionotropic GABA receptor antagonists (Wyatt and Daw, 1976; Caldwell et al., 1978; Ariel and Daw, 1982; Massey et al., 1997) spatially displaced GABAergic inhibition was proposed as a possible mechanism underlying DS.

A controversy within the field was the question if DS is generated within the DSGCs themselves or presynaptically in e.g. an amacrine cell or a network of cells (for review see Vaney et al., 2001). Following a study in turtle (Borg-Graham, 2001), experiments in rabbit indicated that the inhibitory GABAergic as well as the excitatory input to the DSGCs is directionally tuned (Taylor and Vaney, 2002; Fried et al., 2002). DS is, thus, very likely computed presynaptic to the DSGCs (see also 1.4.3). Although it might be hard to imagine how the bipolar cell input to DSGCs (Cohen and Miller,

[6] There is a small non-directional zone on the side of a DSGC's receptive field that is encountered first by a stimulus from the preferred direction. This is an important finding in itself as it favors an inhibition displaced towards the null side (Barlow and Levick, 1965).

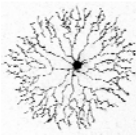

1995; Kittila and Massey, 1997) could be directional (see also 4.4), studies indicate that the directional excitatory input to DSGCs is actually both glutamatergic and cholinergic (Fried et al., 2005). When the cholinergic excitatory input (Ariel and Daw, 1982) is blocked, however, DSGC responses still remain DS (Ariel and Daw, 1982; Kittila and Massey, 1997), indicating that cholinergic input does not essentially contribute to DS. It does seem to symmetrically enhance responses to motion though (He and Masland, 1997). Further, it has also been suggested that for grating or sine-wave stimuli acetylcholine (ACh) does play a role in DS (Grzywacz et al., 1998).
It is also clear that other parallel and subsequent mechanisms, such as postsynaptic sharpening of the directional tuning in the DSGCs (Oesch et al., 2005), contribute to retinal DS as well.

1.4.2 Requirements for direction selectivity

At this point it seems helpful to give a brief overview of the formal requirements for the computation of DS as well as the suggested mechanisms in the retina (for review see Borst and Egelhaaf, 1989; Hildreth and Koch, 1987). Barlow and Levick (1965) proposed a model, which relies on a time-delay between excitatory and inhibitory input and, as a result, a vetoing of excitation by inhibition. This is similar to a more formal model, the 'correlation detector', derived from behavioral experiments in insects (Hassenstein and Reichardt, 1956). In the correlation detector the direct signal is combined with a low-pass filtered signal via a non-linear element: a multiplicator (Fig. 9 A, B). Contemplating this, it becomes apparent that a linear operation, like a summation of the signals, would lead to an output of equal size (= same integral) independent of the direction of motion, although not necessarily to the same temporal shape (waveform). A non-linear operation, e.g. multiplication or 'veto', would result in a clear direction-dependent difference, i.e. different amplitudes and integrals, in response (Fig. 9 A, B). Thus, for 'real' direction selectivity (cf. Borg-Graham and Grzywacz, 1992) a non-linear element is necessary (see also Borst and Egelhaaf, 1989 and Poggio and Reichardt, 1973).
There have been multiple suggestions to how a correlation detector could be implemented in the retina. Most proposals involve some kind of displaced and time-delayed inhibition, either onto the DSGC itself or onto a presynaptic cell (Vaney, 1990; Borg-Graham and Grzywacz, 1992), with the interaction between inhibitory and

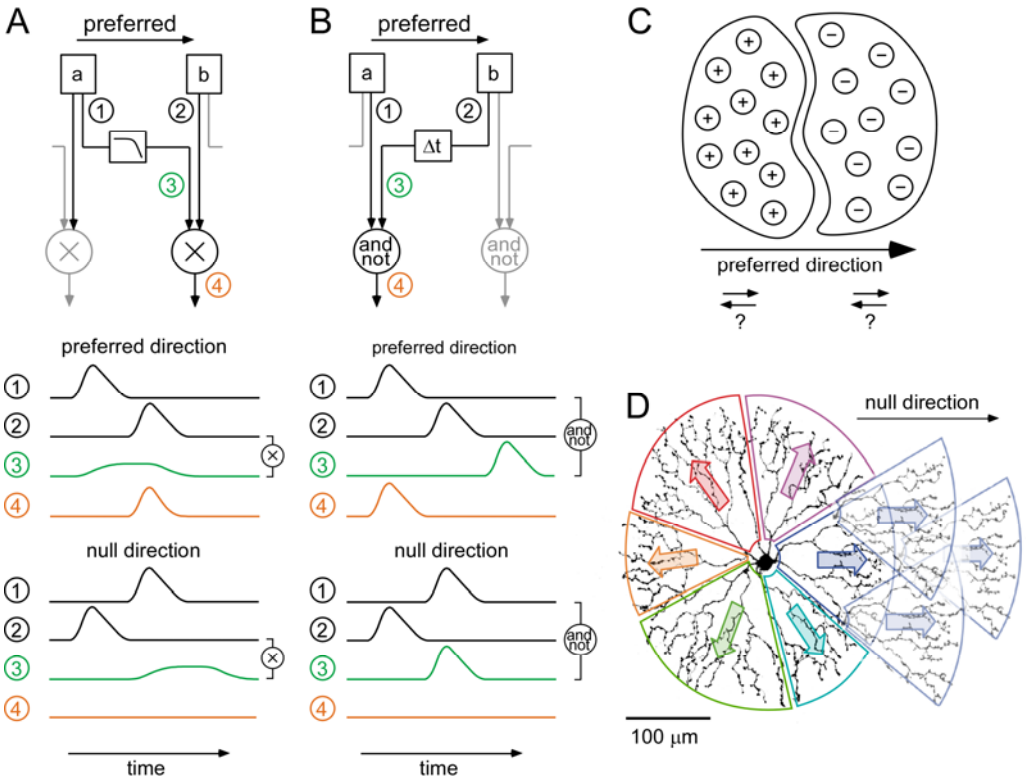

Fig. 9 Models of direction selectivity.
A. Simplified version of the Hassenstein-Reichardt correlation detector (1956). The elements **a** and **b** depict light detection units. The signal from **a** is low-pass filtered and multiplied with the signal from **b** causing a response in preferred but no response in null direction. Traces below the scheme are from the locations 1 to 4 **B.** Model analog to A., but derived from the type of correlation detector described by Barlow and Levick (1965). In this scheme a boolean operation is used: a time-delayed (*Δt*) signal vetoes (*'and not'-element*) a signal arriving in synchrony (*see traces for null direction*). Barlow and Levick suggested an inhibitory synapse as the neuronal equivalent to the *'and-not'* gate **C.** Fictive DSGC receptive field composed of an excitatory and an inhibitory half. It becomes immediately apparent that this model can not explain the properties of a retinal DSGC receptive field, as the direction of movements restricted to a small sub-region of the receptive field would not be recognized (*adapted from* Masland, 2003). **D.** Modernized version of the co-transmission model proposed by Vaney (1990). Each dendritic sector of a starburst amacrine cell (SAC) acts as a largely independent DS computational unit (*'preferred' directions depicted by arrows*). Multiple sectors (from several SACs) of a certain direction preference (*e.g. blue*) could be connected to one type of DSGC. As connections between SACs and DSGCs seem to be predominantly GABAergic (Fried et al., 2002; Lee et al., 2006), the SAC 'preferred' direction would inhibit the respective DSGC in this direction, thus defining its null-direction.

excitatory input generating the non-linearity, e.g. in terms of shunting inhibition (Torre and Poggio, 1978; Koch et al., 1983; Taylor et al., 2000). A non-linearity could also be incorporated in the computation as a threshold mechanism, e.g. in the form of a voltage-gated conductance (Tukker et al., 2004). It has been suggested that the spatial displacement in the mechanism could be caused by laterally displaced inhibitory and excitatory receptors (e.g. Borg-Graham and Grzywacz, 1992) or synaptic elements (Dacheux et al., 2003), the time-delay by waves of intracellular Ca^{2+}, propagating through the dendrites of an involved cell (Barlow, 1996).

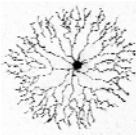

1.4.3 The role of starburst amacrine cells

> It is possible that for this amacrine cell the functional unit is not the whole cell, but local regions of the dendritic plexus, a plexus made up of elements from many overlapping cells.
>
> **Tauchi and Masland, 1984**

The role of one type of cell presynaptic to the DSGC has been controversely discussed for over 20 years. Increasingly this cell, the cholinergic amacrine cell (Masland and Mills, 1979), also known as 'coronate' (Hughes and Vaney, 1980) or 'starburst' (Famiglietti, 1983b) cell, emerges as an essential player.

Starburst amacrine cells (SACs) exist in two subpopulations, an ON and an OFF type (Famiglietti, 1983b), whose dendrites stratify within a very narrow band (~ 2 µm, Masland and Mills, 1979) in the ON and OFF sublamina of the IPL, respectively (Fig. 2; Fig. 8 B). The somata of the ON SACs, or displaced amacrine cells, are located in the ganglion cell layer (Famiglietti, 1983b; Tauchi and Masland, 1984) and can thus be electrically recorded from more conveniently than the somata of OFF SACs in the inner nuclear layer. They exhibit non-spiking (but see Bloomfield, 1992; Gavrikov et al., 2003) graded responses to ON stimuli within their receptive field, which correlates with the dendritic field, and an inhibitory surround (Taylor and Wässle, 1995; Peters and Masland, 1996; Euler, 2002; Zheng et al., 2004).

The SAC morphology is conserved throughout all vertebrate species in which these cells have been studied (Perry and Walker, 1980). It is not only striking because of its radially symmetric dendritic branching pattern (Hughes and Vaney, 1980; Famiglietti, 1983b), but also because of the intriguing distribution of input and output synapses: Input synapses from bipolar and amacrine cells are dispersed all over the dendrites, whereas output synapses are restricted to approximately the outer third of the dendritic branches (Figs. 6 B, 10 A), with both kinds of synapses often localized on characteristic swellings or varicosities (Famiglietti, 1983a; Famiglietti, 1991). The unique 'starburst' morphology has inspired several biophysical SAC models, which propose that the dendritic segments are electrically isolated from the soma and thus could represent the functional subunits of SACs (Fig. 10 A; Miller and Bloomfield, 1983, Poznanski, 1992, Velte and Miller, 1997). In contrast to most other retinal cells SACs feature an extremely high overlap of their dendrites (30-70 fold, Tauchi and Masland, 1984; anticipated by Vaney et al., 1981b; Famiglietti, 1983b), which co-fasciculate with each other (Tauchi and Masland, 1985), with the dendritic branches of

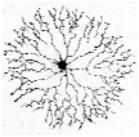

the ON/OFF (Famiglietti, 1992a; Vaney and Pow, 2000) and with the ON DSGCs (Famiglietti, 1992a), creating a lattice-like meshwork. It has been shown that DSGCs receive direct cholinergic input (Masland and Ames, 1976; Ariel and Daw, 1982; Kittila and Massey, 1997) and since SACs are probably the only ACh-releasing neurons of the retina[7] (Baughman and Bader, 1977; Masland and Mills, 1979) it is likely that they are the neurons to provide the DSGCs with this cholinergic input.

Masland and coworkers were the first to suggest a role of SACs in the DS mechanism by proposing that the SAC dendritic plexus could provide the substrate for the local direction selective subunit in the ON/OFF DSGC receptive field (Masland et al., 1984a). In 1988 two groups discovered that the cholinergic amacrine cells are also GABAergic (Brecha et al., 1988; Vaney and Young, 1988), two 'conventional' neurotransmitters[8] within one neuron being thought of as a rarity in the central nervous system (CNS) at this time (Vaney and Young, 1988). Consequently, both groups suggested the SAC to be the source of excitatory as well as inhibitory input to DSGCs. Shortly after, Vaney (1990) put forward a co-transmission model in which the SAC dendritic sectors function as independent subunits. In this model the dendritic segments are asymmetrically connected to DSGCs, with cholinergic input only from those sectors pointing in the preferred direction of a respective DSGC and symmetric GABAergic input (Fig. 9 C).
Meanwhile, both ACh and GABA release have been shown to be Ca^{2+} dependent (O'Malley and Masland, 1989; O'Malley et al., 1992; Zheng et al., 2004). It is still unclear though if the transmitters are localized to different vesicles or dendritic compartments and if different mechanisms control their release.

In the last ten years evidence for an essential role of SACs in the DS computation has accumulated. For instance it has been demonstrated that ablating a large fraction of the SAC population (Yoshida et al., 2001; Amthor et al., 2002) abolishes direction selectivity (but not light-responsiveness) in DSGCs. With double patch-clamp recordings is has been shown that DSGCs receive direct SAC inhibition coming from the null-side of their receptive field but lack SAC input coming from the preferred side (Fried et al., 2002; Lee et al., 2006). Nevertheless, despite numerous attempts no study

[7] At least in the rabbit. In the ground squirrel retina another population of cholinergic amacrine cells has been described. These cells do not costratify with the DSGC dendrites however (Cuenca et al., 2003; see also 4.4.1).
[8] 'Conventional' meaning: glutamate, GABA, glycine and ACh. Neuropeptides or neuromodulators are often co-released in addition to one of these transmitters.

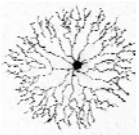

to date has demonstrated convincing morphological evidence of asymmetric connectivity (Dong et al., 2004, Famiglietti, 2002).

In 2002 Euler and colleagues were able to directly demonstrate DS signals in the dendritic tips of ON SACs (Euler et al., 2002): They used functional imaging to show that light stimuli moving outward from the soma to the dendritic tips (centrifugal) evoke large [Ca^{2+}] transients in the tips of the dendrites, whereas inward moving stimuli (centripetal) did not (Fig. 10). Because ACh and GABA are released in a Ca^{2+} dependent manner (O'Malley and Masland, 1989; Zheng et al., 2004), the DS [Ca^{2+}] responses should represent DS neurotransmitter release. This study also confirmed the relative isolation of dendritic segments as [Ca^{2+}] transients are only evoked in the sector which is stimulated by light.

Thus it seems that the currently most convincing scheme for the generation of DS involves an already directional inhibitory input to a DSGC from null-side SAC segments, which point in its null-direction (Fig. 9 D).

One important question regarding SACs has nonetheless not been solved: How and where is DS generated in the SAC dendrites?

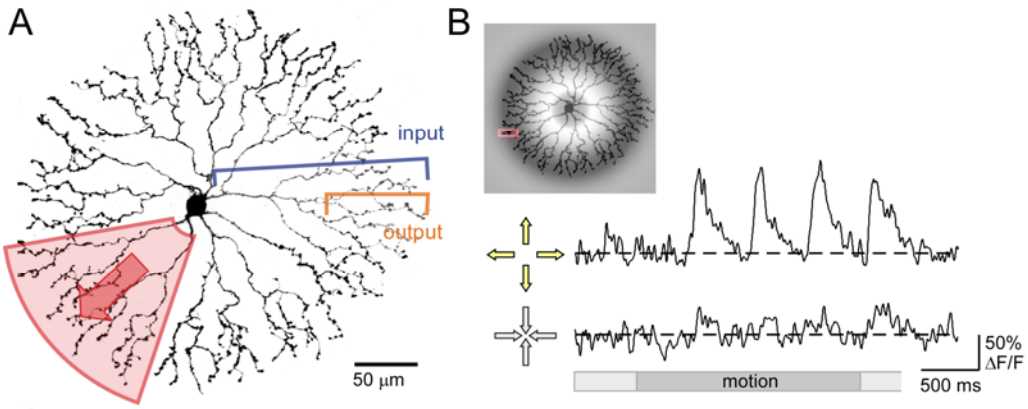

Fig. 10 The starburst amacrine cell.
A. Rabbit starburst amacrine cell (SAC). The cells have 3-5 primary branches terminating in up to 80 dendritic tips; the overall length of SAC dendrite in one rabbit retina has been calculated to ~ 2 km (Tauchi and Masland, 1984). The input synapses are distributed along the whole dendrite, whereas the outputs are restricted to the outer third of the dendritic tree (*see text*). The red sector depicts what is currently viewed as a 'functional' unit of the SAC. Each of these sectors has the directional preference from soma to dendritic tips (*outward, see* B.). **B.** [Ca^{2+}] response measured in a dendritic tip (*red box in inset*) to an outward or inward-moving circular sine-wave (*overlay in inset*). When the stimulus moves in outward direction there are large [Ca^{2+}] responses; the signals to inward motion are minimal. *Picture will appear in a modified form in* (Euler and Hausselt, *in preparation*)

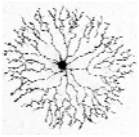

As already proposed by Rall (1964), a summation of electrical inputs along a dendrite can lead to a larger signal at its centrifugal end. This suggestion was seized by later models of SAC dendritic DS (Miller and Bloomfield, 1983; Borg-Graham and Grzywacz, 1992) and was recently extended to an elaborate biophysical model demonstrating a directional difference 'measured' in the SAC dendritic tips in response to outward *vs*. inward motion (Tukker et al., 2004). In contrast to this model most models rely on interactions of excitatory and especially inhibitory inputs between SACs and between SACs and other amacrine cells (e.g Borg-Graham and Grzywacz, 1992), with a recent study suggesting that an inhibitory SAC network alone can create DS in these cells (Münch and Werblin, 2006). Recently some investigators have come up with more unconventional ideas as to the computation of DS in SACs: For example, Gavrikov et al. (2003) propose a chloride gradient within the dendrites of SACs, leading to opposite effects of GABA at different dendritic eccentricities.

The purpose of this study was to investigate constraints for DS in SAC dendrites and to begin to explore the properties of the underlying biophysical mechanism.

❋

Chapter II

Methods

Animals and tissue preparation

Imaging and visual stimulation

Electrophysiology

Data analysis

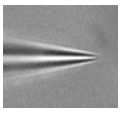

2.1 Animals and tissue preparation

Animals used were six to ten week old (i.e. adult) New Zealand White rabbits or, in some experiments, pigmented animals (Charles River or Harlan Winkelmann, Germany). No systematic differences in the responses were observed between albino and pigmented rabbits (T. Euler, personal communication), therefore data from the two strains were pooled. All procedures had been approved by the local animal care committee and were in accordance with the law of animal experimentation issued by the German Government (Tierschutzgesetz).

Preparation of the retina whole-mount was performed according to the following protocol: After at least two hours of dark adaptation the animals were first deeply anesthetized by an intramuscular injection of Ketamine (50 mg/kg body weight; Curamed Pharma GmbH, Germany) and Xylazine (10 mg/kg body weight; Rompun, Bayer, Germany) and then sacrificed with a lethal dose of Sodium Pentobarbital (160 mg/kg body weight; Narcoren, Merial GmbH, Germany) injected into the ear vein.

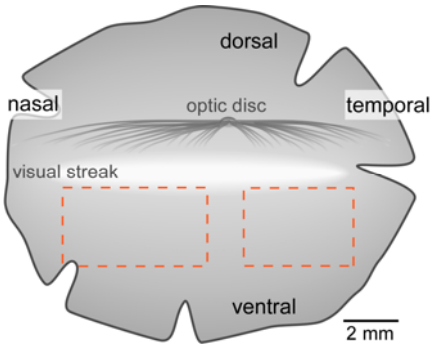

Fig. 11 Schematic drawing of a retina flatmount. Flattened rabbit retina from the left eye, ganglion cell layer facing upwards. The two orange boxes just below the visual streak (*lighter gray*) indicate the sites from which tissue was taken for the recordings.

Immediately after death one eye was enucleated. All the following steps were performed in oxygenized (95% O_2, 5% CO_2) Ames medium (Sigma-Aldrich, Germany or USBiological, USA) at room temperature. After hemi-dissecting the eye at the ora serrata lens and vitreous were removed and the retina was carefully dissected from the rest of the eyecup. A piece of retina (4-25 mm^2) was cut ventral to the visual streak and slightly peripheral to the midline (Fig. 11). This piece of retina was then either glued to a coverslip with tissue glue (CellTak, Becton Dickinson GmbH, Germany) or

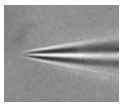

mounted on a piece of nitrocellulose filter paper (#AABP02500; Millipore GmbH, Germany) in which ~ 1-2 mm-diameter holes had been punched to allow infrared (IR) illumination from below. The coverslip or filter paper holding the retina was then transferred to the recording chamber, where it was held down at the bottom of the chamber by a U-shaped platinum wire and continuously superfused with warm (~ 36°C) oxygenized Ames medium at a flow rate of approximately 2-4 ml/min. The rest of the retina was kept in a light-proof chamber in oxygenized Ames medium at room temperature for later use.

2.2 Imaging and visual stimulation

Multi-photon fluorescence microscopy (Denk et al., 1990) was used to image the structure of the tissue (see 2.3 and Fig. 6) as well as calcium signals in indicator-filled cells (Denk and Detwiler, 1999; Euler et al., 2002) during visual or electrical stimulation. The setup (the 'Eyecup Scope', Fig. 12) was specifically designed by W. Denk and coworkers (*manuscript in preparation*) to meet the requirements of opto-physiological measurements and simultaneous light stimulation in whole-mounted retina or eyecup preparation (see also 1.3.1). The 'eyecup scope' is basically an episcopic microscope equipped with a high-NA (numerical aperture) objective lens, through which both the excitation light of the laser and the visual stimulus are delivered to the tissue. This is made possible by a sophisticated system of dichroics, mirrors and adjustable lenses within the arms of the microscope. The optical paths for multi-photon fluorescence imaging and visual stimulation are described in detail in the following two sections.

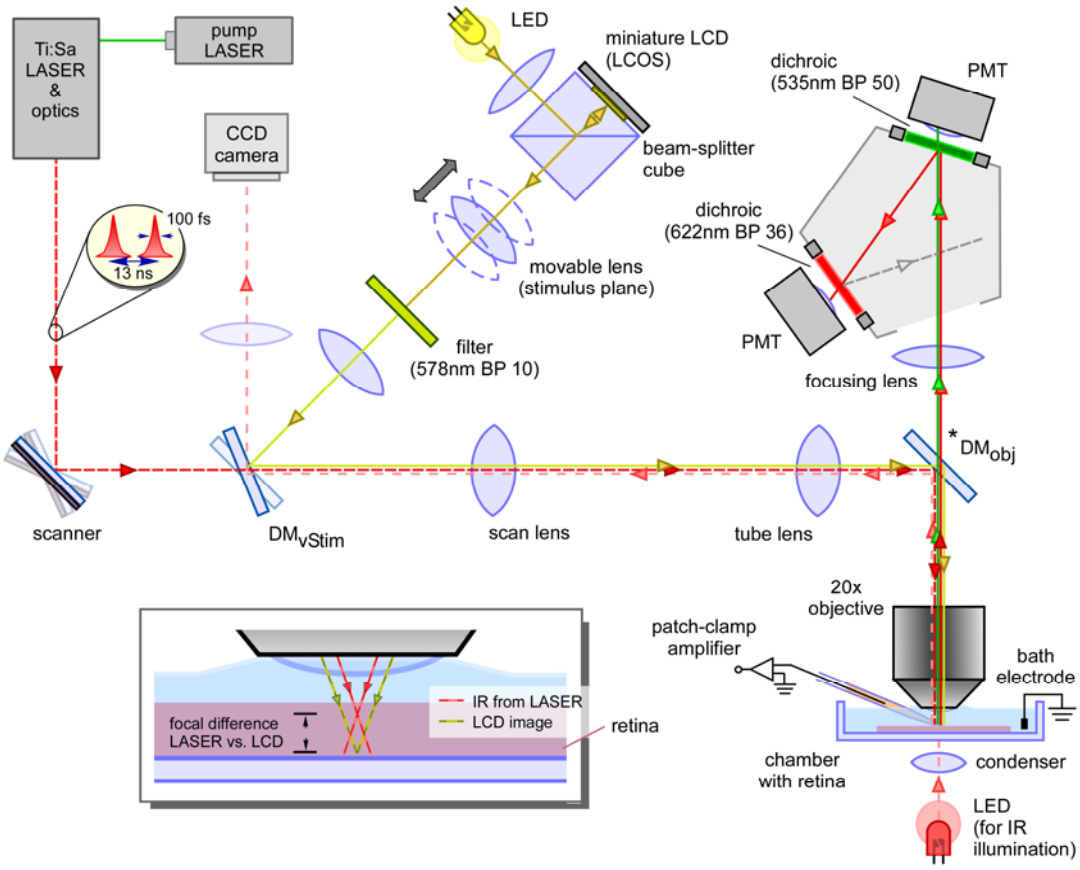

Fig. 12 Illustration of the 'Eyecup Scope'.
Shown are (*from left to right*) the path of the IR excitation laser (*red dashed line*) that converges with the path from the light stimulus (yellow line) at the dichroic DM_{vStim} before being directed via the dichroic DM_{obj} (* *for transmission spectrum see Fig. 13*) through the objective into the tissue. Fluorescence signals (*green and red lines*) pass through DM_{obj} to the photomultipliers (*top right*). A quasi-DIC image of the tissue is created by IR illumination via a condenser from below the recording chamber (*light red dashed line*) and recorded with a CCD camera (*upper left*). The inset shows the offset between the laser focus and the visual stimulus image. *Further details are described in sections 2.2.1 and 2.2.2*.

2.2.1 Two photon microscopy and [Ca^{2+}] imaging

The light source for the multi-photon microscope – a Ti:sapphire laser (Mira Optima 900-F) – is pumped with continuous wave light (532 nm) by a 10 W solid state laser (Verdi, both Coherent Co., USA) and generates quasi-monochromatic (bandwidth ~ 10 nm) 100 fs pulses at 76 MHz. The wavelength of the excitation laser was adjusted to wavelengths between 920 and 930 nm to limit the activation of photoreceptors. This wavelength range is also suitable for exciting the fluorescent dyes used in this study: Sulforhodamine (SR-101, Sigma-Aldrich; emission peak 586

nm; Fig. 4) and derivatives of Oregon-Green 488 (OGB-1, OGB-2, OGB-6F, Molecular Probes, Europe; emission peak 526 nm; Fig. 4).

The intensity of the laser beam is controlled with a Pockel's cell (Conoptics Inc., USA; Model 350-50, with Model 302 driver). The beam is collimated and directed onto the scanners – a pair of orthogonally oriented mirrors (3 mm aperture) fixed to two independent scanner motors (6200; both Cambridge Technologies, USA) – which control the XY-position of the beam in the focal plane of the objective. After the scanners the beam passes a scan lens and a microscope tube lens (# MXA220-18, Nikon, Germany). These are arranged such that the light from the scan lens is focused on the focal plane of the tube lens, and that they work as a telescope (both depicted in Fig. 12). The laser beam is thus collimated and expanded before it is reflected by a custom-made dichroic mirror (DM_{obj}, Chroma Technology Corp., USA; described in more detail in Fig. 13) into the objective (20x water immersion, 0.95 W, XLUMPlanFI, Olympus, Germany) and focused into the retina. Due to this expansion the laser beam slightly overfills the back aperture of the objective and, thus, ensures a full utilization of the high NA, maximizing the resolution of a focused spot at the diffraction limit.

The ballistic and multiply scattered photons emitted from the multi-photon excitation volume (see 1.3.1 and Fig. 5) that are collected by the microscope objective pass the

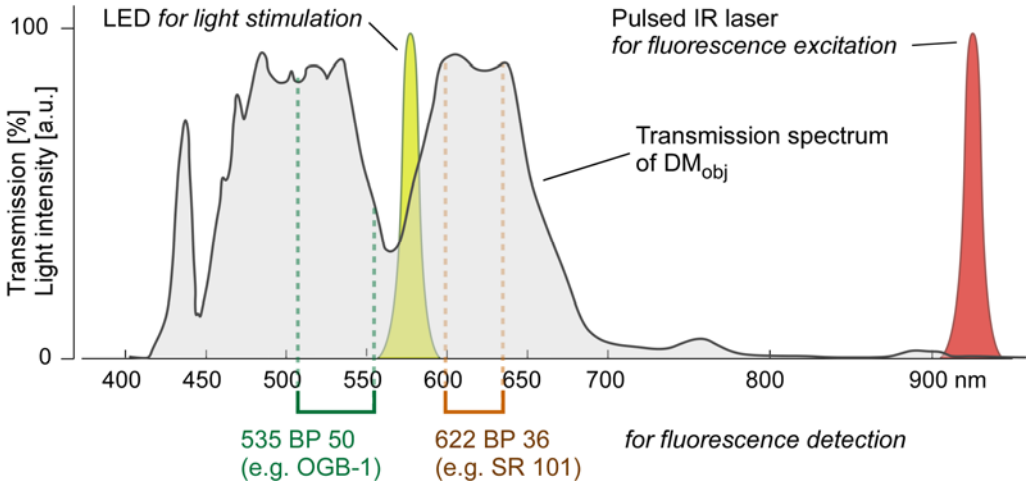

Fig. 13 Transmission spectrum of DM_{obj}
The dichroic mirror (*see Fig. 12*) is custom-designed for combining visual stimulation and multiphoton microscopy within one microscope arm. It features high transmission in a narrow band around 440 nm and two broad bands at longer wavelengths (~ 450-550 nm and 570-670 nm). Fluorescent light within these ranges is thus passed to the photomultipliers (*see Fig. 12*). IR light (longer than 700 nm) as well as blue (shorter than 420 nm and ~ 450 nm) and 'yellow' (~ 560 nm) are partially reflected by the dichroic. Hence, the excitation laser (~ 928 nm) as well as light used for visual stimulation (in this case at 578 nm) are reflected into the tissue.

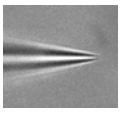

dichroic mirror (DM_{obj}, Figs. 12 and 13) towards the detector head. To ensure that all the light that leaves the objective reaches the detectors, a collecting lens focuses a de-magnified image of the back aperture of the objective onto the first detector (all detectors: #R6357 photomultiplier tubes (PMTs), Hamamatsu, USA; Fig. 12). A dichroic mirror in front of this first detector transmits a defined band of wavelengths (535 nm, bandpass 50 nm, for 'green' fluorescent dyes; Chroma Technology Corp. part # HQ 535/50 nm) and reflects other wavelengths onto the second detector. The second detector is equipped with a similar dichroic mirror, which transmits another wavelength band (622 nm, bandpass 36 nm, for 'red' fluorescent dyes; Chroma Technology Corp. part # HQ 622/36 nm). Such a 'decimating' detector arrangement allows the distribution of the fluorescence light to up to 4 detectors, however, in the experiments described here only two channels were used.

The imaging-software CfNT (Confocal for Windows NT, originally written at Bell Labs by R. Stepnoski and modified extensively by M. Müller, MPImF) running under Microsoft Windows XP, coordinates the movements of the scan mirrors as well as the acquisition of the fluorescence signal. One fluorescence image (a frame) is generated by scanning an area in the focal plane of the objective lens line by line (8 to 512 lines per image) with the excitation laser, while the emitted light is collected. Each line is divided into short sections (termed pixels, usually between 64 and 512 per line), which, since the beam is moving, correspond to 'time slots' for the collection of photons. In this study, the scan rate was varied between 1 to 4 ms per line, which, depending on the number of lines per frame, results in a large range of possible scanning frequencies. For the acquisition of time-elapsed fluorescence 'movies' frames with 8 lines (per 2 ms) at 64 pixels per line (62.5 Hz frame rate) were used here, unless otherwise noted. The morphology of cells filled with a fluorescent dye was recorded using frames with 512 lines at 512 pixels per line – hence temporal resolution was sacrificed in favor of spatial resolution.

To allow movements over the tissue in x-, y- and z-direction the objective lens is mounted on a set of three motor-driven translational stages (one for each axis; Sutter Instruments, USA, MP285-3Z), which can be moved in 0.04 µm increments.

2.2.2 Visual stimulation

Light stimuli were generated using Windows software (custom-written by T.Euler, MPImF) compiled with Delphi7 (Borland, USA).

In some of the initial experiments a through-the-condenser stimulus system was used in which light stimuli were output via a video projector (Astrobeam 530; A+K, Germany, 80 Hz frame rate; 800 x 600 pixels), band pass-filtered (600 nm, BP 20 nm, Omega Filters, Germany), and focused through the sub-stage condenser (0.32 NA; Zeiss, Germany) onto the photoreceptors (~ 4.4 µm/pixel; app. 130 - 2000 photons s^{-1} μm^{-2} for 600 nm)

For most experiments the custom designed visual stimulator of the 'eyecup scope' was used. It shares the second half of the optical path with the excitation laser beam (Fig. 12). Light stimuli are displayed on a miniature liquid-crystal-on-silicon (LCoS) display that has been removed from a commercial head-mounted computer monitor (i-visor DH-4400VP, Cybermind Interactive, Netherlands, or, later, i-glasses VGA; EST, Germany, 30 or 60 - 100 Hz frame rate; 800 x 600 pixels). A collimated beam from a yellow LED (peak ~ 590 nm) that is band pass-filtered (578 nm, BP 10 nm, laser clean-up filter Z578/10, Chroma Technology Corp.) is used for illumination.

The monochromatic output from the stimulator passes scaling and focus-correction optics to create a nearly collimated image that can be adjusted in the depth of its final focus in the tissue (see Fig. 12, movable lens). This correction is implemented to focus the light stimulus within the photoreceptor layer while the laser beam is focused in a different plane (e.g. the in the IPL), in which the imaging is performed – as both are transmitted to the tissue by the same objective lens (see inset, Fig. 12). In these experiments the focus of the light stimulus was set to ~ 100 µm below the objective focus which approximates to the distance between ON-type starburst amacrine cell dendrites in the inner plexiform layer and the photoreceptor layer in rabbit retina.

After the correction optics the image impinges on a dichroic mirror (DM_{vStim}, Chroma Technology Corp.) which reflects visible light but transmits near infrared (IR) and thus, the laser beam (Fig. 12). The image then passes the scan and tube lenses and the dichroic mirror DM_{obj} (Figs. 12 and 13) to be finally focused by the objective into the retina. The stimulus LED on the other hand is focused on the back aperture of the objective and thus is projected onto the retina as a collimated beam, ensuring uniform luminance of the image from the LCoS display. The Leica XLUMPlanFL objective lens (20x, water immersion) was chosen for two reasons: First, its extensive field of

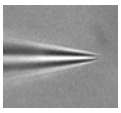

view (~ 1 mm diameter) allows the projection of an image onto the retina that is sufficiently large to cover and exceed the receptive field of the studied retinal neurons. Second, it has a high NA (0.95), which is mandatory for high resolution laser scanning fluorescence imaging.

The stimulus resolution on the retina is ~ 2.1 µm/pixel with approximately 10 - 40 kilophotons s^{-1} μm^{-2} for 578 nm (measured with an Optical Power Meter, Model 840, Newport, Germany). Stimulus contrast (C) is calculated using

$$C = \frac{L_{MAX} - L_{MIN}}{L_{MAX} + L_{MIN}} \tag{1}$$

with the light values L_{MIN} and L_{MAX} the minimal and maximal pixel values, respectively, occurring in a particular stimulus pattern. The gray values used here were always chosen from the linear range of the respective display device. The velocities of the moving stimuli (gratings, circular waves) ranged from 0.1 to 2 mm/s (temporal frequencies: 0.5 to 10.5 Hz).

Circular-wave stimuli consisted of expanding or contracting concentric sinusoidal waves (first term in eqn. 2; Fig. 14) that were centered on the cell. The wave vector was set to 1 cycle per stimulus radius (r_{Max}). The pixel values (P) for the stimuli were calculated using

$$P(r,i) = \sin\left[2\pi \cdot \left(\frac{r}{r_{Max}} + i \cdot \frac{f_{Stim}}{f_{Display}}\right)\right] \cdot \exp\left[-\left(\left(r - r_{0,Filter}\right) \cdot \frac{2}{w_{Filter}}\right)^4\right], \tag{2}$$

with the distance from the stimulus center (soma) r (in µm; $0 \le r \le r_{Max}$), the stimulus frequency f_{Stim}, the display refresh frequency $f_{Display}$, and the frame index i. To avoid sharp edges and to restrict the motion to roughly the outer two thirds of the SAC dendrites the resulting sine wave was filtered with a 'doughnut-shaped' super-Gauss (second term in eqn. 2) with $r_{0,Filter} = 0.5 \cdot r_{Max}$, and $w_{Filter} = 0.562 \cdot r_{Max}$ (Fig. 14 B). To get the desired contrast the intensities of the stimulus pixels were, finally, scaled by

$$P'(r,i) = \frac{P(r,i)+1}{2} \cdot (L_{MAX} - L_{MIN}) + L_{MIN}\,. \tag{3}$$

For most SACs recorded (dendritic field diameters ~ 280 to 360 µm) r_{Max} = 192 µm, which means that the annular area with the circular wave covered the area between ~ 45 and ~ 147 µm from the stimulus center (soma). For the few cells that had smaller

or larger dendritic fields r_{Max} of 128 or 256 µm was used, respectively; this will be mentioned. For the data shown in Figs. 19, 22 and 23 r_{Max} = 192 µm, and the stimulus was presented either behind masks of background gray values or smoothed with a Gaussian of different values for $r_{0,Filter}$ and w_{Filter}. The sizes of the obtained rings are mentioned in the respective sections (see Results). The background of the stimulus projection area is set to the mean intensity of the circular wave.

All of the circular waves used followed the same general motion protocol: (i) Static presentation of the wave for one second, (ii) outward motion for two seconds, (iii) static presentation for two seconds, (iv) inward motion for two seconds, (v) static presentation for one second. Then the condition (e.g. wave configuration, contrast velocity etc.) was changed and the sequence re-started. The whole protocol (all conditions) was repeated three times per condition unless otherwise noted.

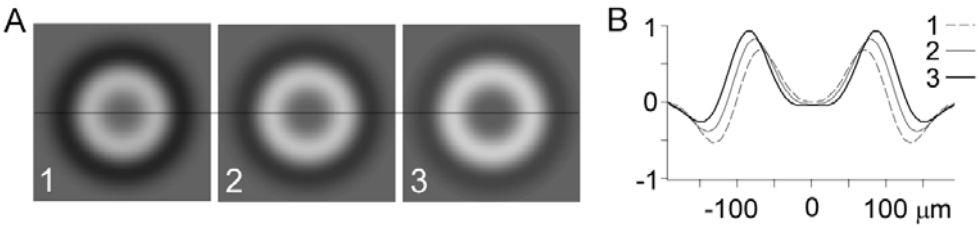

Fig. 14 Circular sinewave stimulus.
A. Example of three consecutive frames from an expanding circular sinewave (contrast 73%) with 128x128 pixels. **B.** The profile of each frame along a line through the center is plotted. For details see 2.2.2.

2.2.3 Other visualization

The tissue in the recording chamber could also be illuminated by an infrared (IR) LED from below (via a condenser). Using an IR-sensitive CCD camera (Fig. 12) a quasi-DIC image of the tissue was displayed on a computer monitor in real-time. This image was used to view the surface of the retina to find an appropriate area where the tissue was flat as well as to access a cell with the patch electrode. At lower magnification (Plan 4x/0.1W objective, WD30, Nikon) the IR quasi-DIC image was used to locate the electrode in the recording chamber.

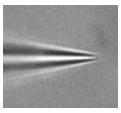

2.3 Electrophysiology

To find particular cell types for electrophysiology or dye-injection the tissue was stained by adding the fluorescent dye sulforhodamine 101 (3 to 7 µM; Sigma-Aldrich) to the extracellular medium. The dye filled the intracellular space allowing, for example, to identify ON starburst amacrine cells with ~ 98% success rate, using soma diameter (~ 10 µm; Famiglietti, 1983b; Masland et al., 1984b) and characteristic round shape (Euler et al., 2002; see also Fig. 6 A). Sulforhodamine was also used as an indicator for tissue health, as dying cells in the retina strongly accumulate the dye and thus brightly fluoresce. Immediately after establishing electrical access to a cell the perfusion system was switched to sulforhodamine-free medium to reduce fluorescence background and preempt any sulforhodamine fluorescence-mediated photo damage. The wash-out was completed before optical recordings commenced.
Starburst amacrine cells were recorded with the whole-cell tight-seal (patch-clamp) technique (Hamill et al., 1981; see Introduction and Fig. 7), which allows a much better electrical control of the cell and a much improved signal-to-noise ratio than with the sharp microelectrodes used in a previous study (Euler et al., 2002).

After locating a starburst cell soma (see above) using sulforhodamine fluorescent imaging, the following procedure was performed under IR illumination: First, a hole was made in the inner limiting membrane next to the targeted cell by scratching a patch pipette over the retinal surface and extended by 'blowing' extracellular medium between the cell bodies. Cellular debris, including Müller-cell membranes, was removed using the same pipette as a 'vacuum cleaner' after its tip had been broken off. When the targeted cell was freely accessible a fresh patch electrode was inserted into the chamber for the recording. To keep the tip of the electrode clean, constant pressure was applied to the electrode, while its resistance was monitored. As soon as the electrode touched the cell, the pressure was relieved and the resistance began to rise. The command voltage (V_{COM}) was then switched to -75 mV. As soon as a stable Giga-seal (see 1.3.2) had formed brief (0.1 to 0.5 ms) 1 V pulses were applied to rupture the cell membrane and achieve the whole-cell configuration.
The reference electrode in the recording chamber was an Ag/AgCl wire or pellet. Data were recorded using a current/voltage clamp amplifier (Multiclamp 700A, Axon Instruments, USA) in combination with pClamp 8 software (Axon Instruments) and analyzed off-line with IgorPro (Wavemetrics, USA).

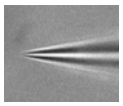

The somatic membrane potential (V_m) was digitized at 5 to 10 kHz and low-pass filtered at 2 kHz. In voltage-clamp mode the current (I_m) was digitized at 5 to 25 kHz and low-pass filtered at 1 kHz. The voltages (both V_m and V_{COM}) were corrected off-line by subtracting 15 mV for the liquid junction potential. The liquid junction potential[9] (Fenwick et al., 1982) was calculated (JPCalc by P. H. Barry, as implemented in Clampex, Axon Instruments) and measured and ranged (depending on the intracellular solution) from 14 to 16 mV and 17 to 18 mV, respectively. Voltage-clamp recordings were, in addition, compensated off-line for series resistance (R_{series}, 23 to 75 MΩ).

Patch-electrodes (3 to 12 MΩ) were pulled from borosilicate glass (O.D.: 1.0 mm, I.D.: 0.58 mm, with filament; Hilgenberg GmbH, Germany) on a laser puller (P-2000; Sutter Instruments) or a filament puller (DMS-Universal puller, Zeitz, Munich, Germany) and backfilled with intracellular solution. Chemicals were purchased from Sigma-Aldrich unless noted otherwise. For current clamp recordings a K^+-based solution (modified from Field and Rieke, 2002) was used, which contained (in mM): K-aspartate (or, with identical results, K-gluconate) 110-120, KCl 5-10, NaCl 5, HEPES 5-10, $MgCl_2$ 0-1, Mg-ATP 1, Na_2-GTP 0.1-1. For voltage-clamp experiments K-aspartate (or K-gluconate) and KCl were replaced by equal amounts of Cs-methanesulfonate and CsCl, respectively, to reduce K^+ currents. In some experiments 0.2-0.5 mM $CaCl_2$, 2-5 mM HEDTA (N-(2-Hydroxyethyl)ethylenediamine-N,N',N'-triacetic acid) and NMG (4-N-methyl-D-glucamine) were added to buffer and elevate the $[Ca^{2+}]$, with no discernable effect on the results. To some solutions a 'recovering solution' composed of 1 mM ATP, 1 mM GTP, 10 mM Na_2- or K_2-Phosphocreatine was added (Warrier et al., 2005). To replenish ATP and GTP 50 Units of Creatine Phosphokinase were added to these IC-solutions freshly before each experiment. The intracellular solution always contained one of the $[Ca^{2+}]$ indicator dyes listed above to allow visualization and $[Ca^{2+}]$ imaging of the recorded cells. Usually OGB-1 was used at a concentration of 100 µM unless otherwise noted. There were no discernable differences in the electrical responses when using different dyes.

In some experiments neurotransmitter receptors or channels were blocked pharmacologically. Most pharmacological agents were applied with the perfusion medium and purchased from Sigma-Aldrich (exceptions are indicated): GABAzine (SR-95531; $GABA_A$-selective; 25-50 µM), Picrotoxin (non-selective ionotropic

[9] The steady potential difference that is caused when solutions containing different ion concentrations and ions with different mobilities come into contact.

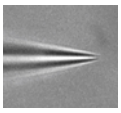

GABA receptor antagonist; 300 µM) and TPMPA (1,2,5,6-tetrahydro- pyridine-4-yl-methylphosphinic acid; $GABA_C$-selective; 50-75 µM) were used to block GABAergic transmission. To study voltage-gated sodium channels QX-314 (N-(2,6-Dimethylphenylcarbomoylmethyl) triethylammonium bromide, 5 mM in the intracellular solution; Tocris, Germany) or Vinpocetine ((3α, 16α)-Eburnamenine-14-carboxylic acid ethyl ester, 30-40 µM) were used. Apart from Cd^{2+} ($CdCl_2$, 5-90 µM) the antibiotic Neomycin (2.5 - 250 µM) and MVIIC ω-conotoxin (blocks P/Q- and N-type, 70-200 nM, Aloman, Israel) were used to block voltage-gated calcium channel subtypes.

2.4 Data analysis

2.4.1 Fluorescence signals

Fluorescence (*F*) data from imaged cells were spatially averaged over so-called regions of interest (ROI) that covered a 2-80 µm-long section of a dendrite, temporally filtered (box car filter with a 42 ms window) and background corrected by subtracting *F* from a ROI placed next to the dendrite. For each response

$$\Delta F(t)/F_0 = (F(t) - F_0)/F_0 \qquad (4)$$

was calculated with F_0 the pre-stimulus *F* averaged over 100 to 500 ms. For quantification the area under the trace

$$(A_{Ca} = \int_{t_1}^{t_2} (\Delta F(t)/F_0)\,dt) \qquad (5)$$

for a defined time interval ($t_1 < t < t_2$) was calculated (as in Euler et al., 2002).
To estimate the Ca^{2+} activation curves (Figs. 29 and 30) of the voltage-gated calcium channels in the imaged dendrite A_{Ca} was plotted as a function of V_{COM}. In order to compare different cells A_{Ca} for each cell was normalized to the [Ca^{2+}] response at V_{COM} = -35 mV taken from the interpolated [Ca^{2+}] *vs.* V_{COM} relationship for this cell. The

interpolation was done using a spline fit (as implemented in IgorPro). The data points pooled from all cells were then fitted using a current *vs*. voltage (*I vs. V*) curve for voltage-gated channels (adapted from eqn. 1 in Scholze et al., 2001):

$$A_{Ca}\left(V_{COM}\right) = A_{Ca,0} + g \cdot \frac{V_{COM} - E_{rev}}{1 + \exp\left(\left[V_{50} - V_{COM}\right] / V_{Slope}\right)} \qquad (6)$$

with the somatic command potential V_{COM} and the free parameters $A_{Ca,0}$ (offset), g (maximal conductance), V_{50} (half-activation voltage) and V_{Slope} (the slope voltage).
For the experiment shown in 3.6.1 (Fig. 30) owing to the large variability of the data points the tentative fit only converged when E_{rev} was set to a defined value. The Ca^{2+} reversal potential is difficult to determine as different Ca^{2+} channels are usually highly selective for Ca^{2+} but do exhibit some permeability for e.g. Na^{+} (Zamponi, 2005). In addition, the intracellular Ca^{2+} concentration is much lower than the extracellular Ca^{2+} concentration (Hille, 2001) and difficult to measure exactly, making the calculation of the Nernst potential very error prone. For this fit an E_{rev} of 50 mV was used.

2.4.2 Electrical signals

To quantify the electrical response to circular-wave stimuli a spectral analysis was performed using the discrete Fourier transformation[10]. Data are presented using the power spectrum, which contains only the squared amplitudes of each frequency component, and a plot depicting the phase of each frequency component (wrapped to $-\pi$ and π; for details see Fig. 15 B, D). The FFT function in the IgorPro software was employed; it relies on the Cooley-Tukey algorithm (Cooley and Tukey, 1965).
During a discrete Fourier transformation the time-series to be analyzed is iterated and thus spurious frequencies can be introduced if the signals contain large and fast components, such as a stimulus-onset transient. Therefore only trace segments that contained an integer number of stimulus cycles were used and the onset of the motion

[10] Fourier transforms are used to decompose a signal into its frequency components, i.e. a time-series (here the response to a sinusoidal stimulus) is transformed into a frequency-spectrum (hence, spectral analysis).

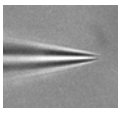

response was excluded (Fig. 15 A, C, black frame). Additionally, the analysis window was shifted in 50-ms steps along the trace until the difference between data trace and its 'reconstruction' from the first four frequency components (see below) was minimal. Four frequency components were extracted from this analysis: the DC component V_0 (at 0 Hz), the fundamental V_1 (at f_1) – which corresponds to the stimulus frequency – and the second and third harmonics, V_2 (at $2 \cdot f_1$) and V_3 (at $3 \cdot f_1$), corresponding to I_0, I_1, I_2, and I_3 for voltage-clamp measurements. These four components (each comprising amplitudes and, except for V_0 or I_0, phases) are sufficient to capture the response characteristics, as can be seen from the inverse transformation back into a time-series ('reconstruction', see inset, Fig. 15 D). Only cells with a robust light-evoked voltage response (≥ 2 mV) to out-going motion of the standard circular-wave stimulus at the lowest used stimulus contrast ≥ 45 % were included. To facilitate the comparison between cells normalized asymmetry indices ($AI_{0...3}$) of each frequency component were calculated:

$$AI_n = \frac{V_{n,EXP} - V_{n,CON}}{V_{n,EXP} + V_{n,CON}} \tag{7}$$

with n=1, 2 or 3. A positive *AI* means that out-going motion evokes larger amplitudes for this particular frequency component. Note that, because only amplitude but no phase information is used, an *AI* equal to zero does not imply identical waveforms. *AI* distributions were fitted with Gaussian functions in IgorPro (Wavemetrics) with a bin size of 0.05.

While the absolute phases depend on the origin of the time window, the 'relative phases' calculated as

$$\phi_n / n - \phi_m / m \tag{8}$$

(with ϕ_n and ϕ_m the absolute phases of the frequency components f_n and f_m respectively, and $m = n + 1$) do not, and thus can be used to characterize the waveforms (Fig. 15 C). Since the amplitudes of the frequency components mostly captured the directional differences very well, the phases were used seldom to characterize the response traces.

All averages are given as mean ± standard error of the mean (SEM), with the SEM calculated as $\sigma / \sqrt{n}$, with σ the standard deviation and n the number of data points.

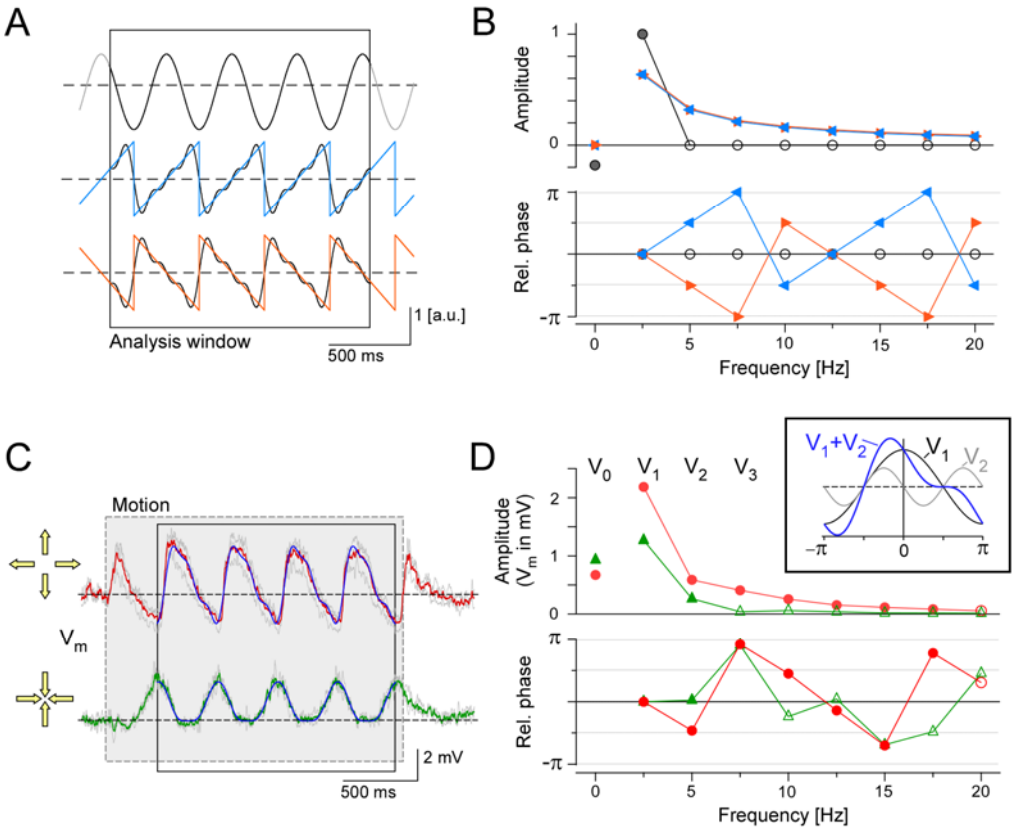

Fig. 15 Fourier decomposition for the quantification of electrical responses
A: Example periodical traces (simple sinewave in black and sawtooth in blue and orange) and their reconstructions from the first three FFT components (V_0 *and* V_1, V_2, V_3 and their phases) in black. The analysis window (*black frame*) includes an integer number of cycles. **B:** Amplitudes (*top*) and relative phases ($\phi_2 - 2\cdot\phi_1$, *bottom*) *vs.* frequency (f), from the FFT of the waveforms shown in A. Symbols (V_0 at f=0; V_1 at f_1; V_2,V_3 ... at $2\cdot f_1$, $3\cdot f_1$, ...) correspond to discrete frequencies from FFT; connecting lines are only a guide for the eye. The sawtooth waves contain higher harmonics whereas a sinewave consists only of the fundamental frequency. Phases are shifted by $\pi/2$ or $-\pi/2$ for the blue and orange sawtooth, respectively. **C:** Typical SAC somatic voltage response to expanding (*red*) and contracting motion (*green*) of a circular sinewave (as in Fig. 17); *gray*: individual trials, *red* and *green*: averages for n=3 trials; *blue*: reconstructed waveforms; *black frame*: analysis window. **D**: Amplitudes and phases from the FFT of the averaged responses in C. Note that the phases for the expanding motion decrease almost linearly except when wrapping around (at $-\pi$, π) – similar to the phases of the orange sawtooth in A. Reconstructions of the waveforms using $V_{0\text{-}3}$ and their phases are shown as blue traces in C. The inset illustrates that adding a double frequency component (V_2) shifted by $-\pi/2$ to a sinewave (V_1) yields a steeply-rising waveshape reminiscent of the response to expanding motion in C.

Statistical significance of differences was evaluated using the Whitney-Mann rank sum test (implemented in PAST, vs. 1.43; Hammer et al., 2001). The significance of the difference between a population and zero was tested with the Wilcoxon matched-pair signed-ranks test (Wilcoxon, 1945) implemented in Matlab (Mathworks, USA) with $p \leq 0.05$ considered as significant $(*)$ and $p \leq 0.01$ as highly significant $(**)$.

❋

Chapter III

Results

Electrical responses to light

Calcium responses to light

Variation of visual stimulus parameters

Pharmacology

Voltage clamp experiments

Voltage-induced changes in calcium

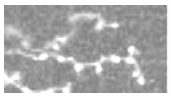

3.1 Electrical responses to light

In the hand of most groups starburst amacrine cells (SACs) do not generate action potentials (APs) that can be electrically measured at the soma – but respond to light with graded potentials (Taylor and Wässle, 1995; Peters and Masland, 1996, Euler et al., 2002; but see Bloomfield, 1992; Gavrikov et al., 2003). Unlike in spiking neurons, where the membrane voltage at the soma (or the initial segment of the axon) is directly translated into an AP firing rate, the membrane voltage at the soma of a SAC does not have direct functional relevance for the cell's output. It is the membrane potential at the distal dendrites that determines the SAC's output, as this is the site of neurotransmitter release (Famiglietti, 1983a; Famiglietti, 1991). Yet, the soma is the only place where SACs can be recorded electrically and even weak electrotonic coupling of the dendritic sectors to the soma (Velte and Miller, 1997) can provide information about electrical events in the dendrites – such as the signals underlying directional [Ca^{2+}] responses (Fig. 10 B).

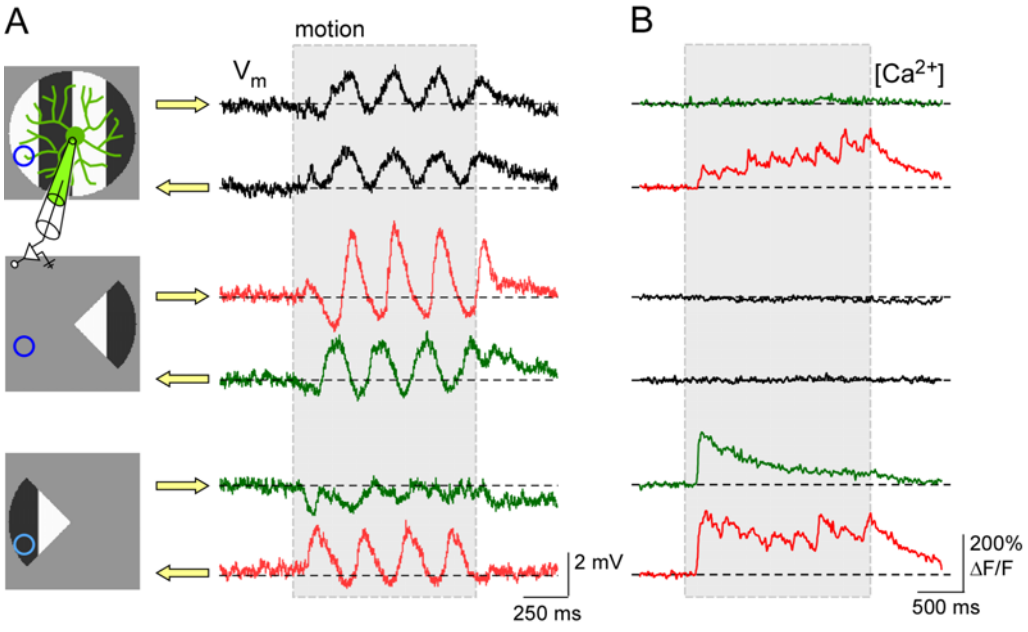

Fig. 16 **A.** Voltage responses from a SAC to black and white gratings moving in two different directions behind a circular mask or sector masks. Movement from the soma of the cell (schematically shown in green, *top panel*) towards the dendritic tips evokes larger responses (*red traces*) than movement in the opposite direction (*green traces*). **B.** [Ca^{2+}] responses to similar stimuli (but at a higher temporal frequency) from a different cell, optically recorded at the location indicated with the blue circles on the panels in A. The first pair of traces in A shows that a grating does not induce a DS response in the SAC soma. The response in the dendritic tip however (*first pair of traces in B*) is DS. This DS is only reflected in the somatic response when for example a similar grating is used that covers approximately a sector of the dendritic tree (*second and third pair of traces in A*).

When SACs are probed with full-field moving grating stimuli somatic voltage responses are not directional (Fig. 16 A upper traces; Euler et al., 2002), probably because signals from different branches arrive at the soma with different, even opposite, phases and cancel. Cancellation can be avoided by restricting stimulation to a part of the dendritic tree, by e.g. moving either a bar (Gavrikov et al., 2003) or a spot of light (Peters and Masland, 1996) to and fro only between the soma and the distal dendrites, or by masking a moving grating stimulus so that it only covers a part of the dendritic tree (Fig. 16 A, middle and lower traces). Other special stimuli can ensure that the DS signals from different branches are in phase and reinforce at the soma. This was achieved here by using sinusoidal circular wave stimuli moving outward and inward (Fig. 17, 14; for detailed description see 2.2.2), which caused, respectively, large or minimal [Ca^{2+}] responses in the dendrites (Fig. 17 A).

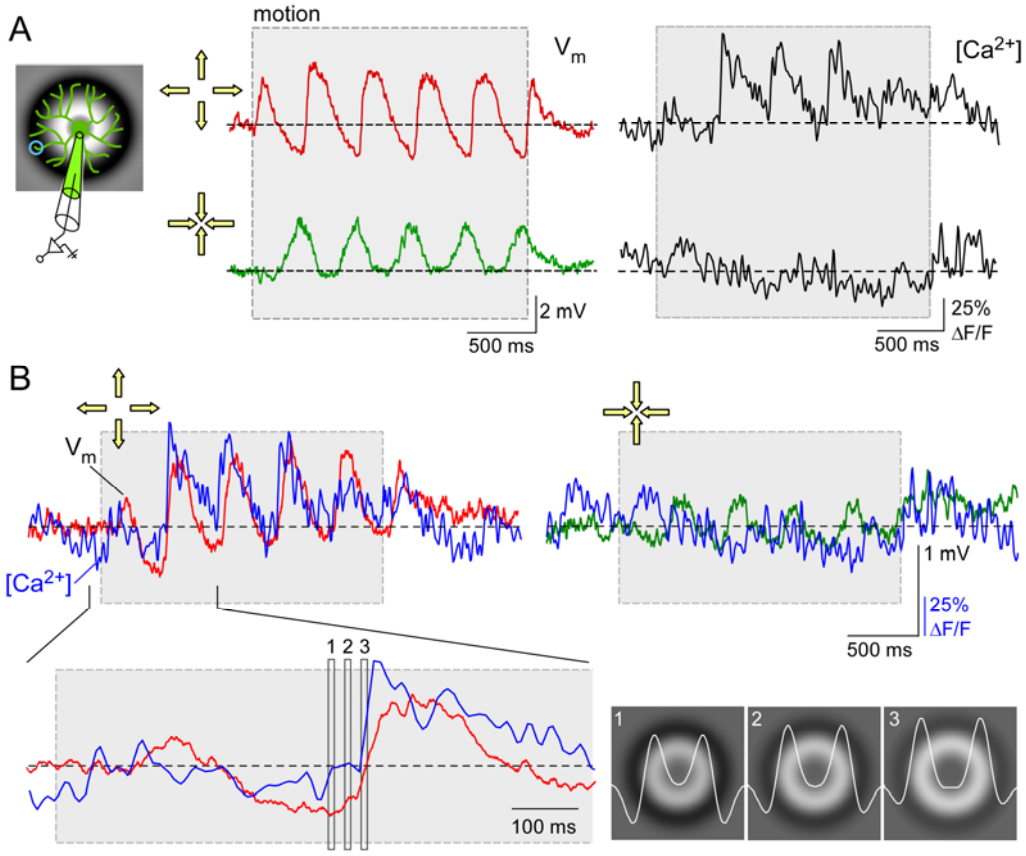

Fig. 17 **A.** Voltage (averages from 3 trials) and [Ca^{2+}] responses of a SAC to a circular wave (*top trace* outward, *bottom trace* inward motion). Outward motion evokes larger and 'steeper' responses (*red traces*) than inward motion (*green traces*) in V_m and [Ca^{2+}]. **B.** Overlay of a voltage response and [Ca^{2+}] response showing that the steep rise in [Ca^{2+}] and V_m occurs simultaneously and at the point where the bright 'edge' of the circular wave stimulus enters the outer half of the dendritic tree (*single trials, see magnified section of the traces*).

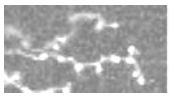

These circular wave stimuli were centered on the SAC soma and roughly covered its dendritic arbor and, thus its receptive field (Taylor and Wässle, 1995). All of the recorded cells were ON (displaced) starburst amacrine cells, which show a sustained depolarization with a transient component to bright stimuli in their receptive field and a smaller hyperpolarization when the surround is illuminated (Taylor and Wässle, 1995; Peters and Masland, 1996). In total, 121 cells were recorded using the whole-cell tight-seal patch clamp technique (Hamill et al., 1981). Only the cells with robust light responses (83 cells) were further analyzed. Immediately after gaining electrical access to a cell, the resting potential was measured. The averages were -62 ± 1 mV (n = 58; range: -26 to -82 mV) with the K^+-based intracellular solution and -48 ± 1 mV (n = 25; range: -35 to -58 mV) with the Cs^+-based solution; the latter was used for voltage-clamp recordings. The average input resistance was 164 ± 21 MΩ (n = 17; range: 83 to 478 MΩ). There was no discernable difference in the shape or size of the light-induced responses for the different fluorescent indicators and/or intracellular solutions.

When presenting a circular wave stimulus SACs usually showed a larger response for expanding then for contracting motion (Fig. 17). Further, the responses had a clearly non-sinusoidal wave shape, particularly there was a ‘sharp rise’ to expanding motion e.g. Fig. 17 A). This indicates the presence of higher harmonic frequencies in the responses – these are multiples of the stimulus frequency or ‘fundamental’[11]. A sensitive way to quantify harmonic frequencies in periodic responses such as those evoked by the circular wave stimuli, is spectral analysis using Fast Fourier Transform (FFT, see Fig. 15). As can be seen in the reconstructions of the responses from the first four FFT components (amplitudes and phases of V_0 to V_3; blue curves in Fig. 15 C) the response waveforms are often well approximated with only a few harmonic components.

A linear system, which can be described as the sum of its parts, never generates any 'new' frequencies. Thus, the presence of higher harmonics, for a single frequency (sinusoidal) input, is an unequivocal indicator of nonlinearity, and the amplitudes of the harmonics can be used to quantify the nonlinearity (Egelhaaf et al., 1989). Additionally, this kind of analysis obviates the need for a measurement of the absolute response amplitude, which is less reliable because of high-frequency noise (especially at the peaks of the traces, see e.g. Fig. 27 B) and/or slower fluctuations in membrane potential. Amplitudes can in principle be deduced from the reconstructed waveforms

[11] The circular wave stimulus is sinusoidal (see Fig. 17 B) and therefore contains a single frequency component.

(Fig. 15 C), but more information about a response is obtained when analyzing the FFT components separately. Thus, the overall response amplitudes were not used.
As already expected from the response waveforms, circular-wave stimuli generated responses with fundamental and higher harmonic components that were larger for expanding than for contracting stimuli (Figs. 15 D and 18 A); this was most evident for the harmonics (V_2 and V_3). The relative phases ($\phi_2 - 2\cdot\phi_1$) clustered near -π/2 for expanding motion (Fig. 18 B), indicating a steep rise in the response (see inset in Fig. 15 D), even for traces where this waveform cannot easily be seen. Responses to contracting motion typically contained much smaller harmonic amplitudes, indicating a more sinusoidal waveform. For contracting stimuli the broad distribution of $\phi_2 - 2\cdot\phi_1$ indicates a lack of correlation between fundamental and 2nd-harmonic phases (Fig. 18 B). In the histogram only cells with $V_2 \geq 0.3$ mV were included, as phase measurements become meaningless for amplitudes close to or below the noise level.

To compare different cells (also with respect to different stimulus parameters or pharmacology) a normalization in the form of directional-asymmetry indices AI_1, AI_2 and AI_3 (see eqn. 7) was used. In almost all cells, expanding motion evoked larger fundamental responses ($AI_1 > 0$ in 90 % of the cells) with higher harmonic content

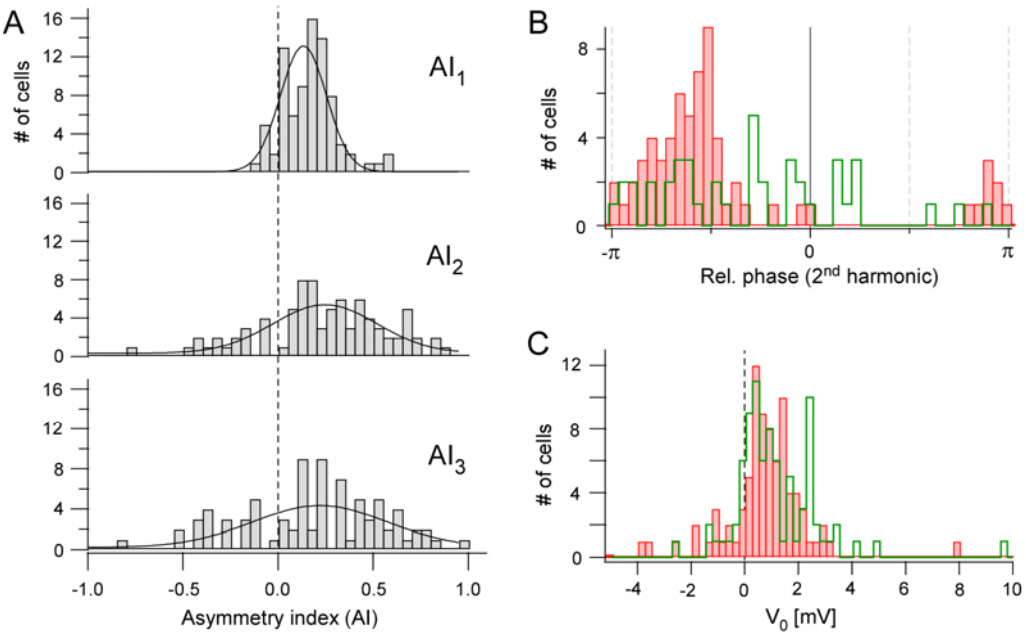

Fig. 18 **A.** Distributions of the asymmetry indexes AI_1, AI_2 and AI_3 (n=83 cells, all AIs are significantly different from zero with $p_{AI1, AI2, AI3} \leq 0.0001$) and gaussian fits; stimuli: 2.5 - 3 Hz; 46 - 73% contrast. **B.** Histogram of the relative phase shift ($\phi_2 - 2\cdot\phi_1$) between fundamental and second harmonic (*red:* outward, *green:* inward motion; n=41 cells; only responses with $V_2 \geq 0.3$ mV included) **C.** Distribution of V_0 (n=83, same cells as in A) for outward (*red*) and inward (*green*) motion.

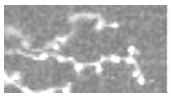

($AI_2 > 0$ in 80 %, $AI_3 > 0$ in 73 % of cells), as the distributions of AI_1, AI_2, and AI_3 show (Fig. 18 A). The peak positions of the Gaussian fits for the *AI* distributions are (n=83 cells): $AI_1 = 0.13 \pm 0.01$, $AI_2 = 0.25 \pm 0.04$, and $AI_3 = 0.22 \pm 0.07$. The *AIs* are significantly different from zero (AI_1: $p \leq 2.32 \cdot 10^{-13}$; AI_2: $p \leq 1.92 \cdot 10^{-7}$; AI_3: $p \leq 5.80 \cdot 10^{-5}$). The replacement of intracellular K^+ by Cs^+ had no significant influence on the AIs; with K^+: n=58, $AI_1 = 0.13 \pm 0.01$, $AI_2 = 0.27 \pm 0.03$, $AI_3 = 0.19 \pm 0.05$; with Cs^+: n=25, $AI_1 = 0.14 \pm 0.02$, $AI_2 = 0.17 \pm 0.07$, and $AI_3 = 0.28 \pm 0.01$ (from Gaussian fits). The difference in the average DC components (V_0) for out-going (0.7 ± 0.2 mV) and in-going (1.1 ± 0.2 mV) stimuli was small (~ 0.4 mV) but significant (n=83, $p \leq 2.74 \cdot 10^{-4}$; Fig. 18 C). For K^+ and Cs^+ the DC components were not significantly different and, thus, were pooled. For a complete summary of all the averages and p-values see Appendix A.

3.2 Calcium responses to light

Dendritic [Ca^{2+}] responses (Fig. 17) to visual stimuli were seen in only 9 out of 50 optically-recorded cells with the patch-electrode attached, while electrical responses to visual stimulation were present in all 50 cells. In half of the cells (8 of 16) that remained intact after the patch electrode had been retracted, light-evoked [Ca^{2+}] responses developed after about 15 minutes ('recovery', e.g. Fig. 19, see also 4.2.3). When present, dendritic [Ca^{2+}] responses were very similar to those observed in cells dye-loaded via high-resistance microelectrodes (Euler et al., 2002 and X. Castell, personal communication). The overall time course of the [Ca^{2+}] responses was analogous to that of the electrical measurements, however the amplitude differences between outward and inward motion were often more pronounced than for the somatic voltage responses, resulting in a large [Ca^{2+}] signal for outward and a much smaller (or even no discernable) [Ca^{2+}] signal for inward motion (Fig. 17). As in the previous recordings (Euler et al., 2002) the [Ca^{2+}] responses exhibited some variability in amplitude, temporal structure and strength of directionality (see e.g. Fig. 17 A; Fig. 19 D).

Often, there seemed to be a delay between the first upward voltage deflection and the [Ca^{2+}] responses to the same stimulus (see Fig. 17 A and Fig. 21 C for outward motion). This can however be explained by the time course of the circular wave stimuli: For most stimuli (e.g. Fig. 17 A) the first increase in V_m is elicited by only half

a period of the sinewave and is thus smaller (and not included in the FFT interval, see Fig. 15 C). Apparently a 'whole' period of the signal is required for a maximal voltage and [Ca^{2+}] response. In the nine cells in which simultaneous optical and electrical recordings succeeded, [Ca^{2+}] rose sharply, roughly simultaneously with the somatic voltage, as the bright phase of the circular wave entered the distal section (annulus) of the dendritic arbor (Fig. 17 B).

Also, which part of the SAC's dendritic tree the stimulus covered had an influence on the [Ca^{2+}] response: In Fig. 19 the [Ca^{2+}] responses of two different cells are shown, that were recorded after the patch electrodes had been removed and the cells had 'recovered'. In both cases the standard circular wave stimulus was presented, but covered by gray masks which left rings of different width and at different diameters uncovered. For the first cell the outer diameter of the motion-presenting ring decreased until only the proximal dendrites were stimulated. An additional stimulus covered only the distal half of the dendrites. For the latter configuration the largest difference between the [Ca^{2+}] response to outward and to inward motion was seen (Fig. 19 D), whereas the smaller stimuli induced smaller responses (Fig. 19 B and C). The finding is reminiscent of the voltage results to similar stimuli (Figs. 22 and 23 E). Unexpected was the small directional difference in [Ca^{2+}] response to the 'standard' configuration observed in this cell (Fig. 19 A). As mentioned, however, there is quite some variability between the [Ca^{2+}] responses of different cells and at different dendritic recording sites.

The rings in the second set of stimuli had the same narrow width (50 µm) but covered different 'eccentricities' of the SAC's dendritic field, from the proximal part of the dendritic field into the surround of the cell. Here, the largest differences in [Ca^{2+}] responses between outward and inward motion were induced by the first and the third configuration (Fig. 19 E and G). At first sight it might be surprising that [Ca^{2+}] responses were measured even when the moving stimulus did not reach the recording site (Fig. 19 E and G). It is important to note however, that the respective **sector** of the dendritic field was still stimulated and that although the different dendritic sectors of a SAC have been shown to act as largely 'independent' computational units (Euler et al., 2002), the processing **within** one sector is correlated. The difference in responses to the first three stimulus configurations (Fig. 19 E to G) probably reflects usual variability (X. Castell, personal communication), but [Ca^{2+}] responses in too few cells were recorded to systematically analyze this. The strong [Ca^{2+}] response to surround

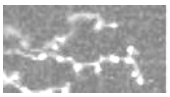

stimulation (Fig. 19 H) is noteworthy as it confirms an, in this case motion dependent, input from other cells (see also 4.1.1).

The variability seen in the [Ca^{2+}] responses is 'averaged' in the electrical responses, which can be interpreted as an integrated signal from all dendrites, and are thus a more reliable measure when probing the general mechanism underlying dendritic DS in SACs.

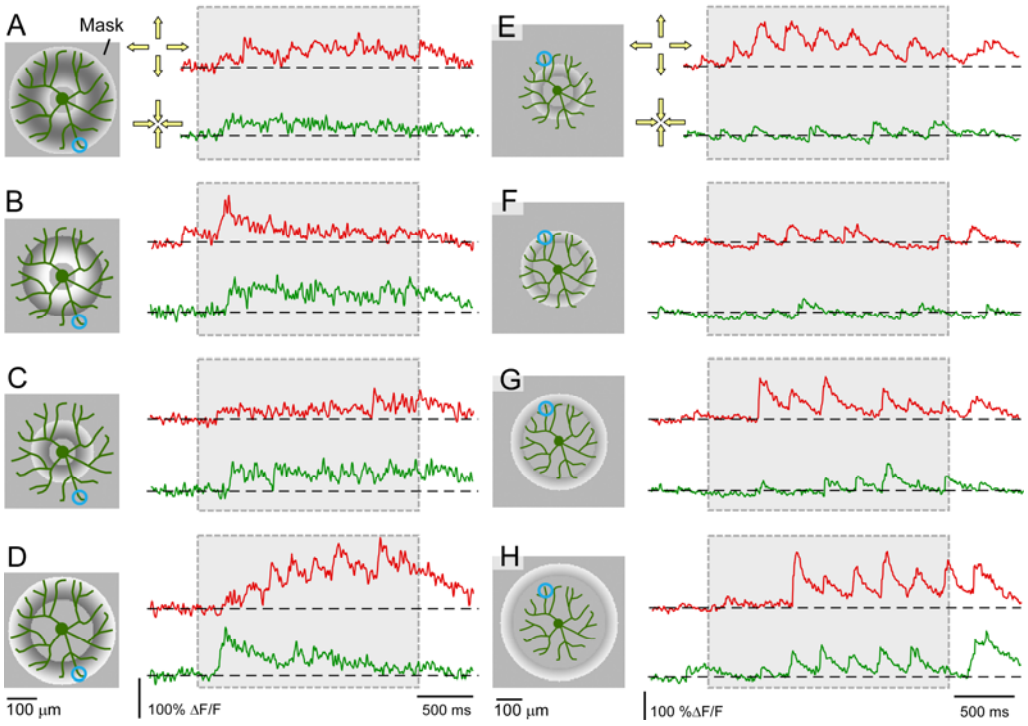

Fig. 19 [Ca^{2+}] responses from two cells (*recording locations indicated by blue circle*, outward motion: *red*, inward motion: *green*) to circular sine-wave stimuli (2.5 Hz) covered with masks of different diameters **A.-D.** One cell, diameter of masks: 360-90 µm, 270-90 µm, 210-90 µm, 360-210 µm, respectively. **E.-F.** Second cell, diameter of masks: 460-360 µm, 380-280 µm, 300-200 µm, 220-120 µm, respectively.

3.3 Variation of visual stimulus parameters

To further characterize dendritic DS in SACs and to determine the constraints for the underlying computation several parameters of the circular waves, such as contrast, velocity or dendritic coverage, were varied while the electrical responses were measured at the soma. The circular wave stimuli were presented at either 2.5 or 3 Hz, except when the temporal frequency (velocity) itself was the independent parameter.

3.3.1 Contrast

To determine if DS in SACs is limited to a certain range of contrasts circular wave stimuli with different light values were designed and the following contrasts (see eqn. 1) were presented to SACs: 72 %, 46 %, 29 %, 20 % and 10 % for 8 cells (Fig. 20 A-D), and 73 %, 57 %, 35 %, 23 % and 12 % for another 5 cells (Fig. 20 E, F). The second set of cells was recorded after the exchange of the LCoS display in the stimulator (see 2.2.2).

For the first group of cells the amplitude of the fundamental, V_1, increased almost linearly with contrast (Fig. 20 B), albeit with a smaller slope for inward than for outward motion. For outward motion the 2nd harmonic (V_2) increased roughly linearly with contrast, whereas for inward motion V_2 was indistinguishable from the (no-motion) background for all but the highest contrast (72 %, Fig. 20 B). This supports the notion that non-linearity is large for outward motion and usually as small as the noise for inward motion. The rise above noise level of V_2 for inward motion at the highest contrast could actually be due to saturation effects in the presynaptic pathway.

In the second group of cells V_1 also increased in an approximately linear manner, the slope being similar for inward and outward motion. Due to the small number of cells in this group, there is more variability in the components. Still, it is evident that V_2 for inward motion remains closer to background level even for the highest (73 %) contrast (Fig. 20 E). In both groups the DC component (V_0) increased slightly with contrast with no clear directional preference. The phase difference between fundamental and second harmonic ($\phi_2 - 2 \cdot \phi_1$) is only plotted for the first group of cells; for outward motion it becomes more tightly clustered (near $-\pi/2$) with increasing contrast, indicating a growing 'steepness' of the responses (Fig. 20 C). Except for AI_2 for 10 and 20 % contrast, all *AIs* in the first group of cells (Fig. 20 D) are significantly different from zero. Given the small number of cells in the second group, their *AIs* were not tested for significance (Fig. 20 F). Generally AI_2 was almost always larger than AI_1, indicating that the directional difference is most evident in the activation of non-linearities.

These results show that dendritic DS in SACs, reflected in the voltage response, is not limited to certain contrasts and that there is an especially large directional difference in the second harmonic. Further, high contrasts could induce saturation effects in the presynaptic circuitry. To limit such presynaptic influence on the non-linearity, high contrast stimuli were used as little as possible when other parameters were varied.

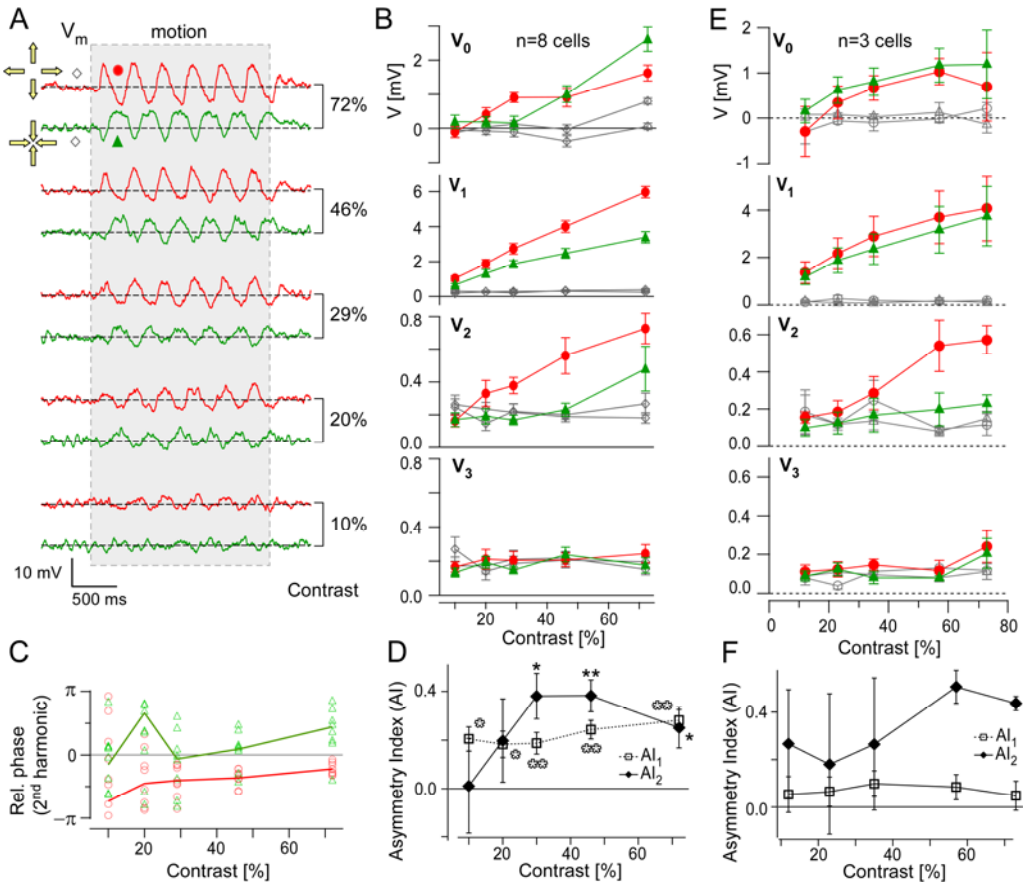

Fig. 20 **A.** Voltage responses evoked by circular wave stimuli (3 Hz, contrasts from 10 to 72%), traces are averages of 3 trials, (outward motion *red*, inward *green*). **B.** Amplitudes of DC (V_0), fundamental (V_1), and harmonics V_2 and V_3 as functions of stimulus contrast (average of 8 cells). No-motion data (*gray symbols*) included **C.** Relative phases of 2nd harmonic ($\phi_2 - 2 \cdot \phi_1$) as a function of the contrast (same cells as in B). **D.** Asymmetry indexes AI_1 (*open squares*) and AI_2 (*filled diamonds*) plotted as functions of contrast; asterisks indicate significance of difference from zero (*open symbols: AI_1; closed symbols: AI_2*; * $p < 0.05$; ** $p < 0.01$; cells from B). **E.** and **F.** Plots equivalent to B and D but with a second group of cells (n=5) and contrasts from 12 to 73%

3.3.2 Velocity

To test if the DS asymmetry in SACs changes with velocity the dependence of the amplitudes of the fundamental and the harmonics on the stimulus velocity was measured in 5 cells (Fig. 21). With a fourfold change in speed (from 0.5 to 2 mm/s or

2.5 to 10.5 Hz) V_0, V_1, and V_2 varied only slightly. Somewhat larger changes were seen for V_3, which fell by a factor of almost 3, possibly due to capacitive filtering at higher frequencies. For all velocities tested fundamental and harmonic amplitudes were always larger for outward than for inward motion.

A recording of $[Ca^{2+}]$ signals as a function of velocity (from a cell in patched state, Fig. 21 C) shows a strong outward-motion response for the two lower velocities, which is consistent with the directional preference of the electrical responses. The small $[Ca^{2+}]$ response to the highest velocity might be due to cellular variability. Unfortunately, because of the lack of stimulus-evoked $[Ca^{2+}]$ signals in most of the patch-clamped cells, this could not be confirmed in other cells.

In summary, for the range of velocities tested, SAC responses exhibited clear fundamental and second harmonic DS that did not change much for velocity.

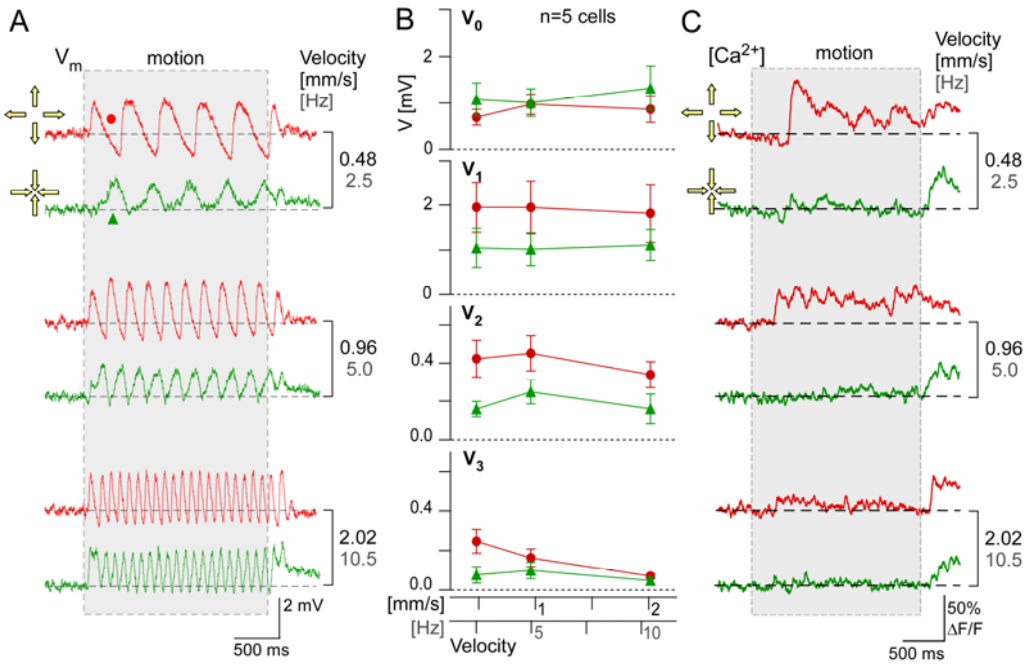

Fig. 21 **A.** Voltage responses evoked by circular wave stimuli with three different velocities, traces are averages of 3 trials, (outward motion *red*, inward *green*). **B.** Amplitudes of DC (V_0), fundamental (V_1), and harmonics V_2 and V_3 as functions of velocity (average of 5 cells). **C.** $[Ca^{2+}]$ responses from a different cell to the same stimulus, averages of 3 trials (outward motion: *red*, inward: *green*)

3.3.3 Dendritic coverage

The next step was to look for the radial location of the dendritic 'direction discriminator'. This was done by testing where along the length of the dendrite motion had to be presented to activate direction-selective nonlinearities. In a first group of cells the 'standard' circular wave stimulus was used, but covered with gray masks, so that rings of different width and dendritic 'eccentricity' remained uncovered. The outer and inner diameters were 360 - 90 µm, 270 - 90 µm, 210 - 90 µm and 360 - 210 µm (Fig. 22 A, B, C and D, respectively). In a second (smaller) group of cells the edges of the ring within which the motion was presented were smoothed (using Gaussians) to minimize possible non-linear 'edge' effects; here the diameters were approximately 350 - 110 µm, 195 - 60 µm, 350 - 200 µm and 545 - 380 µm (Fig.

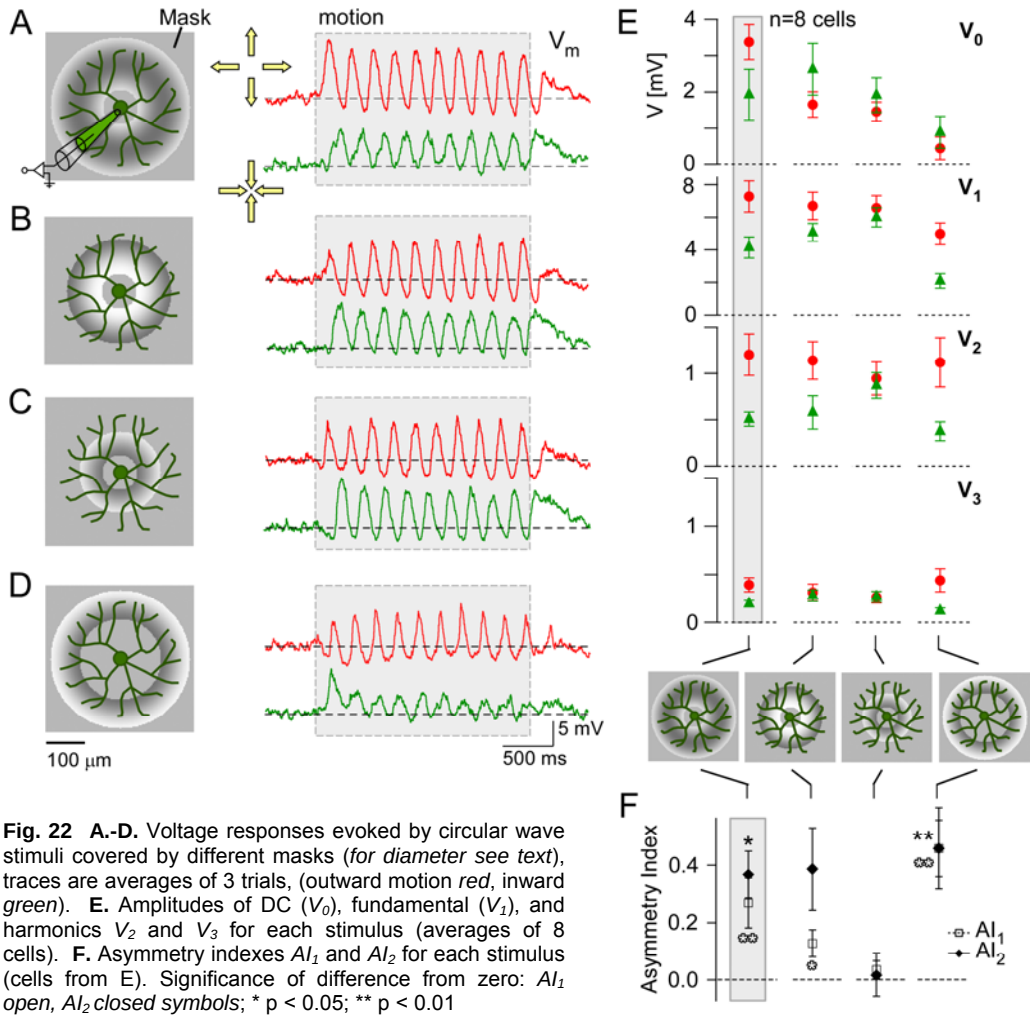

Fig. 22 **A.-D.** Voltage responses evoked by circular wave stimuli covered by different masks (*for diameter see text*), traces are averages of 3 trials, (outward motion *red*, inward *green*). **E.** Amplitudes of DC (V_0), fundamental (V_1), and harmonics V_2 and V_3 for each stimulus (averages of 8 cells). **F.** Asymmetry indexes AI_1 and AI_2 for each stimulus (cells from E). Significance of difference from zero: AI_1 *open*, AI_2 *closed symbols*; * $p < 0.05$; ** $p < 0.01$

23 A, B, C and D, respectively). Note that in the second set of stimuli the last configuration presented motion outside the SAC's dendritic field. To obtain comparable coverage of the receptive field of different SACs by the stimuli, only cells with very similar dendritic radii were chosen for further analysis (First group: 300 to 354 µm, second group: 310 to 335 µm).

Reducing the stimulus size (Figs. 22 B,C and 23 B) led to a reduction in directional sensitivity, mostly due to an increase in the amplitude for contracting motion. The responses to inward and outward stimuli became more similar for both fundamental (V_1) and harmonic responses (V_2, V_3). For the first group of cells AI_1 was reduced consecutively for the smaller stimuli, AI_2 fell to almost zero only for the smallest stimulus. In the second group of cells AI_1 and AI_2 were reduced to almost zero for the second stimulus configuration.

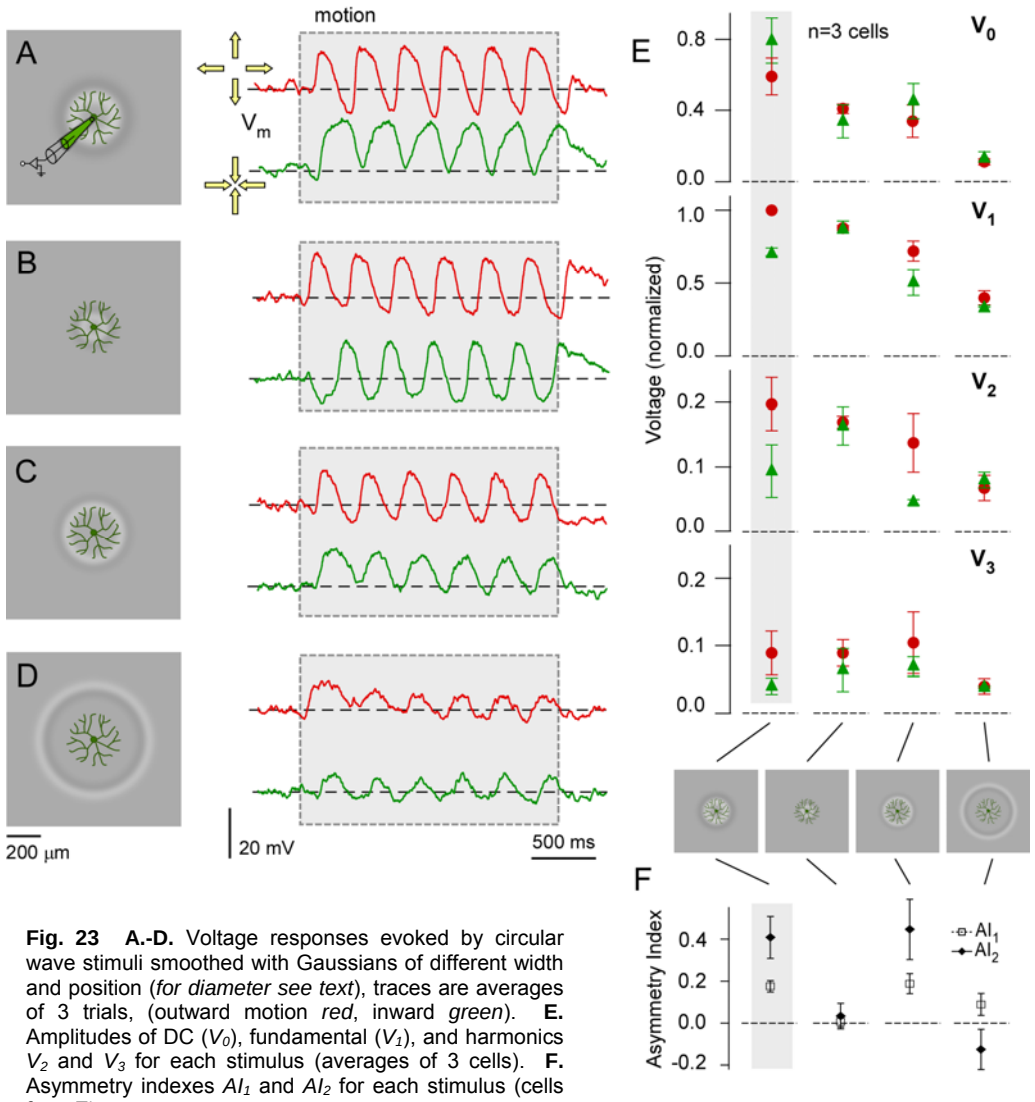

Fig. 23 **A.-D.** Voltage responses evoked by circular wave stimuli smoothed with Gaussians of different width and position (*for diameter see text*), traces are averages of 3 trials, (outward motion *red*, inward *green*). **E.** Amplitudes of DC (V_0), fundamental (V_1), and harmonics V_2 and V_3 for each stimulus (averages of 3 cells). **F.** Asymmetry indexes AI_1 and AI_2 for each stimulus (cells from E).

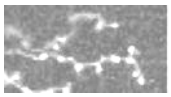

When the masked region in the center was enlarged, restricting motion to the outer dendrites (Figs. 22 D and 23 C), direction selectivity increased for V_1, V_2, and V_3. Comparing the *AIs* of the 'standard' stimulus response (Figs. 22, 23 A) with this configuration reveals an increase for AI_1 as well as AI_2 for both groups (for numbers see Appendix A). For the standard stimulus and the stimulation of the distal dendrites AI_1 and AI_2 were both significantly different from zero, whereas for the first smaller stimulus (Fig. 22 B) only AI_2 was significantly different from zero (test only for first group of cells, numbers: see Appendix A). The stimulus configuration in which motion was presented to the surround of the cells (used only in the second set of cells) evoked merely small non-directional responses (Fig. 23 D).
Taken together this suggests that the 'direction discriminator' is located in the distal section of the dendrite. This is consistent with the finding that voltage and $[Ca^{2+}]$ rise steeply at the time that the bright 'edge' of the stimulus enters the distal half of the dendritic tree (Fig. 17 B).

The DC component V_0 showed no clear directionality in any except the 'standard' stimulus configuration for the first subset of cells; V_0 varied slightly and was smallest when most of the center region was masked (Fig. 22 E). For the second subset of cells V_0 exhibited a small but 'inverse' direction-selectivity for the 'standard' and the 'outer dendrites' configuration (Fig. 23 E).

3.4 Pharmacology

3.4.1 GABA receptor antagonists

The restriction of visual motion to the dendritic field of the recorded SAC – as it was done for most of the stimuli used here – makes effects from the inhibitory surround unlikely. Nevertheless, the tight meshwork of SAC (Tauchi and Masland, 1985) and possibly other amacrine cell dendrites in the inner plexiform layer may result in the activation of inhibitory connections, even by a stimulus designed to cover only the dendritic field of the recorded SAC. Since it has also been shown that SACs do interact via GABAergic synaptic transmission (Zheng et al., 2004) and GABAergic inhibition has been proposed to be a crucial component in SAC DS (Borg-Graham and Grzywacz, 1992; Gavrikov et al., 2003; Münch and Werblin, 2006) the effect of

GABA receptor blockers on the somatic voltage responses and their DS was measured. $GABA_A$ receptors, which are necessary for directional selectivity in DSGCs (Kittila and Massey, 1995 and 1997), are located on both SACs (Greferath et al., 1993; Zhou and Fain, 1995) and DSGCs (Jeon et al., 2002). $GABA_C$ receptors – also ionotropic but with higher GABA affinity and different kinetics – are located on

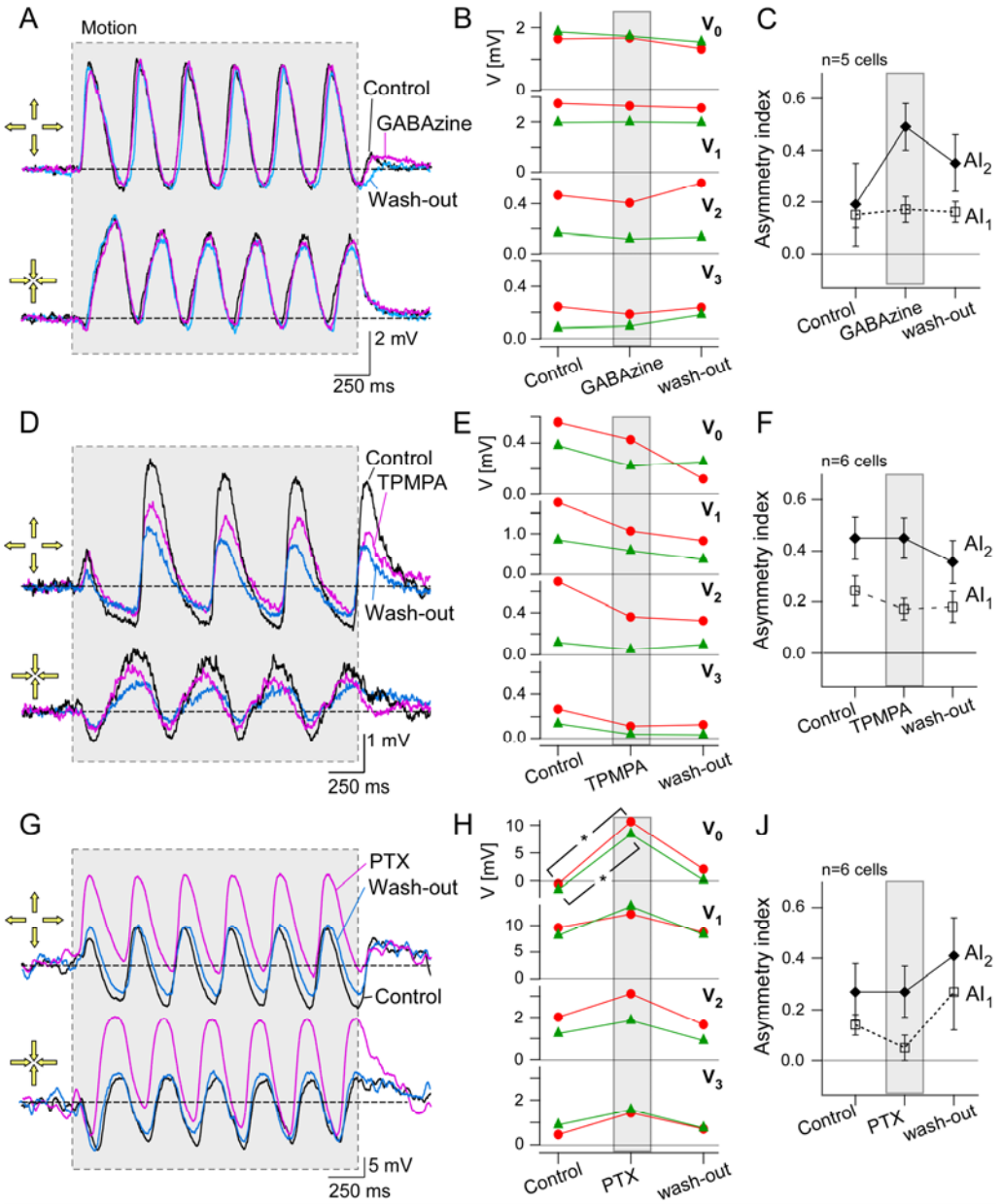

Fig. 24 Voltage responses to circular wave stimuli recorded before (control, *black*), during (*pink*) and after (wash-out, *blue*) bath application of different GABA-receptor antagonists. **A, D, G**. Overlay of traces (averages of 3 trials) to facilitate comparison. **B, E, H.** Amplitudes of DC (V_0), fundamental (V_1), and harmonics V_2 and V_3 for the examples depicted in A, D and G (outward motion *red circles*, inward *green triangles*; *gray box*: data recorded during drug application; asterisks indicate significance of difference from zero with $p < 0.05$). **C, F, J.** Asymmetry indexes AI_1 (*open squares*) and AI_2 (*filled diamonds*), averages of several cells (n in each panel). *Note: for TPMPA washout n=5*

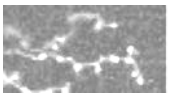

bipolar cells (Feigenspan et al, 1993; Enz et al., 1996) and could thus mediate indirect inhibition of starburst cells (Taylor and Wässle, 1995). $GABA_C$ receptors are probably not essential for DS in the ganglion cells (Massey et al., 1997) but have been suggested to affect DS in starburst amacrine cells (Gavrikov et al., 2003).

GABAzine, a specific $GABA_A$ antagonist, induced no reduction of V_1 or V_2 DS (Fig. 24 A-C), which is consistent with dendritic [Ca^{2+}] measurements (Euler et al., 2002). In fact, AI_2 increased, but not significantly, under GABAzine (for p-values see Appendix A). TPMPA, a specific $GABA_C$ antagonist, did also not change DS significantly in V_1 or V_2 (Fig. 24 D-F). To block all ionotropic GABA receptors simultaneously Picrotoxin (PTX), a widely used but nonspecific GABA-receptor antagonist, was applied. It had no significant effect on the DS of either V_0 , V_1, or V_2 (Fig. 24 G-J). It is surprising though that PTX led to a response enhancement in all components during stimulus motion, for stimuli both moving outward and inward, an effect which was not observed with GABAzine or TPMPA (Fig. 24 G, H). The increase in V_0 was the strongest (from ~ 1 to 5 mV, n=6 cells) and significant ($p_{out} \leq 0.06$, $p_{in} \leq 0.031$).

These results show that the DS of the responses does not require $GABA_{A/C}$ receptor-mediated transmission and also confirm previous findings that dendritic DS in starburst amacrine cells is not weakened by $GABA_A$ antagonists (Euler et al., 2002). Thus, an essential role for inhibitory input in the generation of direction-selective nonlinearities is ruled out. The most likely explanation for the non-linearities that remains is a dendrite-intrinsic mechanism, with voltage-gated channels as the foremost candidates.

3.4.2 Blockers of voltage-gated channels

The correlation between motion-induced [Ca^{2+}] transients and the activation of nonlinearities (Fig. 17 B) suggests a role for voltage-gated Ca^{2+} channels (VGCCs). High voltage activated Ca^{2+} channels of the P/Q and N-types, which can be specifically blocked by Cd^{2+} at low concentrations, have been found in SACs (Cohen, 2001). Consistent with this finding is that various Ca^{2+} channel blockers, among them low concentrations of Cd^{2+}, abolish directional selectivity in DSGCs while leaving their light-responsiveness largely intact (Jensen, 1995). The result for Cd^{2+} was

confirmed (T. Euler, unpublished data), albeit at concentrations of 20 µM rather than the 60-110 µM used by Jensen (1995).

Because the loss of DS in ganglion cells could result from blocking synaptic inputs to DSGCs from SACs or from suppressing DS generation in SAC dendrites the effect of Cd^{2+} on SAC responses was measured. Both AI_1 and AI_2 were reduced by 10 µM Cd^{2+}, but there was only a significant difference between the *AIs* for the washout condition

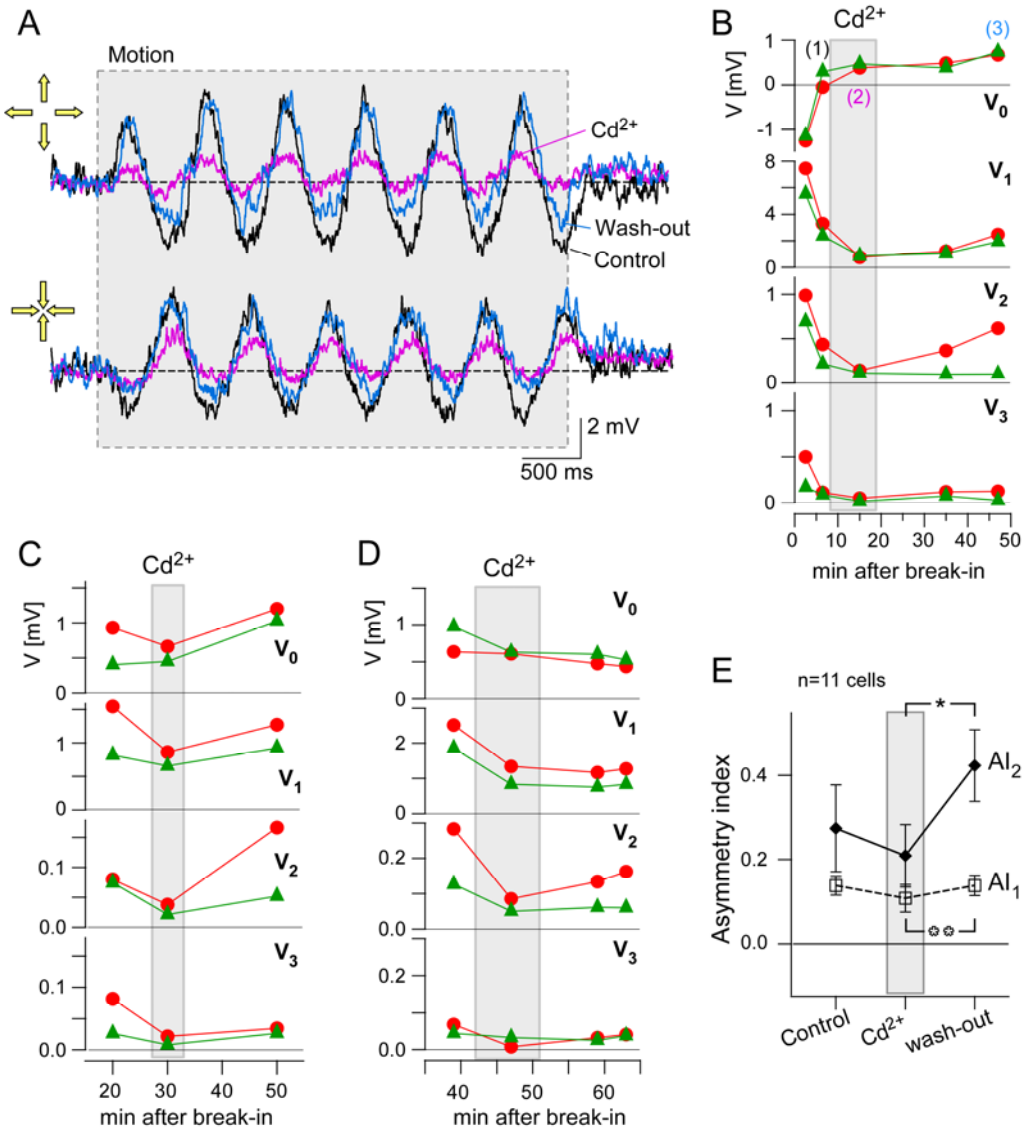

Fig. 25 **A.** Voltage responses to circular wave stimuli (3 Hz, 57% contrast) recorded before (control, *black*), during (*purple*) and after (wash-out, *blue*) bath application of 10 µm Cd^{2+}. Traces are overlaid to facilitate comparison. **B, C, D.** Amplitudes of DC (V_0), fundamental (V_1), and harmonics V_2 and V_3 plotted over time. (in minutes after break-in; outward motion: *red circles*, inward: *green triangles*) for three different cells to illustrate variability. B shows the data from the cell in A. **E.** Asymmetry indexes AI_1 (open squares) and AI_2 (filled diamonds); averages of 11 cells; the asterisks denotes significant differences between Cd^{2+} and washout for AI_1 ($p_{AI1} \leq 0.01$) and AI_2 ($p_{AI2} \leq 0.05$). *Note: washout n=10*

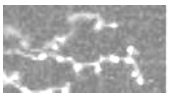

and for the application of Cd^{2+} (Fig. 25; numbers, see Appendix A). The effects of Cd^{2+} were quite variable (see examples, Fig. 25 B-D), probably because of the need to work in the narrow concentration range that leaves the synaptic input from bipolar cells intact, but does show effects on VGCCs in SACs. That higher concentrations of Cd^{2+} eliminated SAC light responses completely (90 µM, 6 cells, results not shown), presumably by blocking synaptic pathways, while lower concentrations had no effect (5 µM, n=1, results not shown) supports this interpretation.

Similar problems were encountered with a more selective blocker of VGCCs (for review see Terlau and Olivera, 2004). The P/Q- and N-type Ca^{2+} channel blocker omega-conotoxin M7C (ω-Ctx M7C), which also reduces the DS of DSGCs without decreasing their light responsiveness (Jensen, 1995), was tested on SACs at three different concentrations. At 200 nM the light response was abolished (data not shown). At 100 nM ω-Ctx M7C reduced V_1 and V_2 strongly for both motion directions (Fig. 26 A, B). A slightly lower concentration (~ 70 nM) of ω-Ctx M7C had a weaker – but again motion direction-independent – effect on the responses (Fig. 26 C, D). For this particular cell the response to a bright 100 ms-spot (~ 100 µm in diameter) was presented between motion trials to monitor the SAC's light response to static stimuli. The response to the spot, which should reflect the synaptic input without motion-induced response components, was reduced by ω-Ctx M7C to the same degree as the motion responses (Fig. 26 D, black circles). This indicates that the ω-Ctx M7C effect was rather due to suppression of bipolar cell input than to a block of directionally activated VGCCs on SAC dendrites. Lower concentrations of ω-Ctx M7C had no discernable effect on the responses, reminiscent of the narrow concentration window of the Cd^{2+} pharmacology.
Neomycin, an antibiotic that also blocks P/Q- and N-Type Ca^{2+} channels (Canzoniero et al., 1993; Keith et al., 1993) and abolishes DS in DSGCs (Jensen, 1996) killed SACs shortly after application and thus could not be used as a specific HVA Ca^{2+} channel blocker in this preparation.
In the light of these variable results this pharmacological approach for studying the role of VGCCs in the DS mechanism was not pursued further.

Voltage-gated Na^+ channels of the tetrodotoxin–resistant (TTXr) Na_V 1.8 type, which have been reported in SACs in the mouse retina (B. O'Brien, personal communication), could also participate in the generation of SAC non-linearity. Unfortunately it is quite difficult to find a specific blocker of these channels that does

not affect other channels (e.g. HVA Ca^{2+} channels) or receptors (H. Terlau, personal communication). One of the few drugs that blocks different types of Na^+ channels, including Na_V 1.8, is the lidocaine-derivative QX-314, which is usually applied intracellularly (Strichartz, 1973). The electrical responses in the cells where 5 mM QX-314 was used, remained completely unchanged over 15 min, although the same solution abolished spikes in ganglion cells within seconds (n=2, data not shown). This may indicate that either the drug does not affect this specific subtype of Na^+ channel at this concentration, or that Na_V 1.8 does not play a role in SAC DS.

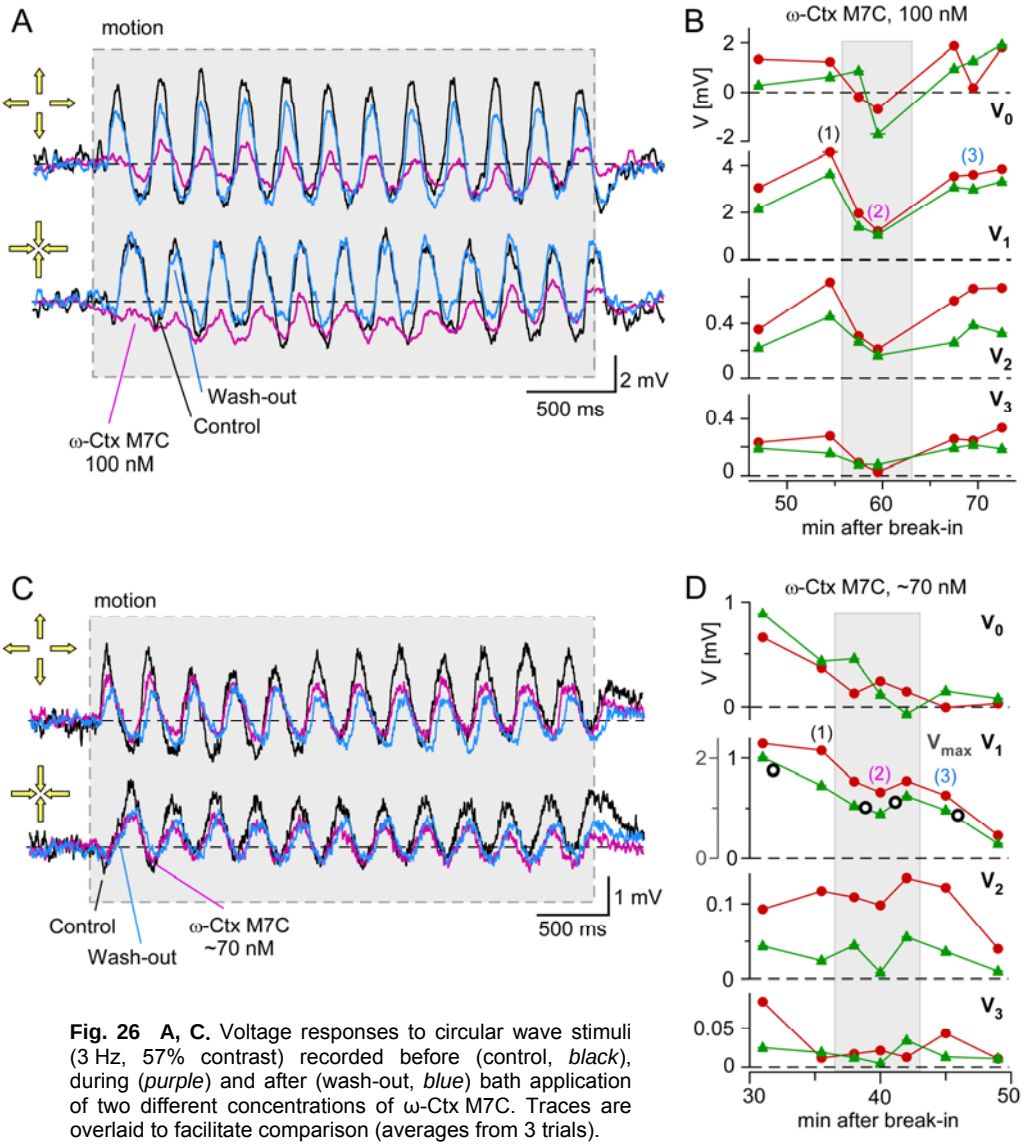

Fig. 26 A, C. Voltage responses to circular wave stimuli (3 Hz, 57% contrast) recorded before (control, *black*), during (*purple*) and after (wash-out, *blue*) bath application of two different concentrations of ω-Ctx M7C. Traces are overlaid to facilitate comparison (averages from 3 trials).

B, D. Amplitudes of DC (V_0), fundamental (V_1) and harmonics V_2 and V_3 plotted over time. (in minutes after break-in; outward motion: *red circles*, inward: *green triangles*). The gray box denotes application of the drug. A and B: application of 100 nM ω-Ctx M7C (n=1). C and D: application of ~ 70 nM ω-Ctx M7C (n=1). The black circles in the V_1 plot in D show voltage amplitudes (*gray ordinate*) to a 100 ms spot of light.

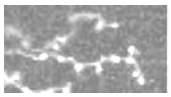

A second drug, Vinpocetine, which has effects on Ca^{2+}/calmodulin dependent cGMP-phosphodiesterase and glutamate receptors (Bönöczk et al., 2000) but has been shown to block Na_V 1.8 channels when applied extracellularly to cultured neurons (Zhou et al., 2003), had such devastating impact on the tissue health (n=3 retinas tested) that this line of experiments was not further pursued.

Taken together most of the pharmacological experiments targeting voltage-gated channels in SACs yielded no conclusive results for or against a certain type of channel. The Cd^{2+} experiments, however, might support an involvement of HVA Ca^{2+} channels in the generation of the SAC non-linearity.

3.5 Voltage clamp experiments

Recordings of SAC currents during somatic voltage steps provide direct information about voltage-gated channels (VGCs) without relying on pharmacology. VGCs have a limited and channel type-specific activation region (Fig. 29 C). Varying the somatic command voltage (V_{COM}) can thus help to establish whether VGCs are involved in DS and response nonlinearity and may help to identify the channel type involved. The current responses (I) evoked by outward and inward motion resembled the voltage responses measured in current-clamp in shape and directional asymmetry (Fig. 27 A, B). During visual stimulation the somatic potential was stepped from -75 mV to voltages between -105 (below which cells became leaky) and -35 mV (protocol, see Fig. 27 A). Both fundamental (I_1) and harmonics (I_2, I_3) were substantially voltage dependent (Fig. 27 C). The DC component I_0 was dominated by currents elicited by the voltage-step protocol and was not further analyzed.
The asymmetry indexes AI_1 and AI_2 behaved very differently as a function of step voltage (Fig. 27 C). The DS of I_1 (AI_1) declined somewhat towards hyperpolarized potentials and was especially small for the two lowest V_{COM}, i.e. negative to the zero-current potential (V_{Rest}). In contrast, AI_2 was largest around the resting potential and decreased slightly for the lowest potential. The 3rd harmonic (I_3), which was close to background (no-motion) levels around the resting potential, became quite substantially directional for stronger hyperpolarization, as can be seen from the difference in currents (Fig. 27 C).

Of all voltage dependencies analyzed, only that of I_1 for contracting motion (green traces in Figs. 27 C) resembled what would be expected from a passive dendrite, i.e. a linear I-V curve reversing at ~ 0 mV. In contrast, I_1 and I_3 for expanding motion and I_2 for both motion directions depended on the holding voltage in a non-linear manner, as would be expected for the activation of voltage-gated channels (VGC). The large amplitudes of AI_2, and I_2 and I_3 for outward motion, at the and negative to the zero-current potential suggest especially strong differential, i.e. directional activation of VGCs around V_{Rest} but also negative to the resting potential. As HVA Ca^{2+} channels

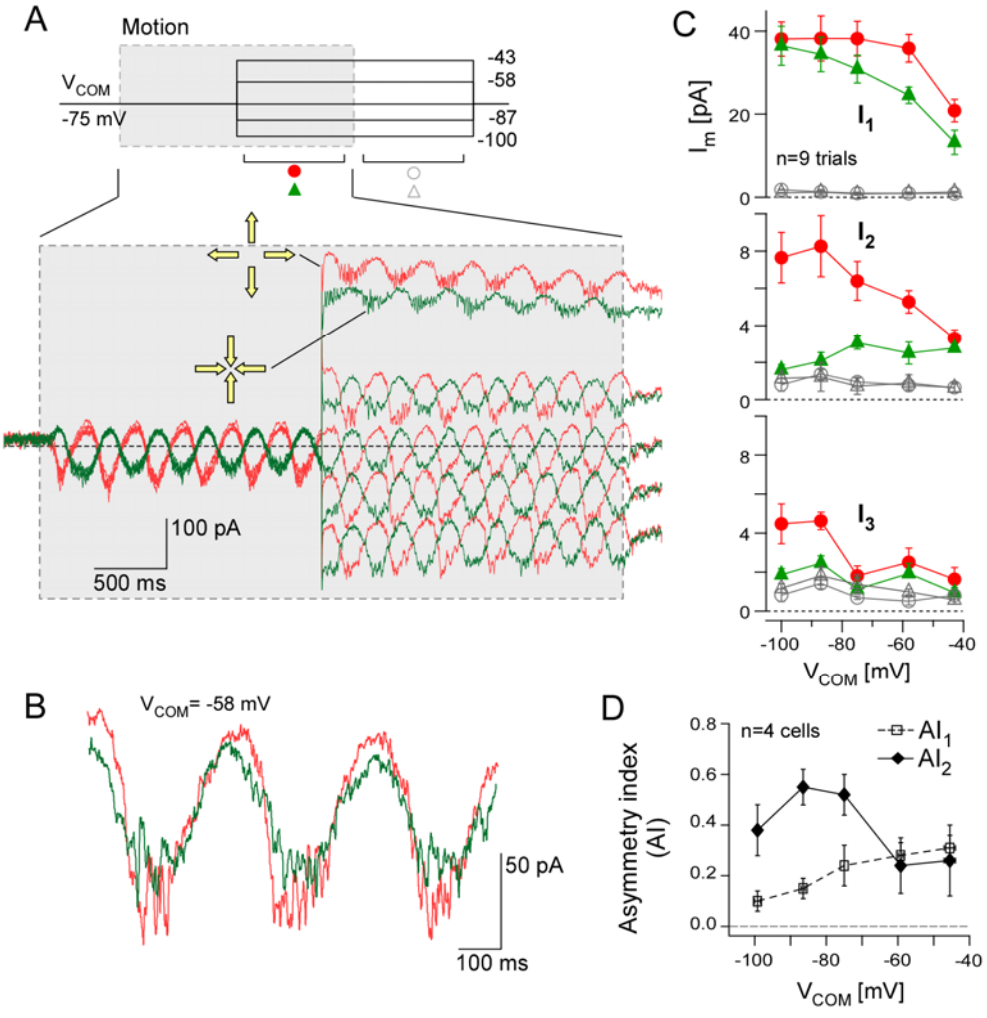

Fig. 27 **A**. Current responses evoked by circular sine-wave stimuli (3 Hz; 46% contrast) in the voltage-clamp mode while the command potential (V_{COM}) was stepped from -75 mV to the potentials indicated (averages of 3 trials; Cs^+-based intracellular solution). The stimulation sequence was repeated for different potentials after a 2 sec break. **B.** Traces for outward (*red*) and inward motion (*green*) from A magnified and aligned (shifted by $\pi/2$) to illustrate the differences in waveshapes. **C.** Amplitudes of the fundamental (I_1), and the 2nd and 3rd harmonics (I_2, I_3) as functions of V_{COM} (averages of 9 trials; same cell as in A, B). Motion (*red and green filled symbols*) and no-motion data (*gray open symbols*), both during the voltage steps are plotted. **D.** Asymmetry indexes AI_1 (*open squares*) and AI_2 (*filled diamonds*) as a function of V_{COM}.

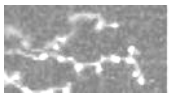

are activated above -40 mV rather than below -70 mV, this seems to suggest an involvement of low voltage-activated (LVA) Ca^{2+} channels, which is surprising in the light of the pharmacological results obtained by Cohen (2001) and Jensen (1995). Cohen used blockers for LVA Ca^{2+} channels and found little effect on SAC Ca^{2+} currents (see 4.2.1).

Another possibility which could reconcile the voltage-clamp data with HVA Ca^{2+} channels is a difference in membrane voltage between the dendritic tips and the soma. If the dendritic tips were more depolarized than the soma, it would seem as if VGCs in the dendrites were activated at more hyperpolarized (somatic) voltages than their activation parameters suggest (for details see 4.2.2). Such a voltage difference is plausible, particularly along the thin proximal dendritic segments of SACs (Famiglietti, 1983b).[12]

3.6 Voltage-induced changes in calcium

More details about the activation range and properties of the dendritic voltage gated Ca^{2+} channels (VGCCs) can be derived from $[Ca^{2+}]$ imaging. To test whether the VGCCs in SAC dendrites (Cohen, 2001) are active when the somatic voltage is near the resting potential, changes in dendritic $[Ca^{2+}]$ during somatic voltage steps were measured (Fig. 28). Substantial voltage-evoked $[Ca^{2+}]$ responses were observed in 20 out of 27 cells. Seven of these cells displayed large "spiky" $[Ca^{2+}]$ "transients" riding on top of the responses (Fig. 28 C), which might reflect events due to Ca^{2+}-induced Ca^{2+} release (see 4.2.3). Light-induced $[Ca^{2+}]$ responses, for which 12 of the 20 cells were tested, were found more often in SACs with spiky transients (3 of 5) than in cells without (1 of 7).

An activation curve (Fig. 29 A) was constructed using only SACs without spiky transients (compare Fig. 28 B) and fitted with eqn. 6 with the half-activation voltage $V_{50} = -48.5 \pm 2.0$ mV and the slope voltage $V_{Slope} = 8.7 \pm 2.0$ mV (n=6 cells; other fit parameters: $A_{Ca,0} = -0.17 \pm 0.08$; $g = -0.016 \pm 0.002$). V_{50} is much lower and V_{Slope} is much larger than the nominal values for VGCCs prominent in SACs ($V_{50} \sim -20$ mV, $V_{Slope} \approx 2.6$ mV, estimated from fitting the data shown in Fig. 4C of Cohen, 2001).

[12] Attenuation of voltages and currents along the SAC dendrites (the space-clamp issue, see 1.3.2) also have to be taken into account. Details will be discussed thoroughly in paragraph 4.2.2.

Similar to the voltage-clamp experiments this seems to suggest a LVA type of Ca^{2+} channel in the distal dendrites. As mentioned above (3.4) pharmacological experiments do not support this. A comparatively depolarized potential at the dendritic tips with respect to the soma however (see 3.4), would yield an activation of HVA

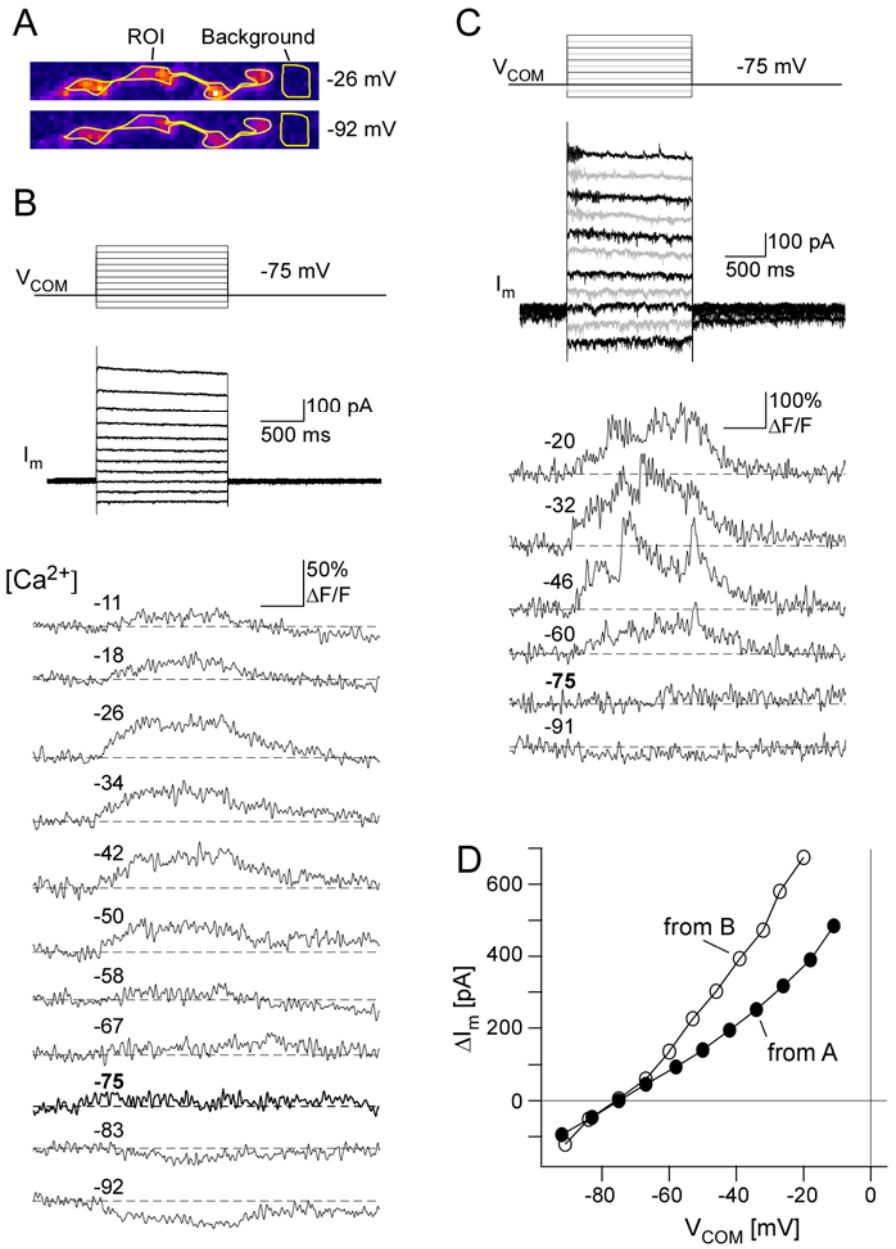

Fig. 28 **A.** Dendritic section from which $[Ca^{2+}]$ responses for B were recorded (*ROI: region of interest*). Averages of 10 frames (160 ms) during two different voltage steps (*step voltage next to images*). **B.** Changes in somatic current (I_m) and dendritic $[Ca^{2+}]$ signals to voltage steps from the dendritic ROI shown in A (single trial data, voltage steps from V_{COM} = -75 mV; $[Ca^{2+}]$ indicator: 100 μM Oregon Green 488 BAPTA-1; Cs^+-based intracellular solution). **C.** Example of spiky $[Ca^{2+}]$ transients riding on responses in a different cell (same protocol as in B). **D.** Somatic current as a function of the step potential (*filled circles*: cell from B, *I(-75 mV)* = -64 pA; *open circles*: cell from C, *I(-75 mV)* = -86 pA).

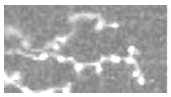

Ca^{2+} channels in the distal dendrites despite the lower potential at the soma (for details see 4.2.2). Such a voltage difference requires a steady inward current near the dendritic tips and an outward current at or near the soma. K^+ channels that are open at the resting potential, and which are not always completely blocked by intracellular Cs^+ used in voltage-clamp experiments (Hille, 2001), could be responsible for such an outward current (Fig. 31). The inward dendritic current would need to flow through channels with a more positive reversal potential, such as glutamate-gated channels, which are known to be tonically activated on SACs (Taylor and Wässle, 1995). Thus, blocking such channels should result in a shift of the Ca^{2+} activation curve closer to what would be expected from HVA Ca^{2+} channels, i.e. towards more depolarized potentials. When applying the AMPA-type glutamate receptor blocker CNQX a reduction in holding current (from -96 ± 2 pA to -76 ± 9 pA; n=5; V_{COM} = -75 mV) was measured, confirming the tonic activation of glutamate receptors in SACs. In addition, CNQX application induced a reversible shift of the [Ca^{2+}] *vs.* V_{COM} curve towards depolarized potentials by 15 mV (Fig. 29 B; n=3 cells; fit parameters: V_{50} = -34 ± 3 mV; $A_{Ca/0}$ = -0.09 ± 0.06; g = -0.019 ± 0.003; V_{Slope} = 10.2 ± 2.2 mV, see eqn. 6).

Thus, a voltage difference between soma and dendritic tips may in fact be responsible for the discrepancy between the activation curves derived from [Ca^{2+}] imaging and the expected activation curves of the Ca^{2+} channels found in SACs (29 C).

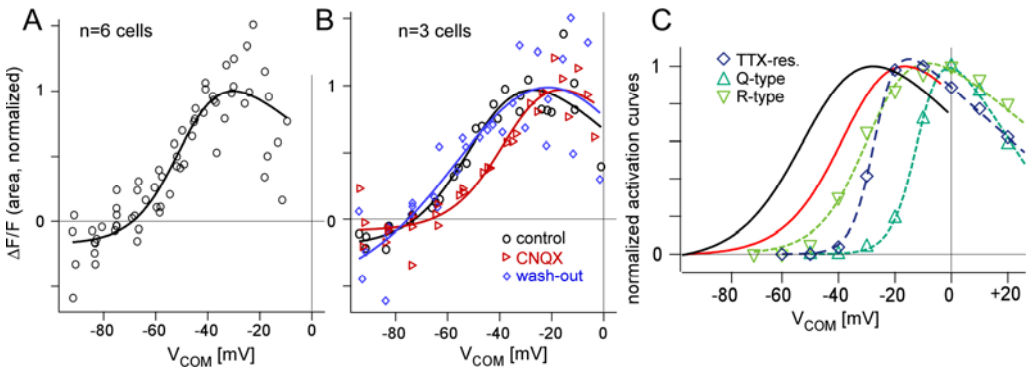

Fig. 29 **A**. [Ca^{2+}] responses (*circles,* for calculation see eqn. 5) as a function of V_{COM} for cells lacking spiky transients; each symbol represents a single response. For each cell the amplitudes were normalized to the response amplitude at -35 mV (see 2.4.1) and fitted (*continuous line*) with an activation curve using eqn. 6. **B.** [Ca^{2+}] vs. V_{COM} before (control, *black circles*), during (*red triangles*) and after (wash-out, *blue diamonds*) bath application of 10 μM CNQX. **C.** Curve fits from A and B (CNQX) overlaid with fits (using eqn. 6) to data from the literature for P/Q-type (*dark green triangles*, from Mori et al., 2000) and R-type (*light green upside down triangles*; from Zhang et al., 1993) Ca^{2+} channels, as well as for TTX-resistant Na^+ channels (*blue diamonds*; from Roy and Narahashi, 1992).

3.6.1 Local dendritic calcium responses

Another way to estimate the voltage-difference between proximal and distal dendrites is the simultaneous recording of $[Ca^{2+}]$ responses to voltage steps along the length of the dendrite (Watanabe et al., 1998). Local Ca^{2+} signals should reflect local Ca^{2+} influx, as long as in these experiments, regarding the short imaging times, little diffusion should take place (Meyer and Stryer, 1991). If there is a more depolarized membrane voltage in the dendritic tips than in the soma, more proximal sites should feature $[Ca^{2+}]$ vs. V_{COM} curves shifted to more hyperpolarized potentials than distal sites. Moreover, the 'steepness' of a voltage-gradient or the 'location' of a voltage-drop could thus be studied. Due to technical constraints it was not possible to image a whole dendrite of ~ 150 µm length. Preliminary data of a 80 µm segment (128x32 pixels, 4 ms per line) from one cell appear to confirm that the 'position' of the $[Ca^{2+}]$ activation curve along the 'voltage'-axis (Fig. 30 A, blue and green curves) indeed depends on the radial dendritic location of the $[Ca^{2+}]$ measurement.

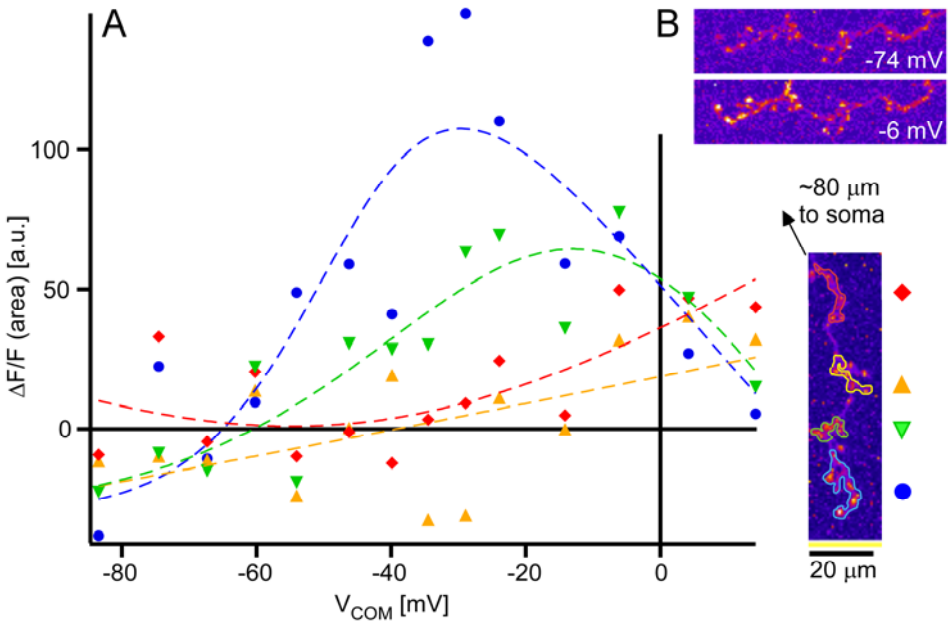

Fig. 30 **A.** $[Ca^{2+}]$ responses recorded at different regions of interest (ROIs) along a dendritic segment of ~ 80 µm length and ~ 80 µm from the soma (*see lower panel*) evoked by voltage-steps (protocol as in Fig. 28) are plotted as a function of V_{COM}. Recordings are fitted with activation curves (using eqn. 6). The $[Ca^{2+}]$ responses are largest at the dendritic tip (*blue circles*) and decrease for ROIs closer to the soma (*green and yellow triangles and red diamonds, respectively*). **B.** Averages from 10 frames (1.28 s) during the voltage-steps to -74 and -6 mV.

Chapter IV

Discussion

Network interactions

Starburst cell intrinsic mechanisms

Models

Outlook

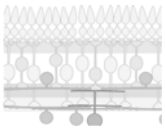

4 Discussion

> The important thing is not to stop questioning. Curiosity has its own reason for existing. One cannot help but be in awe when he contemplates the mysteries of eternity, of life, of the marvelous structure of reality. It is enough if one tries merely to comprehend a little of this mystery every day.
>
> **Albert Einstein**

Ever since starburst amacrine cells (SACs) were first suggested to participate in the direction selective (DS) circuit in the retina (Famiglietti, 1983a; Masland et al., 1984a), ideas about their role in the computation have been diverse (reviewed in Vaney et al., 2001). Only recently studies have shown that the ablation of large numbers of SACs abolishes DS, but not light-responsiveness, in direction selective ganglion cells (DSGCs), indicating that SACs are required for the computation of motion direction in the retina (Yoshida et al., 2001; Amthor et al., 2002). Additionally, $[Ca^{2+}]$ signals in SAC dendrites, likely representing the cell's output signal (O'Malley and Masland, 1989; O'Malley et al., 1992; Zheng et al., 2004), are direction selective (Euler et al., 2002). It still remains controversial which of the different DS mechanisms (or possibly, combination of mechanisms) suggested, if any, underlies the computation of DS in the retina. If one accepts that SACs provide DS ganglion cells with directionally tuned input, one of the important questions is how this elementary asymmetry in SAC DS is generated: through inhibitory and excitatory network interactions or intrinsically within a SAC dendrite. An intrinsic mechanism relies on spatio-temporally structured inputs, but not on an external directionality – in other words, DS is computed by the cell itself. This study shows that at least inhibitory network interactions are not required for SAC dendritic DS and that an intrinsic mechanism, relying on voltage-gated channels within the SAC dendrites, is capable of generating a robust directional signal.

4.1 Network interactions

4.1.1 Inhibition

It has been repeatedly proposed that the computational mechanism leading to starburst amacrine cell DS requires lateral GABAergic inhibition (Masland et al., 1984a; Borg-Graham and Grzywacz, 1992; Gavrikov et al., 2003; Münch and Werblin, 2006), which seems plausible in the light of the following observations: First, blocking ionotropic GABAergic inhibition in the retina (Wyatt and Daw, 1976; Caldwell et al, 1978), or more specifically, $GABA_A$ receptors (Kittila and Massey, 1995 and 1997), abolishes DS responses in DSGCs but not their light-responsiveness *per se*. $GABA_A$ receptors are localized directly on DSGCs (Jeon et al., 2002), as well as on SACs (Greferath et al., 1993; Brandstätter et al., 1995; Zhou and Fain, 1995). Thus, the GABAergic inhibition necessary for retinal DS could act on DSGCs, but also on SACs, or both. Second, release of acetylcholine (ACh), is suppressed by GABA (Massey and Neal, 1979; Massey and Redburn, 1982, Massey et al., 1997). As SACs form the major population of cholinergic neurons in the retina (Masland and Mills, 1979; see also 4.4.1) this indicates that ACh release from SACs is controlled by GABA[13]. Third, the synaptic contacts among SACs (Millar and Morgan, 1987, Mariani and Hersh, 1988; Famiglietti, 1991, but see Brandon, 1987) have recently been demonstrated as mainly GABAergic in the mature retina (Zheng et al., 2004). These findings suggest that GABAergic inputs could play a role in SAC DS.
Further, literally all computational models of DS designed through the decades are based on interactions between excitatory and inhibitory inputs (Hassenstein and Reichardt, 1956; Barlow and Levick, 1965; Torre and Poggio, 1978; Koch et al., 1983; Borg-Graham and Grzywacz, 1992). Thus, it seems an obvious consequence that more recent models dealing with the DS of SAC dendrites also suggest GABAergic mechanisms (Gavrikov et al., 2003; Münch and Werblin, 2006).

In the light of the studies supporting GABAergic input to SACs it had been surprising that the DS of dendritic $[Ca^{2+}]$ signals was not abolished by blocking $GABA_A$ receptor mediated inhibition (Euler et al., 2002). Here this finding was extended to the DS of SAC electrical responses. The application of the GABA receptor blockers GABAzine,

[13] Partially the GABAergic effect on ACh release is mediated via GABA-receptors on bipolar cells (Linn and Massey, 1992).

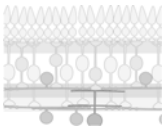

TPMPA and PTX showed that SAC DS does not require ionotropic GABAergic inhibition (Fig. 24).

As SACs have inhibitory surrounds (Bloomfield, 1992; Taylor and Wässle, 1995, Peters and Masland, 1996), and recent double patch-clamp recordings have verified direct $GABA_A$ receptor-mediated inhibitory contacts between SACs in adult rabbit retina (Zheng et al., 2004), it seems intriguing that GABAzine, a highly selective $GABA_A$ receptor blocker, did not change SAC voltage responses to circular wave stimuli at all (Fig. 24 A). However, one has to keep in mind the types of visual stimuli used here: Most stimuli were restricted to the dendritic field of the recorded SAC and did not extend into the surround. Thus, the lack of GABAzine effects might simply be due to the fact that neighboring SACs (and other amacrine cells) were poorly stimulated. The voltage recordings from the cells stimulated with a 'surround' ring (Fig. 23 D-F) show small but consistent responses to motion, which supports this view.[14] Remarkably, the responses evoked by this stimulus are not DS. In favor of an inhibitory, non-directional surround input is the finding that the $GABA_{A/C}$ receptor blocker PTX uniformly enhances voltage responses to motion in both directions (Fig. 24 G, H). Higher contrast stimuli elicit a motion-induced DC depolarization, which is also non-directional (cf. V_0 in Fig. 20 B and E). This depolarization may be counter-balanced by motion-induced surround inhibition, thus preventing non-directional activation of voltage-gated Ca^{2+} channels (VGCCs) and neurotransmitter release.
It is quite possible that for stimulus configurations other than those tested here, e.g. for full-field moving gratings, one will find an effect of GABA receptor blockers on the DS of SACs. For such stimuli lateral inhibition could relay directional information from adjacent SACs, thereby enhancing the directional tuning of the SACs' dendrites and contribute to the robustness of retinal DS. On the other hand, it has been shown that DS in ON/OFF DSGCs is suppressed when the surround moves in synchrony with the center stimulus (Chiao and Masland, 2003). A speculative but alluring notion is that this effect could already be coded at the SAC level by directional inhibition between neighboring SACs.

In the light of the results obtained with GABAzine and TPMPA, which are known to efficiently block ionotropic GABA receptors, it is surprising that PTX showed an effect on the voltage responses (Fig. 24 G-J). One possible explanation is that $GABA_A$

[14] The quite large $[Ca^{2+}]$ response to the narrow surround ring in Fig. 19 H may reflect input from the SAC surround. Since, however, this result was obtain so far for only one cell it remains to be seen in future experiments how consistent this finding is.

receptors on SACs may have a reduced sensitivity to GABAzine because of their unique subunit composition (Brandstätter et al., 1995). They contain the δ subunit, which is known to extensively modify $GABA_A$ receptor properties (Saxena and MacDonald, 1994). Another possibility is that at the concentration needed to completely abolish GABA-induced currents in SACs (~ 300 µM, see Fig. 4D, E in Zhou and Fain, 1995) PTX could also affect glycine receptors (Wang and Slaughter, 2005), which are also present on SACs (Zhou and Fain, 1995). Glycine does not seem to play an essential role in the generation of retinal DS (Caldwell and Daw, 1978; Daw and Ariel, 1981) and block of glycine receptors does not strongly alter reciprocal GABAergic inhibition between SACs (Zheng et al., 2004). Nevertheless, a glycinergic 'control' inhibition from other amacrine cells is conceivable.

Ultimately, the inhibitory interactions among SACs could enhance and/or sharpen SAC DS (Münch and Werblin, 2006) and may well play an important role for the robustness of DS at the ganglion cell level. Also, it cannot be excluded that there are parallel DS mechanisms that rely on lateral inhibition. Nonetheless, the results presented here demonstrate that an inhibitory network is not a requirement for SAC dendritic DS.

4.1.2 Excitation

Another possible explanation for SAC DS is that these cells receive directionally-tuned excitatory input, e.g. from bipolar cells. The excitatory input SACs receive manifests itself in a non-rectifying light-evoked synaptic current (Taylor and Wässle, 1995), which should increase with hyperpolarization due to a stronger driving force. If this excitatory input were already directionally tuned, clamping a SAC to more hyperpolarized potentials should thus preserve or even increase the DS of the fundamental current response (I_1). Instead, I_1 becomes less DS at strongly hyperpolarized potentials (Fig. 27 D), which is inconsistent with excitation being directional.

As inhibitory input is not essential for SAC DS and excitatory input to SACs seems not to be DS it is most likely that an intrinsic dendritic computation in SACs forms the basis of their directional selectivity.

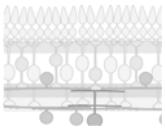

4.2 Starburst cell intrinsic mechanisms

The striking morphology of the starburst amacrine cell (Hughes and Vaney, 1980; Famiglietti, 1983b) with its resemblance of a starburst firework display has always fascinated researchers. The dendritic overlap of SACs is extremely high (30-70 fold, Tauchi and Masland, 1984; Vaney et al., 1981b; Famiglietti, 1983b) and the resulting dendritic plexus has early been proposed as an important functional feature of SACs, as for instance the spatial resolution in such a fine meshwork would be extremely great (Masland et al., 1984a).

Several models address the electrotonic properties of the SAC morphology (Miller and Bloomfield, 1983; Poznanski, 1992; Borg-Graham and Grzywacz, 1992; Velte and Miller, 1997; Tukker et al., 2004) and many ideas have been developed regarding the intriguing distribution of input and output synapses along the SAC dendrite (e.g. Vaney, 1990). That the morphology of SACs alone, in terms of its electrotonic properties and its distribution of inputs over the dendritic tree, can generate a directional voltage response in the distal dendrites (Borg-Graham and Grzywacz, 1992; Poznanski, 1992) was recently confirmed by Tukker et al. (2004) in a very comprehensive and sophisticated biophysical model. Other recent studies have developed ideas for DS mechanisms based on intrinsic SAC properties such as a Cl^- gradient (Gavrikov et al., 2003; see 4.3) or intracellular Ca^{2+}-signalling (Barlow, 1996).

4.2.1 Voltage gated channels and direction selectivity

> […] the rules that underlie the expression of ion channels and their characteristic somatodendritic distributions are key to understanding how the functional phenotypes of neurons arise and are related to each other.
>
> **Migliore and Shepherd, 2005**

Although voltage-gated channels (VGCs) have often been mentioned as possible candidates for the non-linearity necessary for the DS computation, they have rarely served those models other than as thresholding elements that convert the voltage signal into synaptic release (e.g. Tukker et al., 2004; for details see 4.3). One has to

keep in mind, however, that SAC are widely considered to be non-spiking[15] (Taylor and Wässle, 1995; Peters and Masland, 1996; Euler, 2002; Zheng et al., 2004, but see Bloomfield, 1992; Gavrikov et al., 2003) and that the number of studies on dendritic and Ca^{2+} spikes in computational neuroscience has only recently started to flourish (for review see e.g. Migliore and Shepherd, 2005). On the other hand, VGCs in retinal interneurons have been assigned various roles, e.g. supporting spikes as a means of signal propagation in axon-bearing amacrine cells (Taylor, 1996), but also participating directly in signal processing: In the A2 amacrine cells Na^{+}-spikes have been shown to act as 'local signal boosters' that accelerate light responses (Boos et al., 1993).

Several lines of evidence indicate that SACs also use VGCs for signal processing, in this case for the generation of dendritic DS. First, the presence of a substantial 2nd harmonic component (V_2) in the SAC electrical responses even for lower-contrast expanding stimuli (Fig. 20 B, E) demonstrates that an electrical nonlinearity is involved in SAC DS. Second, as GABA receptor blockers did not change fundamental or harmonic components of the voltage responses (see also 4.1.1 and Fig. 24), the nonlinearity cannot be generated by GABAergic network effects. Third, the non-linearity is unlikely to be introduced by a presynaptic pathway (see 3.3.1). Even if there was a presynaptic nonlinear contribution, it should be non-DS, because the excitatory input is not DS (see 4.1.2). Fourth, the voltage-dependence of the light-evoked currents, and especially of the non-linearity, (cf. 3.5) suggests an activation of VGCs. All of this is highly indicative of a differential, i.e. direction-dependent activation of voltage-gated channels on the SAC dendrites.
In support of a concerted activation of VGCs for outward motion is also the clustering of the relative phases ($\phi_2 - 2 \cdot \phi_1$) between fundamental and 2nd harmonic at negative values around $-\pi/2$ (Fig. 18 B). This shows that even when it is not obvious as a steep slope of the response trace, nonlinearity occurs mainly during the rising phase of the fundamental. This and the steep rise in $[Ca^{2+}]$ for outward motion (Fig. 17 A) suggest that the distal-dendritic potential rests near the threshold of regenerative events (e.g. Ca^{2+} spikes).[16]

[15] See next footnote.
[16] The crossing of this threshold under certain circumstances might also be the reason that action potentials have been reported in some (Bloomfield, 1992; Gavrikov et al., 2003) but not all (Taylor and Wässle, 1995; Peters and Masland, 1996; Euler et al., 2002) SAC electrical recordings. It is also possible however, that dendritic spikes cannot be recorded at the soma due to centripetal attenuation, as suggested by Velte and Miller (1997).

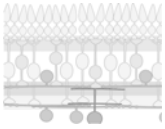

Unfortunately both the voltage-clamp and the pharmacological experiments failed to identify the types of VGCs involved. The Ca^{2+} and Na^{+} channel blockers simultaneously compromised transmission in the presynaptic pathways or did not act as selectively as expected (3.4.2). It cannot be excluded that TTX-resistant voltage-gated Na^{+} channels (O'Brien, personal communication) are involved; the pharmacological experiments were inconclusive in this respect. The only statistically significant result pointing to an involvement of a certain type of VGC on SACs was the difference in AI_1 and AI_2 between the application 10 µM Cd^{2+} and washout (Fig. 25 E). Low concentrations of Cd^{2+} selectively block HVA P/Q- and N-type Ca^{2+} channels. These HVA Ca^{2+} channels (and probably R-type Ca^{2+} channels) have been found in SACs (Cohen, 2001) and are thus the most likely candidates responsible for the nonlinearity.

Also that pharmacological block of N- and P/Q-type Ca^{2+} channels results in a loss of DS in DSGCs (Jensen, 1995) supports the view that these subtypes play an important role in DS computation. Because N- and P/Q-type channels contribute ~ 70% of the Ca^{2+} current in SACs (Cohen, 2001), the analysis has been focused on these types.

It is unlikely that T-type or low-voltage activated (LVA) L-type channels (Lipscombe et al., 2004) contribute significantly, because SAC Ca^{2+} currents are not sensitive to Ni^{2+} (Cohen, 2001), which blocks T-type channels more effectively than other Ca^{2+} channels (Fox et al., 1987), or Nifedipine, which inhibits L-type channels (Cohen, 2001).[17]

Considering that only HVA but no LVA Ca^{2+} channels appear to be present in SACs (Cohen, 2001), the results of the voltage-clamp experiments are surprising for two reasons. First, the shallow maximum of I_2 as a function of the somatic command potential (Fig. 27 C) was unexpected, as the current provided by HVA channels – assuming decent voltage control of the cell – should have been suppressed completely by hyperpolarization beyond their activation range (Fig. 29 C). That this was not possible, within the range of holding potentials that the cells would tolerate, indicates that there is voltage attenuation between soma and dendrite (see below and 4.2.2). The second surprise was that the DS of I_2 was largest at rather hyperpolarized command

[17] So far immunocytochemistry has not provided any insights concerning the Ca^{2+} channel subunits expressed in SACs. Labeling with antibodies against several VGCC subunit subtypes in rat shows strong expression of the P/Q-type Ca^{2+} channel in the whole inner plexiform layer (Xu et al., 2002; 2003), making a localization to specific cell types difficult. The two (of at least four) subunit types of the L-type channel which were analyzed in these studies seem to be localized exclusively on bipolar cells and possibly Müller cells (Xu et al., 2002), not on the processes of other cells in the inner plexiform layer. Nevertheless there are other L-type subunits and T-type Ca^{2+} channel subunits, which were not studied.

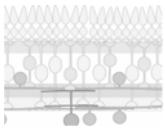

potentials (Fig. 27 C, D) and not at V_{Rest}. Generally, one would expect that the cells should feature maximal 'direction discrimination' near their resting state and not when they are somatically hyperpolarized. In addition HVA Ca^{2+} channels, which likely underlie the harmonic currents, are activated at voltages more positive than -40 mV, rather than below -70 mV (Fig. 29 C). These unexpected findings could also be explained by a difference in membrane voltage between the dendritic tips and the soma, instead of by LVA Ca^{2+} channels (see 3.5 and 3.6). If the dendritic tips were more depolarized than the soma, VGCs in the dendrites would seem to be activated at more hyperpolarized (somatic) voltages than their activation range would suggest.

Before discussing the hypothesis of a dendritic voltage-difference in detail (4.2.2), the plausibility of a contribution from VGCCs can be assessed mathematically: One can estimate whether the number of Ca^{2+} channels needed to generate the measured 2nd harmonic current (I_2) is consistent with the size of the Ca^{2+} currents reported by Cohen (2001). Since only moderate voltage modulations are considered, any I-V curve (including that for a voltage-gated channel) can be expanded into a Taylor series. This was done here, for the time being neglecting inactivation and kinetic aspects. The channel properties of the P/Q-type Ca^{2+} channels (data from the literature, Guia et al., 2001; Mori et al., 2000) were used, because, as mentioned, N- and P/Q-type channels contribute ~ 70% of the Ca^{2+} current (Cohen, 2001). When assuming a voltage modulation amplitude of 5 mV (Fig. 17 A) ~ 930 P/Q-type channels are needed to account for the measured I_2 of 8 pA (for V_{COM} = -90 mV, Fig. 27 C; for calculations see Appendix B, courtesy of W. Denk, from Hausselt et al., *submitted for publication*). In comparison, about ~ 300 channels are necessary to account for the Ca^{2+} conductance seen in SACs (~ 4 nS, Cohen, 2001). The discrepancy in the estimates of channel number might simply reflect the fact that they are based on measurements from different preparations and, thus, probably are affected differently by dendritic voltage attenuation and current shunting. It is not unlikely that the voltage modulation in the dendrite is for example twice as large as the modulation measured in the soma (Velte and Miller, 1997). If this was the case and if the current from the dendrite was attenuated by the same factor, the number of channels obtained would be half as large (465) and thus in closer agreement with the number estimated using Cohen's data. This calculation shows that the assumption of dendritic Ca^{2+} channels generating the harmonic currents is not unreasonable.

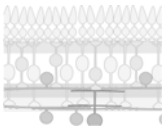

A direction-dependent amplification of synaptic input currents by VGCs could also explain why the fundamental component (V_1) is larger for outward than for inward motion (e.g. Fig. 15 D), a finding that passive biophysical models do not predict (Rall, 1964; Tukker et al., 2004). One way to picture such signal amplification is that the negative slope conductance (Koch, 1999) which occurs in a certain region of the VGCs' activation range compensates some of the native, including synaptic, conductance and thus increases the cell's input resistance. This in turn leads to a larger, i.e. amplified, voltage change for a given input current. The size of the negative slope conductance that could be provided by P/Q-type channels peaks at -12.2 mV where it reaches ~ 1/(130 MΩ) for ~ 930 channels, as are needed to account for I_2 (see above; for calculations see Appendix B, courtesy of W. Denk, from Hausselt et al., *submitted for publication*). This value is comparable to the light-induced synaptic conductance (around ~ 3.7 nS = 1/(270 MΩ); deduced from Fig. 4B in Taylor and Wässle, 1995), and therefore significant amplification could be provided. The slope conductance depends strongly on the voltage, i.e. the location on the activation curve and becomes negligible below the activation range. This means that no VGC-based amplification should occur at very hyperpolarized potentials, which is consistent with the observed decrease in DS for V_1 towards more hyperpolarized command potentials (Fig. 27 D).

4.2.2 Somato-dendritic voltage difference

One problem when investigating dendritic processing is that it is not only impossible to record electrically from most of the dendrite, but that it is also difficult to control the voltage in parts of the dendrite that are remote from the electrode location (the 'space clamp' problem, see 1.3.2). This is particularly problematic in SACs (Velte and Miller, 1997), where the dendritic connections between the soma and distal branches are very thin (Famiglietti, 1983b) and synapses are tonically activated (Taylor and Wässle, 1995). Therefore, the dendrite acts as a voltage-divider (Fig. 31) and voltage attenuation needs to be explicitly considered.

Earlier optical measurements from SAC had shown that dendritic [Ca^{2+}] can be transiently reduced by stimulation of the cell's surround (Euler et al., 2002), suggesting that even at rest (i.e. with constant, uniform illumination) there is a steady-state Ca^{2+} influx. The [Ca^{2+}] *vs.* voltage-step data confirms this as, when V_{COM} is more

hyperpolarized than the resting potential (V_{Rest}), there is a decrease in (distal) dendritic [Ca^{2+}] – indicating reduced Ca^{2+} influx. This is likely due to the deactivation of Ca^{2+} channels when the voltage becomes hyperpolarized relative to the channel activation range (Fig. 28 B). This indicates that when the soma is clamped to the zero-current potential (~ V_{Rest}) the dendritic voltage is within the activation range of VGCCs. These data, similar to the voltage-clamp experiments (see 3.5 and 4.2.1), seem to suggest that Ca^{2+} influx is not through HVA Ca^{2+} channels (see 3.6 and activation curves, Fig. 29 C). Yet, LVA channels were not found in SACs (see 4.2.1; Cohen, 2001). An alternative explanation that reconciles HVA Ca^{2+} channels with the data is that the measured Ca^{2+} activation curve (Fig. 29 A) is shifted by attenuation of the somatic control voltage via R_{Long}, the longitudinal dendritic resistance (Miller and Bloomfield, 1983; Borg-Graham and Grzywacz, 1992; Velte and Miller, 1997), in combination with a distal leak conductance ($1/R_{Leak}$) that has a reversal potential positive to the somatic resting potential (Fig. 31), such as CNQX-sensitive glutamate receptors. This idea is supported by the finding that blocking (tonically activated) CNQX-sensitive glutamate receptors reversibly shifts the activation curve closer to where it would be expected (Fig. 29 B).

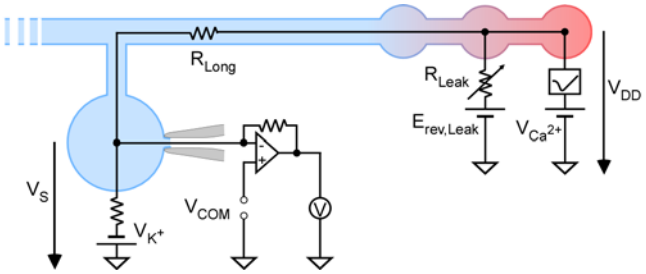

Fig. 31 Proposed dendritic voltage-divider
Shown are the somatic voltage V_S and the K^+ leak conductance with the reversal potential V_{K+} as well as a simplified patch clamp circuit with the command potential V_{COM}. Elements of the voltage-divider causing a voltage drop between dendritic tips and soma (with $V_{DD} > V_S$) are the longitudinal dendritic resistance R_{Long}, the leak conductance R_{leak} (e.g. tonically activated glutamate receptors), the reversal potential $E_{rev,leak}$ and a voltage-gated channel (*here* Ca^{2+})

The properties of such a dendritic voltage divider (Fig. 31) can be roughly estimated by comparing the activation parameters (V_{50} = -48.5 mV, V_{slope} = 8.7 mV) obtained from the [Ca^{2+}] *vs.* V_{COM} data (Fig. 29 C and Table 1) to those measured in electrotonically compact cells, such as *Xenopus* oocytes (Zhang et al., 1993) which exhibit little or no voltage attenuation. The relationship between distal voltage (V_{DD}) and somatic voltage (V_S) is

$$V_{DD} = E_{rev,Leak} + \frac{R_{Leak}}{R_{Leak} + R_{Long}} \left(V_S - E_{rev,Leak} \right), \qquad (9)$$

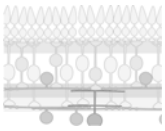

with $E_{rev,Leak}$ the reversal potential of the distal leak. Changes in the somatic voltage reach the dendritic tips attenuated by the factor $\gamma = R_{Leak} / \left(R_{Leak} + R_{Long} \right)$. Since the apparent (measured) V_{slope} is increased by approximately $1/\gamma$ (see Appendix B for details), γ describes the transformation of the measured activation curve into the activation curve expected for a certain Ca^{2+} channel. Further, $E_{rev,Leak}$ can be calculated to find out if it is in the predicted range (e.g. similar to that of glutamate receptors). For the P/Q-type channel $\gamma = 4.56/8.7 = 0.524$, (for V_{slope} values see Table 1).

Activation curve/Ca^{2+} channel type	V_{50} in mV	V_{slope} in mV
$[Ca^{2+}]$ *vs.* V_{COM}	-48.5 ± 2.0	8.7 ± 2.0
$[Ca^{2+}]$ *vs.* V_{COM} with CNQX	-34 ± 3	10.2 ± 2.2
fit from Cohen (2001) data	-20	2.6
P/Q-type fit (data from Mori et al., 2000)	-10.9 ± 0.5	4.56 ± 0.35
R-type fit (data from Zhang et al., 1993)	-27.5 ± 2.1	8.57 ± 1.09
TTX-r Na^+ channel fit (data from Roy and Narahashi, 1992)	-26.9 ± 0.2	4.00 ± 0.15

Table 1. Fit parameters V_{50} and V_{Slope} from different voltage-gated channels and data sets

To obtain an estimate for the reversal potential of the distal leak ($E_{rev,Leak}$) eqn. 9 can be solved with V_S set to the apparent half-activation voltage (V_{50S}) and V_{DD} to the actual half-activation voltages (V_{50VC}), leading to $E_{rev,Leak} = \left(V_{50VC} - \gamma V_{50S} \right) / \left(1 - \gamma \right)$. For the P/Q-type currents $E_{rev,Leak}$ = 30.5 mV.

While the attenuation factor (γ) of ~ 0.5 for P/Q-type channels is plausible, the leak reversal potential is too high to be consistent with a glutamate receptor-mediated 'leak'[18] current. In this estimate several aspects have not been taken into account, though: (i) There could be persistent currents (Hodgkin and Huxley, 1952) through VGCCs or voltage-gated Na^+ channels (O'Brien, personal communication). These would increase the slope of the activation curve and shift $E_{rev,Leak}$ to more positive potentials, because the current following activation of these VGCs depolarizes the dendrite, leading in turn to an accelerated activation of VGCs. (ii) The channel activation curves used for comparison (Fig. 29 C) were measured using Ba^{2+}, which not only shifts the activation range of VGCCs to more positive values (e.g. Zhang et al., 1993), but also increases the open-channel conductance (reviewed in Sather,

[18] Glutamate receptors can be considered as providing a 'leak' conductance here, as at least some of them are tonically active.

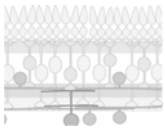

2005). Both effects could increase the slope of the I-V curve under conditions of imperfect voltage clamp.

The preliminary data from [Ca^{2+}] recordings along the dendrite (Fig. 30) indicates that the voltage attenuation, measured as shift of the Ca^{2+} activation curve, is smaller at more proximal sites, and therefore supports the idea of a voltage gradient. A problem with these measurements is, however, that the [Ca^{2+}] responses are larger in the dendritic tips – in accordance with earlier results (Euler et al. 2002) as well as with unpublished observations (X. Castell, personal communication), showing that [Ca^{2+}] transients evoked by light stimulation are usually larger in the distal than in the more proximal dendrite. The smaller proximal responses make the curve-fitting less reliable (2.4.2).

To maintain a difference in resting membrane potential a constant outward current at or close to the soma is required to counterbalance the dendritic tonic inward current. This outward current is likely carried by K^+. A potassium channel of the $K_V3.1$ subtype, which seems to be more densely distributed on the soma and the proximal than on the distal dendrites has been described in SACs (Ozaita et al., 2004). This channel has been suggested to promote the relative electrical isolation of SAC dendritic sectors, but it is unclear if it would be active at low enough voltages to carry a constant outward current near the soma. It may seem puzzling that intracellular Cs^+ which was used in the voltage-clamp experiments (see 3.5) to block K^+ channels did not abolish the voltage-gradient. Many K^+ channels however are incompletely blocked by intracellular Cs^+ (see 3.6 and Hille, 2001). A reduction of the gradient by suppressing K^+ channels – e.g. with high extracellular concentrations of Tetra-ethyl ammonium chloride (TEA-Cl) as it would be necessary to inhibit the channels Ozaita et al. (2004) described – was not attempted, because K^+ channels in retinal cells upstream of the SAC would also be blocked, likely leading to unpredictable effects on the light response.

Considering the evidence presented here, the voltage-divider hypothesis does reconcile the voltage-step evoked [Ca^{2+}] signals (Fig. 29 A) and the course of the motion-induced currents as a function of voltage (27 C, D) with the notion that HVA Ca^{2+} channels underlie the voltage-activated dendritic currents in SACs.

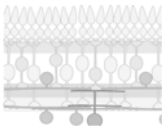

The question remains: what is the advantage of a depolarized membrane potential in the SAC distal dendrites? An obvious consequence is that even small changes in synaptic input currents (e.g. as caused by low-contrast motion stimuli) would strongly modulate VGCs if the membrane potential was near or within their activation range. The possible functional relevance this has for the dendritic computation of DS is discussed in detail in section 4.3.

4.2.3 Calcium induced calcium release

Recently, Barlow (1996) has suggested an involvement of intracellular Ca^{2+} signaling and Ca^{2+}-induced Ca^{2+}-release (CICR) in the SACs as a potential signal delay mechanism that matches the temporal requirements for the 'vetoing' inhibition proposed by Barlow and Levick (1965) (see 1.4.2). While the biochemical machinery necessary for CICR has been found in cultured GABAergic amacrine cells (Hurtado et al., 2002; Warrier et al., 2005), these cells were not classified further and it is currently not yet clear whether CICR is present in SACs.

Nevertheless, some findings presented here point to the possibility of CICR in SACs. The first hint is the loss of light stimulus-induced $[Ca^{2+}]$ transients during most whole-cell recordings (see 3.2). This is not due to a loss of VGCC function, as depolarizing steps in voltage-clamp recordings can still evoke an increase in $[Ca^{2+}]$ (Fig. 28, 30). Also, in retinal ganglion cells recorded under similar conditions dendritic $[Ca^{2+}]$ responses persist (Oesch et al., 2005), suggesting the loss of light-induced $[Ca^{2+}]$ responses to be SAC specific. CICR is potentially sensitive to wash-out of cellular components during whole-cell recording and might be required in SACs to generate detectable $[Ca^{2+}]$ responses to light stimuli. This is supported by the observation that cells exhibiting spontaneous spiky $[Ca^{2+}]$ transients (Fig. 28 C), which may reflect CICR activity, are also more likely to show light-induced Ca^{2+} responses (see 3.6).

The persistence of DS electrical responses (in the fundamental as well in the harmonics) in the absence of any light stimulus-induced $[Ca^{2+}]$ transients suggests, however, that the DS computation in SACs as such is independent of CICR. It remains to be explained why, if Ca^{2+} fluxes through VGCCs underlie the nonlinear currents, they cannot be detected as changes in Ca^{2+}-dependent fluorescence. During a 100 ms

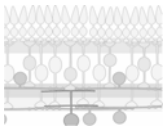

period (the rising phase of the stimulus at 2.5 Hz) about $32 \cdot 10^{-18}$ mol of Ca^{2+} enters the cell (estimated using a single channel conductance $\alpha = 7.4$ pS, 500 VGCCs, and $\Delta V =$ 10 mV; see Appendix B). This is only roughly 10% of the total amount of $[Ca^{2+}]$ indicator ($\sim 32 \cdot 10^{-17}$ mol), estimated using a volume of the SAC dendrite of 3.2 pL (based on Famiglietti, 1991 and Miller and Bloomfield, 1983, and a concentration of 100 µM OGB-1; see Appendix B). Accordingly, with only the Ca^{2+} current through VGCCs the change in fluorescence intensity with this amount of indicator would be much less than the light-induced changes actually seen with e.g. sharp electrodes (Euler et al., 2002).

As DS Ca^{2+}-current densities are expected to be rather small in absolute terms – although the ratio between outward and inward motion might still be quite large – it is possible that CICR is needed to amplify $[Ca^{2+}]$ changes to levels that are sufficient for driving Ca^{2+}-dependent (O'Malley et al., 1992; Zheng et al., 2004) synaptic output from SACs. It may actually be impossible to allow entry of sufficient Ca^{2+} through voltage-gated channels to drive release without increasing the Ca^{2+} channel density into a regime where the dendrite becomes electrically unstable, i.e. regenerative events occur. Due to its lack of electrogenicity CICR would circumvent this problem.

Along the same lines the confinement of $[Ca^{2+}]$ increase to 'hotspots', usually co-localized with the varicosities in the outer dendrites (Euler et al., 2002; X. Castell, unpublished data), may be explained by an involvement of local Ca^{2+} stores and Ca^{2+} uptake mechanisms. Such intracellular Ca^{2+} mechanisms could facilitate local processing and thus, local release of neurotransmitter. As suggested in a recent study the two SAC neurotransmitters, acetylcholine and GABA (Masland and Mills, 1979; Brecha et al., 1988; Vaney and Young, 1988), could be released differentially, following the activation of different types of VGCCs (Zhou and Zheng, 2006). Although speculative, it is even conceivable that specific channel types and/or different internal Ca^{2+} signaling pathways are linked to distinct neurotransmitter release-mechanisms.

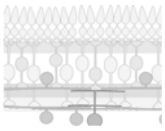

4.3 Models

> Thus, the Hassenstein-Reichardt model […] introduced mathematical techniques and quantitative modeling to biology, clearly demonstrating that our intuition does not reach very far; instead we soon reach the point where the 'pen starts getting smarter than the person holding it'.
>
> **Alexander Borst, 2000**

The essential elements of the computation of motion direction are spatial asymmetry and nonlinearity (Hildreth and Koch, 1987; Borst and Egelhaaf, 1989). In most models of retinal DS they are assumed to be implemented as asymmetric connections and interactions between inhibitory and excitatory inputs, respectively (Hassenstein and Reichardt, 1956; Barlow and Levick, 1965; Torre and Poggio, 1978; Koch et al., 1983). Most models of dendritic DS in SACs follow this scheme, assuming that lateral synaptic inhibition is required for SAC DS (e.g. Borg-Graham and Grzywacz, 1992; Gavrikov et al., 2003).

Some recent models make use of intrinsic neuronal properties. One model e.g. suggests a $[Cl^-]$ gradient along the SAC dendrites generated by a differential distribution of Cl^- importers and exporters, leading to differential effects of GABA at the proximal and distal dendrites (Gavrikov et al., 2003). One problem with this model is that the block of Cl^- transporters in the retina strongly affects the Cl^- reversal potential in many cells, including those presynaptic to SACs. The second issue is that the experimental evidence relies on extracellularly recorded SAC spikes. Considering the controversy regarding SAC spikes, and the question, that if they existed, what their relevance might be, the conclusions from the model are disputable. Further, the Cl^- gradient model depends upon GABAergic transmission. As shown here (4.1.1), GABAergic inhibition is not necessary for SACs to generate DS responses.

A number of models have dealt with the passive electrical properties of SACs (Miller and Bloomfield, 1983; Poznanski, 1992; Borg-Graham and Grzywacz, 1992; Velte and Miller, 1997, Tukker et al., 2004). There is general agreement that the dendritic sectors, which seem to be largely isolated from each other and from the soma, can be considered as functional subunits. In 1964 Rall had shown that sequential summation of synaptic inputs along a passive dendrite can lead to a larger electrical signal at the end of the dendrite towards which the inputs are moving. Applying this concept to the SAC morphology, Miller and Bloomfield (1983) proposed that currents would spread

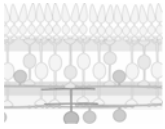

more easily in a centrifugal direction within a SAC dendritic sector than towards the soma. Borg-Graham and Grzywacz (1992) showed with a passive model, that a directional difference in dendritic voltage can be generated due to the electrotonic properties of the SAC morphology alone. This finding was later confirmed with an elaborate but also passive SAC model in combination with more realistic visual stimulation (Tukker et al., 2004). One problem with passive models is that they generate a difference in the shape of the output waves, but not 'real' direction selectivity, which is defined by a difference in the area (integral) of output waves (see also 1.4.2). This means that passive models have to rely e.g. on a thresholding mechanism, such as spike-generation (e.g. Tukker et al., 2004). In one of the models developed by Borg-Graham and Grzywacz (1992) the non-linearity necessary for 'real' DS was generated by the interaction of inhibitory and excitatory input. They pointed out, though, that "if a nonlinear functional is applied to the tip waveform […] the cable *without* inhibition generates a directional response […]". Also Tukker et al. (2004) recognized that "calcium channels could effectively provide a threshold, which amplified DS". Along the same lines, Velte and Miller (1997), who studied spiking and non-spiking models of SACs, wrote that it should "not be difficult to imagine mechanisms in which directionally sensitive differences are generated […] depending on the position and density of spike generating membrane sites".
Another problem of all passive models is that they predict somatic voltage excursions that are larger for inward than for outward motion and this is not consistent with experimental data (Fig. 17; Peters and Masland, 1996; Euler et al., 2002; Gavrikov et al., 2003). Furthermore, the direction-discrimination obtained from purely passive models seems too small to explain how the DS system as a whole is able to prefer e.g. lower contrast preferred-direction stimuli over higher-contrast null-direction stimuli (Merwine et al., 1998).

The data presented in this study suggests that active currents (VGCs), likely provided by HVA Ca^{2+} channels in the SAC's distal dendrites, and a difference in voltage between dendritic tips and soma are important features of the DS computation. The question is how these features can generate a DS output from non-DS inputs.
A seemingly straight-forward explanation is that excitatory synaptic input caused by a stimulus moving outward is summing up along the dendrite (Rall, 1964) and will be amplified more strongly, because the membrane potential in the distal dendrites rests within the VGCs activation range. Inputs elicited by a stimulus moving inward are summed as well but should be less effective in activating the proximal VGCs, because

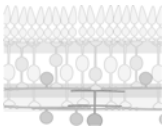

here the membrane potential rests further away from the VGCs' activation range. However, this 'simple' explanation does not take into account dynamic interactions between the synaptic inputs and VGC activity. In addition, or possibly as a result of ignoring the interactions, this 'simple' model fails to capture certain quantitative aspects e.g. why DS in SACs is robust for a relatively large range of contrasts (Fig. 20; Merwine et al., 1998) and why the somatic responses are larger for outward than for inward motion.

In order to explore the effects of a voltage gradient on dendritic VGCs a numerical two-compartmental model was constructed (see Fig. 32, courtesy of W. Denk, from Hausselt et al., *submitted for publication*; see Appendix C). The model is conceptual; it does not incorporate any morphological detail. The two compartments can be thought of as a distal and a more proximal part of a dendritic sector. These two 'locations' were chosen (and the soma was not considered), because data presented here (see 3.3.3) suggest that the DS computational mechanism is likely located near the outer region of the dendritic tree. Both compartments contain, in addition to a linear leak conductance (g_{leak}) and a capacitance (C), a single type of voltage-gated channel (g_D or g_P), which has the properties of a HVA Ca^{2+} channel. The model does not depend on the VGCs being Ca^{2+} channels; other types of VGCs could work as well, but this was not further explored. The compartments are connected by a resistor (R_{long}), representing the longitudinal intra-dendritic current pathway (Fig. 32 A). The moving stimulus is simulated by the injection of phase-shifted sinusoidal currents (Fig. 32 B).

The model shows that even if both compartments are otherwise identical, a gradient in the resting voltages (e.g. -19 mV and -16.5 mV; for other parameters see Appendix C, table 14) between the compartments leads to a strongly DS response: In the more depolarized compartment, which represents the distal dendrites, the "outward" stimulus causes a ~ 8.5-fold larger (fundamental-frequency) voltage amplitude than the "inward" stimulus. The more negative compartment, which represents the more proximal dendrite, also prefers the "outward" stimulus but only moderately so (by a factor of ~ 1.3 for the fundamental; Fig. 32 C). Without a voltage difference between the compartments there is no direction discrimination (Fig. 32 D). The model is consistent with the experimental data in four important ways: (i) Outward motion evokes a larger proximal response, similar to the larger somatic response in the measured voltage responses. (ii) DS is stronger for the second harmonic than for the

fundamental. (iii) Outward stimuli with much weaker contrast evoke larger responses than inward stimuli with high contrast. And (iv) DS is strongly voltage dependent (for details see table 14, Appendix C). These are important features that cannot be reproduced by passive models and therefore strengthen the case for a central role of active conductance in dendritic DS. Nevertheless, the model is only a preliminary one and thus has some drawbacks. It is e.g. limited in its range of stimulus frequencies, and the value used for R_{long} is rather high (see Appendix C). More refined versions of the model (e.g. with more compartments or combinations of VGCs) are expected to resolve these issues. An interesting property of the model is that a strong directional preference is imposed on a symmetrical arrangement of compartments by an only modest voltage gradient (compare panels C and D in Fig. 32), which is likely for the gradient found in SAC dendrites. In the model the proximal compartment is only slightly DS, while strong DS is limited to the distal compartment, which is where it is needed to drive DS Ca^{2+} signals (Euler et al., 2002) and, in turn, DS synaptic release.

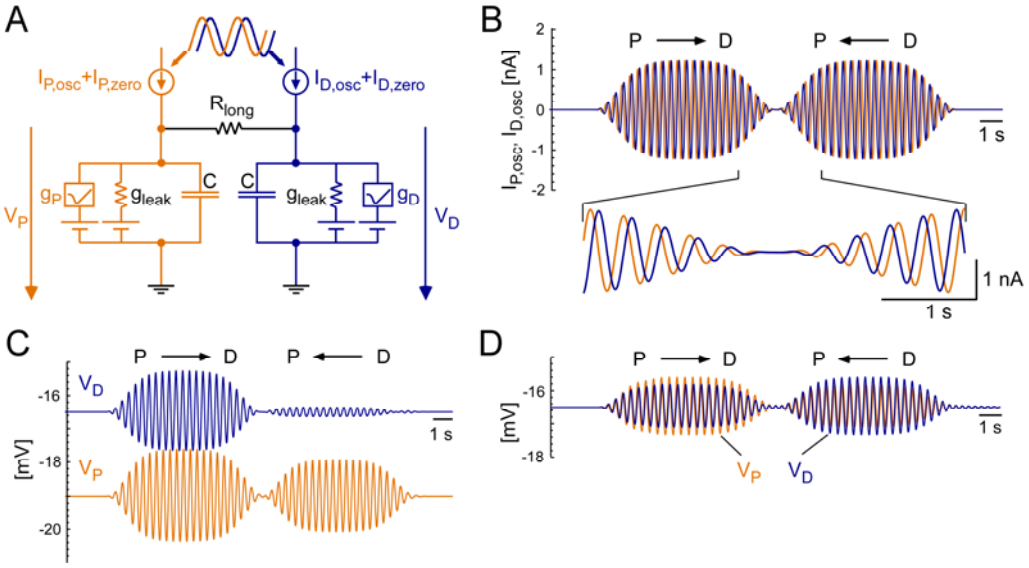

Fig. 32 Two-compartmental model of starburst amacrine cell dendritic direction selectivity
A. Circuit diagram of the two compartments P (proximal) and D (distal), each containing in parallel a capacitor (*C*), a leak conductance (g_{leak}) and a voltage-gated conductance (g_P or g_D). They are connected by a resistor (R_{long}). The inputs from bipolar cells are represented by sinusoidal currents ($I_{P,osc}$ and $I_{D,osc}$) injected into the compartments. The resting potentials are set by additionally injecting DC currents ($I_{P,zero}$, $I_{D,zero}$). Image motion is simulated by setting the relative phase of the sinusoidal currents injected into the two compartments (for details see text). **B.** Sinusoidal input currents injected into the two compartments. During the first stimulation period the current injected into compartment D is delayed relative to compartment P (simulating 'out-going' motion, from P to D). During the second stimulation period the timing is reversed (simulating 'in-going' motion, from D to P). **C.** Voltages in both compartments in response to the injection of oscillating currents from B showing that in both compartments the response is larger when the current in the compartment that has the more depolarized resting potential, in this case compartment D, is delayed. It is this compartment that shows a strong preference for one "motion direction" (*blue trace*). The other compartment has a much weaker preference but for the *same* direction (*orange trace*). **D.** Setting the injected DC current such that both compartments rest at the same potential, causes different preferred directions for both compartments. (For *details see Appendix C.*) *This figure appears in a slightly modified version in Hausselt et al., submitted for publication*

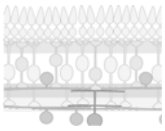

4.4 Outlook

Little by little, one travels far.

J. R. R. Tolkien (1892 - 1973)

Assuming thus, that the initial computation of DS in the retina relies on a difference in voltage along the starburst amacrine cell dendrites, and – possibly as a consequence – a directional activation of dendritic voltage-gated channels, and provided that future studies will confirm this mechanism, how far have we come?

4.4.1 Retinal direction selectivity…

Concerning retinal DS many questions remain to be answered (Fig. 33). First, as mentioned before (1.4.3), the 'mystery' of how the two neurotransmitters are released from SACs is still not solved. It seems to be clear that both acetylcholine and GABA are released via Ca^{2+} dependent mechanisms (O'Malley et al., 1992; Zheng et al., 2004) and that this release is vesicular (Zheng et al., 2004). But are the release mechanisms spatially and/or temporally distinct and if yes, how is this established (cf. Zhou and Zheng, 2006)? Further, neither immunohistochemical (Dong et al., 2004) or ultrastructural studies (Famiglietti, 2002) have been able to find asymmetric connections between SACs and DSGCs. On the other hand, we know from physiological experiments (Fried et al., 2005; Lee et al., 2006) that only SACs on the null-side of a DSGC provide it with inhibitory input, whereas the SACs on the preferred-side do not seem to establish direct functional connections to the DSGC at all – at least none strong enough to drive a ganglion cell when depolarizing a single SAC. This is particularly intriguing as SACs are most likely[19] the only cholinergic neurons (Masland and Mills, 1979; Famiglietti, 1983b, Tauchi and Masland, 1984) in the retina that can provide DSGCs with input. And, in fact, DSGCs have been shown to receive substantial excitatory cholinergic input (Masland and Ames, 1976; Ariel and Daw, 1982; Kittila and Massey, 1997).

[19] There are one or two populations of cholinergic cells in the chicken retina that are not necessarily identical with ON or OFF SACs (Millar et al., 1987, Tumosa et al., 1984). In ground squirrel retina non-SAC cholinergic cells have been described, but they do not co-stratify with DSGCs (Cuenca et al., 2003).

Another puzzle are the findings of several groups indicating that not only the inhibitory but also the excitatory input to DSGCs is directionally tuned (Borg-Graham, 2001; Taylor and Vaney, 2002; Fried et al., 2002). Moreover, pharmacological experiments (Fried et al., 2005) indicate both glutamatergic and cholinergic input to be DS. At the same time it seems to be quite clear that acetylcholine does not have a substantial effect on the direction selectivity of DSGC responses (Ariel and Daw, 1982; Kittila and Massey, 1997; Chiao and Masland, 2002; but see Grzywacz et al., 1998). Considering that only GABA has been found to be essential for DS in ganglion cells (Wyatt and Daw, 1976; Caldwell et al., 1978; Ariel and Daw, 1982; Massey et al., 1997), what kind of information is then conveyed by acetylcholine?

Bipolar cells, which provide the glutamatergic input to DSGCs, generally tile the retina (for review see MacNeil et al., 2004). This raises the question how these cells could deliver DS input to DSGCs of all preferred-direction subtypes at a single retinal location. If neighboring bipolar cells provided different preferred directions, the receptive field of DSGCs should be patchy, which is not the case (Barlow and Levick, 1965). Rendering single axon terminals of bipolar cells DS, e.g. by directional inhibition, would require highly local processing. The most likely candidates for such a hypothetical DS inhibition of bipolar cells, are SACs, which seem to synapse onto bipolar cell terminals only rarely, if at all (Famiglietti, 1991).

Another long-standing question is how many parallel mechanisms within the retinal network are necessary to generate the robust DS responses seen in the ganglion cells. In this context it should be mentioned that only if a large number of SACs is ablated, DS is actually lost in DSGCs (He and Masland, 1997; Yoshida et al., 2001; Amthor et al., 2002), suggesting a great deal of redundancy. Probably diverse ‘presynaptic’ mechanisms, possibly involving other amacrines (Fried et al., 2005), including glycinergic ones, and interactions mediated by $GABA_B$ receptors (Grzywacz and Zucker, 2006), take part in the computation. Further, ‘postsynaptic’ mechanisms are not unlikely, e.g. it has been shown that DS responses are sharpened by dendritic spikes in DSGCs (Oesch et al., 2005).

Possibly one of the most intriguing questions is how this circuit develops. It has been proposed that the SAC plexus serves as a scaffold for DSGC dendrites (Vaney and Pow, 2000) and it is known that DS in DSGCs appears as soon as eye-opening in rabbits (Masland, 1977), suggesting that the circuit develops in the absence of

structured visual input. Yet, how for example the asymmetrical connectivity or the distinct subtypes of DSGCs arise is not known.

Another open question is the functional relevance of retinal DS for higher vision. As direction selective simple cells in the primary visual cortex are thought to compute DS from non-directional input (Priebe and Ferster, 2005; Livingstone, 2005), retinal DSGCs seem not to contribute in the conscious perception of moving objects. ON DSGCs exclusively project to the accessory optic system (Oyster et al., 1971; Buhl and Peichl, 1986), and participate in the optokinetic nystagmus and processing of image-slip due to head- and body-movements (Oyster et al., 1972; for review see Vaney et al., 2001). In contrast, ON/OFF DSGCs project to the DS cells of the lateral geniculate nucleus (Levick et al., 1969) – but it is unclear why. One possibility, though difficult to test, is that ON/OFF DSGCs are necessary for directing attention to fast moving objects anywhere in the field of view (Vaney et al., 2001). Consistent with this possibility is that ON/OFF DSGCs are distributed over the whole retina (Vaney, 1994, Amthor and Oyster, 1995, DeVries and Baylor, 1997), and the fact that they preferentially respond to differential and not to global motion (Barlow and Levick, 1965; Oyster et al., 1972; Wyatt and Daw, 1975).

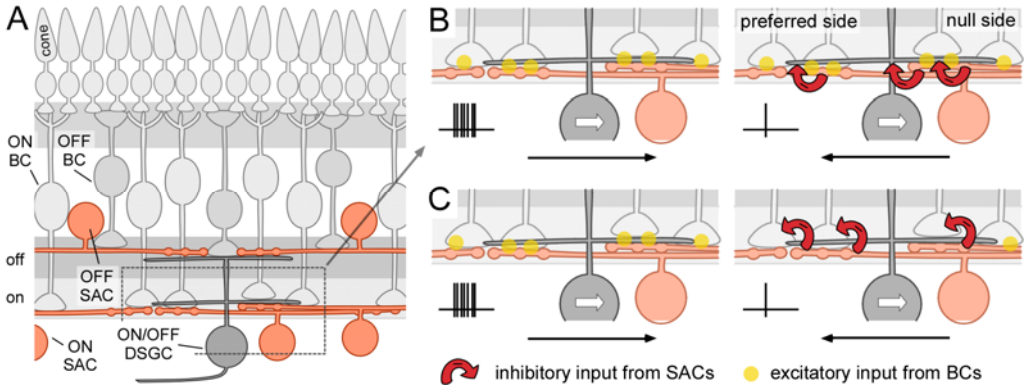

Fig. 33 Possible scenarios of interaction between starburst amacrine and DS ganglion cells
A. Schematic overview of the cells known to be involved in the DS circuit: ON and OFF bipolar and starburst amacrine cells (BC and SAC, respectively) as well as an ON/OFF direction selective ganglion cell (DSGC). Other amacrine cells and horizontal cells are omitted for clarity. **B. & C.** Sections from A (*box in A*) depicting the ON dendritic tree of an ON/OFF DSGC with preferred direction from left to right (*white arrow*), schematic spike trains show DSGC responses, black arrows depict motion direction. **B.** Scenario relying on direct inhibition from SACs to DSGCs. Only the SACs with their dendrites extending in 'null direction' synapse onto DSGCs, providing GABAergic inhibition for stimuli moving in null direction only (right panel) **C.** Scenario depicting inhibition of BCs by SACs (again only with their dendrites extending from the null side of the DSGC). In this theme DSGCs would receive DS excitatory input from BCs. Both scenarios are hypothetical; also a combination is possible. Possible excitatory cholinergic mechanisms are not shown.

4.4.2 …and beyond

The question of how dendritic processing in SACs could generate directional responses goes beyond the DS circuit and touches upon general principles of neuronal computation.

For a long time the prevailing view had been that especially the specific synaptic connectivity of neurons within a network determines information processing, while the computational capabilities of single neurons play only a minor role (e.g. 'integrate-and-fire' model of neurons, for review see Meunier and Segev, 2002). More recently, research has started to concentrate on the computational capabilities of dendrites and on the distribution of the underlying biophysical components, such as voltage-gated ion channels or intracellular signaling machinery (for review see e.g. London and Häusser, 2005).
For few neuronal systems is enough information available to draw a sufficiently complete picture of a single cell type's properties. Neuron types that have been studied in great detail are, for example, mitral cells of the olfactory bulb, neocortical layer V pyramidal neurons, hippocampal CA1 and CA3 cells and cerebellar Purkinje cells. Unlike SACs, these neurons produce conventional action potentials and, hence, provide a 'simple' criterion to measure the cell's output, namely spike rate.[20] For SACs, measuring dendritic [Ca^{2+}] responses, which are though to represent transmitter release (see 1.3.2), is as close as one can currently get to a measurement of the cell's output. For all of the neurons listed above the question remains: how is the spatio-temporal organization processed, such that certain input patterns but not other, potentially very similar ones, initiate action potentials at the soma? Some of the underlying general computational principles are discussed below.

The high density of voltage-gated Na^+ channels in the dendrites of mitral cell and layer V pyramidal neurons, for example, likely underlies action potential back-propagation into their dendrites. Similarly, the ratio of high- to low-voltage activated Ca^{2+} channels and their specific distribution across soma and dendrites determines the criteria under which Purkinje cells and CA3 hippocampal pyramidal neurons generate dendritic Ca^{2+} spikes (for review see Migliore and Shepherd, 2002). Both back-propagating of APs

[20] Expectedly, it is not simple: E.g. in spiking neurons with a high probability of spontaneous transmitter release, subthreshold potentials will also lead to output.

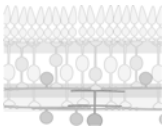

into the dendrites as well as dendritic Ca^{2+} spikes can differentially amplify local inputs (London and Häusser, 2005).
In this context it would be not surprising if Ca^{2+} and possibly Na^{+} channel subtypes in SAC dendrites did play an important role in the processing of spatio-temporal organized input, in this case elicited by different directions of motion. There may even be a differential distribution of Ca^{2+} channel types in SACs, reminiscent of the increase in T-type Ca^{2+} channel density along the dendrites of CA1 hippocampal neurons (reviewed in Johnston et al., 1996).

Other voltage-dependent ion-channels, such as K^{+} channels, can participate in dendritic computation. For example, Ozaita et al. (2004) have described a potassium channel of the $K_V3.1$ subtype in SACs which is likely to facilitate the relative electrical isolation of SAC dendritic sectors proposed by studies (Euler et al., 2002) and models (Miller and Bloomfield, 1983; Poznanski, 1992; Borg-Graham and Grzywacz, 1992; Velte and Miller, 1997). Also NMDA receptors with their Mg^{2+}-sensitive voltage block offer interesting properties. For example, NMDA receptors in layer V pyramidal neurons are responsible for the non-linear summation of synaptic inputs on single thin dendrites (Polsky et al., 2004). In SACs the NMDA receptor-mediated conductance in SACs is small (Zhou and Fain, 1995), however, a computational role for these receptors, especially with regard to a more depolarized resting membrane voltage in the distal dendrites, cannot be completely excluded.

Another computational possibility is a difference in synaptic conductance as a function of dendritic location, which has been described for the apical dendrites of CA1 pyramidal neurons. In contrast to neocortical pyramidal neurons (Williams and Stuart, 2002), in CA1 neurons the input conductance of synapses increases with distance from the soma, yielding an equal signal strength at the soma, independent of dendritic location (Magee and Cook, 2000). Studying local currents in these cells is possible, because their dendrites can be recorded with patch-clamp pipettes. That such dendritic recordings are probably impossible in SACs makes it difficult to study the strength of more distal synaptic inputs along their dendrites. Nevertheless, possible differences in synaptic conductance at different locations along the dendrite should be taken into account when considering dendritic processing in SACs.

To my knowledge, so far no experimental study dealing with computational mechanisms in neurons has described a difference in resting membrane potential

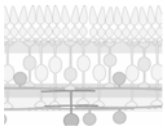

between different dendritic sites. Such a voltage gradient can only be maintained between compartments that are at least partially electrically isolated from each other, or energy costs of e.g. active ion transport may be very high. For decent electrical isolation dendrites have to be sufficiently thin, and such processes are difficult, if not impossible, to access with electrodes in intact neuronal tissue. Indirect methods, as the imaging approach used here, or eventually direct optophysiological measurements using voltage-sensitive dyes, will help to reveal voltage gradients and to understand their functional role.

Ultimately the possible computational mechanisms within single cells are manifold and more and more details will certainly be discovered in the years to come. For the description of DS processing in starburst amacrine cells the hypothesis presented here is surely just the beginning.

❋

5 Literature

Amthor, F. R., Keyser, K. T., and Dmitrieva, N. A. (2002). Effects of the destruction of starburst-cholinergic amacrine cells by the toxin AF64A on rabbit retinal directional selectivity. Vis Neurosci *19*, 495-509.

Amthor, F. R., and Oyster, C. W. (1995). Spatial organization of retinal information about the direction of image motion. Proc Natl Acad Sci U S A *92*, 4002-4005.

Amthor, F. R., Oyster, C. W., and Takahashi, E. S. (1984). Morphology of on-off direction-selective ganglion cells in the rabbit retina. Brain Res *298*, 187-190.

Amthor, F. R., Takahashi, E. S., and Oyster, C. W. (1989). Morphologies of rabbit retinal ganglion cells with complex receptive fields. J Comp Neurol *280*, 97-121.

Ariel, M., and Daw, N. W. (1982). Pharmacological analysis of directionally sensitive rabbit retinal ganglion cells. J Physiol *324*, 161-185.

Armington, J. C., and Adolph, A. R. (1994). Spectral and pattern response in the rabbit retina. J Exp Anal Behav *61*, 247-253.

Barlow, H. (1996). Intraneuronal information processing, directional selectivity and memory for spatio-temporal sequences. Network-Computation in Neural Systems *7*, 251-259.

Barlow, H. B., and Hill, R. M. (1963). Selective sensitivity to direction of movement in ganglion cells of the rabbit retina. Science *139*, 412-414.

Barlow, H. B., Hill, R. M., and Levick, W. R. (1964). Rabbit retinal ganglion cells responding selectively to direction and speed of image motion in the rabbit. J Physiol *173*, 377-407.

Barlow, H. B., and Levick, W. R. (1965). The mechanism of directionally selective units in rabbit's retina.
J Physiol *178*, 477-504.

Baughman, R. W., and Bader, C. R. (1977). Biochemical characterization and cellular localization of the cholinergic system in the chicken retina. Brain Res *138*, 469-485.

Bloomfield, S. A. (1992). Relationship between receptive and dendritic field size of amacrine cells in the rabbit retina. J Neurophysiol *68*, 711-725.

Bönöczk, P., Gulyas, B., Adam-Vizi, V., Nemes, A., Karpati, E., Kiss, B., Kapas, M., Szantay, C., Koncz, I., Zelles, T., and Vas, A. (2000). Role of sodium channel inhibition in neuroprotection: effect of vinpocetine. Brain Res Bull *53*, 245-254.

Boos, R., Schneider, H., and Wässle, H. (1993). Voltage- and transmitter-gated currents of All-amacrine cells in a slice preparation of the rat retina. J Neurosci *13*, 2874-2888.

Borg-Graham, L. J. (2001). The computation of directional selectivity in the retina occurs presynaptic to the ganglion cell. Nat Neurosci *4*, 176-183.

Borg-Graham, L. J., and Grzywacz, N. M. (1992). A Model of the Directional Selectivity Circuit in Retina: Transformations by Neurons Singly and in Concert. In Single Neuron Computation, T. McKenna, S. F. Zornetzer, and J. L. Davis, eds. (Academic Press), pp. 347-375.

Borst, A. (2000). Models of motion detection. Nat Neurosci *3 Suppl*, 1168.

Borst, A., and Egelhaaf, M. (1989). Principles of visual motion detection. Trends Neurosci *12*, 297-306.

Borst, A., and Single, S. (2000). Local current spread in electrically compact neurons of the fly. Neurosci Lett *285*, 123-126.

Boycott, B., and Wässle, H. (1999). Parallel processing in the mammalian retina: the Proctor Lecture. Invest Ophthalmol Vis Sci *40*, 1313-1327.

Brandon, C. (1987). Cholinergic neurons in the rabbit retina: dendritic branching and ultrastructural connectivity. Brain Res *426*, 119-130.

Brandstätter, J. H., Greferath, U., Euler, T., and Wässle, H. (1995). Co-stratification of $GABA_A$ receptors with the directionally selective circuitry of the rat retina. Vis Neurosci *12*, 345-358.

Brecha, N., Johnson, D., Peichl, L., and Wässle, H. (1988). Cholinergic amacrine cells of the rabbit retina contain glutamate decarboxylase and gamma-aminobutyrate immunoreactivity. Proc Natl Acad Sci U S A *85*, 6187-6191.

Buhl, E. H., and Peichl, L. (1986). Morphology of rabbit retinal ganglion cells projecting to the medial terminal nucleus of the accessory optic system. J Comp Neurol *253*, 163-174.

Caldwell, J. H., Daw, N. W., and Wyatt, H. J. (1978). Effects of picrotoxin and strychnine on rabbit retinal ganglion cells: lateral interactions for cells with more complex receptive fields. J Physiol *276*, 277-298.

Canzoniero, L. M., Taglialatela, M., Di Renzo, G., and Annunziato, L. (1993). Gadolinium and neomycin block voltage-sensitive Ca2+ channels without interfering with the Na(+)-Ca2+ antiporter in brain nerve endings. Eur J Pharmacol *245*, 97-103.

Chalupa, L. M., and Werner, J. S. (2003). Preface. In The visual neurosciences, L. M. Chalupa, and J. S. Werner, eds. (Cambridge, MA, USA
London, England, A Bradford Book, The MIT Press), pp. xiii-xiv.

Chiao, C. C., and Masland, R. H. (2002). Starburst cells nondirectionally facilitate the responses of direction-selective retinal ganglion cells. J Neurosci *22*, 10509-10513.

Chiao, C. C., and Masland, R. H. (2003). Contextual tuning of direction-selective retinal ganglion cells. Nat Neurosci *6*, 1251-1252.

Cohen, E. D. (2001). Voltage-gated calcium and sodium currents of starburst amacrine cells in the rabbit retina. Vis Neurosci *18*, 799-809.

Cohen, E. D., and Miller, R. F. (1995). Quinoxalines block the mechanism of directional selectivity in ganglion cells of the rabbit retina. Proc Natl Acad Sci U S A *92*, 1127-1131.

Cole, K. S., and Curtis, H. J. (1939). Electric impedance of the squid giant axon during activity. J Gen Physiol *22*, 649-670.

Cooley, J. W., and Tukey, J. W. (1965). An Algorithm for the machine calculation of compex Fourier series. Math Comp *19*, 297-301.

Cuenca, N., Deng, P., Linberg, K. A., Fisher, S. K., and Kolb, H. (2003). Choline acetyltransferase is expressed by non-starburst amacrine cells in the ground squirrel retina. Brain Res *964*, 21-30.

Dacheux, R. F., Chimento, M. F., and Amthor, F. R. (2003). Synaptic input to the on-off directionally selective ganglion cell in the rabbit retina. J Comp Neurol *456*, 267-278.

Dartnall, H. J., Bowmaker, J. K., and Mollon, J. D. (1983). Human visual pigments: microspectrophotometric results from the eyes of seven persons. Proc R Soc Lond B Biol Sci *220*, 115-130.

Daw, N. W., and Ariel, M. (1981). Effect of synaptic transmitter drugs on receptive fields of rabbit retinal ganglion cells. Vision Res *21*, 1643-1647.

Denk, W., and Detwiler, P. B. (1999). Optical recording of light-evoked calcium signals in the functionally intact retina. Proc Natl Acad Sci U S A *96*, 7035-7040.

Denk, W., Strickler, J. H., and Webb, W. W. (1990). Two-Photon Laser Scanning Fluorescence Microscopy. Science *248*, 73-76.

Devries, S. H., and Baylor, D. A. (1997). Mosaic arrangement of ganglion cell receptive fields in rabbit retina. J Neurophysiol *78*, 2048-2060.

Dong, W., Sun, W., Zhang, Y., Chen, X., and He, S. (2004). Dendritic relationship between starburst amacrine cells and direction-selective ganglion cells in the rabbit retina. J Physiol *556*, 11-17.

Dowling, J. E., and Boycott, B. B. (1966). Organisation of the primate retina: Electron microscopy. ProcRSocLondB *166*, 80-111.

Dübel, J., Haverkamp, S., Schleich, W., Feng, G., Augustine, G. J., Kuner, T., and Euler, T. (2006). Two-photon imaging reveals somatodendritic chloride gradient in retinal ON-type bipolar cells expressing the biosensor Clomeleon. Neuron *49*, 81-94.

Egelhaaf, M., Borst, A., and Reichardt, W. (1989). Computational structure of a biological motion-detection system as revealed by local detector analysis in the fly's nervous system. J Opt Soc Am A *6*, 1070-1087.

Enz, R., Brandstätter, J. H., Wässle, H., and Bormann, J. (1996). Immunocytochemical localization of the GABAc receptor rho subunits in the mammalian retina. J Neurosci *16*, 4479-4490.

Euler, T., Detwiler, P. B., and Denk, W. (2002). Directionally selective calcium signals in dendrites of starburst amacrine cells. Nature *418*, 845-852.

Euler, T., and Hausselt, S. Direction Selective Cells. In Handbook of the Senses, *in preparation*, M. Bevan, F. Editors:, G. Westheimer, A. Kaneko, T. Albright, and R. H. Masland, eds. (Elsevier).

Famiglietti, E. V. (1991). Synaptic organization of starburst amacrine cells in rabbit retina: analysis of serial thin sections by electron microscopy and graphic reconstruction. J Comp Neurol *309*, 40-70.

Famiglietti, E. V. (1992a). Dendritic co-stratification of ON and ON-OFF directionally selective ganglion cells with starburst amacrine cells in rabbit retina. J Comp Neurol *324*, 322-335.

Famiglietti, E. V. (1992b). New metrics for analysis of dendritic branching patterns demonstrating similarities and differences in ON and ON-OFF directionally selective retinal ganglion cells. J Comp Neurol *324*, 295-321.

Famiglietti, E. V. (2002). A structural basis for omnidirectional connections between starburst amacrine cells and directionally selective ganglion cells in rabbit retina, with associated bipolar cells. Vis Neurosci *19*, 145-162.

Famiglietti, E. V., Jr. (1983a). On and off pathways through amacrine cells in mammalian retina: the synaptic connections of "starburst" amacrine cells. Vision Res *23*, 1265-1279.

Famiglietti, E. V., Jr. (1983b). 'Starburst' amacrine cells and cholinergic neurons: mirror-symmetric on and off amacrine cells of rabbit retina. Brain Res *261*, 138-144.

Feigenspan, A., Wässle, H., and Bormann, J. (1993). Pharmacology of GABA receptor Cl- channels in rat retinal bipolar cells. Nature *361*, 159-162.

Fenwick, E. M., Marthy, A., and Neher, E. (1982). A patch-clamp study of bovine chromaffin cells and of their sensitivity to acetycholine. JPhysiol *331*, 577-597.

Field, G. D., and Rieke, F. (2002). Nonlinear signal transfer from mouse rods to bipolar cells and implications for visual sensitivity. Neuron *34*, 773-785.

Fox, A. P., Nowycky, M. C., and Tsien, R. W. (1987). Kinetic and pharmacological properties distinguishing three types of calcium currents in chick sensory neurones. J Physiol *394*, 149-172.

Fried, S. I., Münch, T. A., and Werblin, F. S. (2002). Mechanisms and circuitry underlying directional selectivity in the retina. Nature *420*, 411-414.

Fried, S. I., Münch, T. A., and Werblin, F. S. (2005). Directional selectivity is formed at multiple levels by laterally offset inhibition in the rabbit retina. Neuron *46*, 117-127.

Gavrikov, K. E., Dmitriev, A. V., Keyser, K. T., and Mangel, S. C. (2003). Cation--chloride cotransporters mediate neural computation in the retina. Proc Natl Acad Sci U S A *100*, 16047-16052.

Ghosh, K. K., Bujan, S., Haverkamp, S., Feigenspan, A., and Wässle, H. (2004). Types of bipolar cells in the mouse retina. J Comp Neurol *469*, 70-82.

Glickstein, M. (2003). Vision structure and function: The early history. In The visual neurosciences, L. M. Chalupa, and J. S. Werner, eds. (Cambridge, MA, USA London, England, A Bradford Book, The MIT Press), pp. 3-13.

Golgi, C. (1883). Recherches sur l'histologie des centres nerveux. Arch Ital Biol *4*, 92-123.

Göppert-Mayer, M. (1931). Über Elementarakte mit zwei Quantensprüngen. Annalen der Physik *9*.

Greferath, U., Grünert, U., Möhler, H., and Wässle, H. (1993). Cholinergic amacrine cells of the rat retina express the d- subunit of the $GABA_A$-receptor. NeurosciLett *163*, 71-73.

Grzywacz, N. M., Amthor, F. R., and Merwine, D. K. (1994). Directional hyperacuity in ganglion cells of the rabbit retina. Vis Neurosci *11*, 1019-1025.

Grzywacz, N. M., Amthor, F. R., and Merwine, D. K. (1998). Necessity of acetylcholine for retinal directionally selective responses to drifting gratings in rabbit. J Physiol *512*, 575-581.

Grzywacz, N. M., and Zucker, C. L. (2006). Modeling Starburst Cells' GABAB Receptors and Their Putative Role in Motion Sensitivity. Biophys J *91*, 473-486.

Guia, A., Stern, M. D., Lakatta, E. G., and Josephson, I. R. (2001). Ion concentration-dependence of rat cardiac unitary L-type calcium channel conductance. Biophys J *80*, 2742-2750.

Hamill, O. P., Marty, A., Neher, B., Sakmann, B., and Sigworth, F. J. (1981). Improved patch-clamp techniques for high-resolution current recording from cells and cell-free membrane patches. Pflugers Arch *391*, 85-100.

Hammer, Ø., Harper, D. A. T., and Ryan, P. D. (2001). PAST: Paleontological Statistics software package for education and data analysis. Paleontologia Electronica *4*, 9.

Hassenstein, B., and Reichardt, W. (1956). Systemtheorische Analyse der Zeit-, Reihenfolgen- und Vorzeichenauswertung bei der Bewegungsperzeption des Rüsselkäfers Chlorophanus. Zeitschrift für Naturforschung *11b*, 513–524.

He, S., and Masland, R. H. (1997). Retinal direction selectivity after targeted laser ablation of starburst amacrine cells. Nature *389*, 378-382.

He, S., and Masland, R. H. (1998). ON direction-selective ganglion cells in the rabbit retina: dendritic morphology and pattern of fasciculation. Vis Neurosci *15*, 369-375.

Hildreth, E. C., and Koch, C. (1987). The analysis of visual motion: from computational theory to neuronal mechanisms. Annu Rev Neurosci *10*, 477-533.

Hille, B. (2001). Ion channels of excitable membranes, 3rd edn (Sunderland, MA, USA, Sinauer Associates, Inc.).

Hodgkin, A. L., and Huxley, A. F. (1952). A quantitative description of membrane current and its application to conduction and excitation in nerve. JPhysiol *117*, 500-544.

Hughes, A., and Vaney, D. I. (1980). Coronate cells: displaced amacrines of the rabbit retina? J Comp Neurol *189*, 169-189.

Hurtado, J., Borges, S., and Wilson, M. (2002). Na(+)-ca(2+) exchanger controls the gain of the ca(2+) amplifier in the dendrites of amacrine cells. J Neurophysiol *88*, 2765-2777.

Jensen, R. J. (1995). Effects of Ca2+ channel blockers on directional selectivity of rabbit retinal ganglion cells. J Neurophysiol *74*, 12-23.

Jensen, R. J. (1996). The antibiotic neomycin abolishes directional selectivity in rabbit retinal ganglion cells. Gen Pharmacol *27*, 1405-1407.

Jeon, C. J., Kong, J. H., Strettoi, E., Rockhill, R., Stasheff, S. F., and Masland, R. H. (2002). Pattern of synaptic excitation and inhibition upon direction-selective retinal ganglion cells. J Comp Neurol *449*, 195-205.

Johnston, D., Magee, J. C., Colbert, C. M., and Cristie, B. R. (1996). Active properties of neuronal dendrites. Annu Rev Neurosci *19*, 165-186.

Kalloniatis, M., and Tomisich, G. (1999). Amino acid neurochemistry of the vertebrate retina. Prog Retin Eye Res *18*, 811-866.

Kandel, E. R., Schwartz, J. H., and Jessell, T. M. (2000). Principles of neural science, 4th edn (New York, St.Louis, San Francisco, McGraw-Hill).

Kao, Y. H., Lassova, L., Bar-Yehuda, T., Edwards, R. H., Sterling, P., and Vardi, N. (2004). Evidence that certain retinal bipolar cells use both glutamate and GABA. J Comp Neurol *478*, 207-218.

Keith, R. A., Horn, M. B., Piser, T. M., and Mangano, T. J. (1993). Effects of stimulus intensity on the inhibition by omega-conotoxin GVIA and neomycin of K(+_-evoked [3H]norepinephrine release from hippocampal brain slices and synaptosomal calcium influx. Biochem Pharmacol *45*, 165-171.

Kittila, C. A., and Massey, S. C. (1995). Effect of ON pathway blockade on directional selectivity in the rabbit retina. J Neurophysiol *73*, 703-712.

Kittila, C. A., and Massey, S. C. (1997). Pharmacology of directionally selective ganglion cells in the rabbit retina. J Neurophysiol *77*, 675-689.

Koch, C. (1999). Biophysics of computation - Information processing in single neurons (New York, Oxford, Oxford University Press).

Koch, C., Poggio, T., and Torre, V. (1983). Nonlinear interactions in a dendritic tree: localization, timing, and role in information processing. Proc Natl Acad Sci U S A *80*, 2799-2802.

Koulen, P. (1999). Clustering of neurotransmitter receptors in the mammalian retina. J Membr Biol *171*, 97-105.

Kuffler, S. W. (1953). Discharge patterns and functional organization of mammalian retina. JNeurophysiol *16*, 37-68.

Kuner, T., and Augustine, G. J. (2000). A genetically encoded ratiometric indicator for chloride: capturing chloride transients in cultured hippocampal neurons. Neuron *27*, 447-459.

La Berge, A. (1999). The History of Science and the History of Microscopy. Perspectives on Science *7*, 111-142.

Lee, S., Kim, K., and Zhou, Z. J. (2006). Detection of functional cholinergic and GABAergic communications between starburst amacrine cell and direction selective ganglion cell. Paper presented at: ARVO#2676 (Ft. Lauderdale, FL).

Levick, W. R., Oyster, C. W., and Takahashi, E. (1969). Rabbit lateral geniculate nucleus: sharpener of directional information. Science *165*, 712-714.

Lichtman, J. W., and Conchello, J. A. (2005). Fluorescence microscopy. Nat Methods *2*, 910-919.

Linn, D. M., and Massey, S. C. (1992). GABA inhibits ACh release from the rabbit retina: a direct effect or feedback to bipolar cells? Vis Neurosci *8*, 97-106.

Lipscombe, D., Helton, T. D., and Xu, W. (2004). L-type calcium channels: the low down. J Neurophysiol *92*, 2633-2641.

Livingstone, M. S. (2005). Directional inhibition: a new slant on an old question. Neuron *45*, 5-7.

London, M., and Hausser, M. (2005). Dendritic computation. Annu Rev Neurosci *28*, 503-532.

MacNeil, M. A., Heussy, J. K., Dacheux, R. F., Raviola, E., and Masland, R. H. (2004). The population of bipolar cells in the rabbit retina. J Comp Neurol *472*, 73-86.

MacNeil, M. A., and Masland, R. H. (1998). Extreme diversity among amacrine cells: implications for function. Neuron *20*, 971-982.

Magee, J. C., and Cook, E. P. (2000). Somatic EPSP amplitude is independent of synapse location in hippocampal pyramidal neurons. Nat Neurosci *3*, 895-903.

Mariani, A. P., and Hersh, L. B. (1988). Synaptic organization of cholinergic amacrine cells in the rhesus monkey retina. J Comp Neurol *267*, 269-280.

Masland, R. H. (1986). The functional architecture of the retina [review]. Scientific American.

Masland, R. H. (2001a). The fundamental plan of the retina. Nat Neurosci *4*, 877-886.

Masland, R. H. (2001b). Neuronal diversity in the retina. Curr Opin Neurobiol *11*, 431-436.

Masland, R. H. (2003). Direction selectivity in retinal ganglion cells. In The visual neurosciences, L. M. Chalupa, and J. S. Werner, eds. (Cambridge, MA, USA
London, England, A Bradford Book, The MIT Press), pp. 451-462.

Masland, R. H., Ames, A., and Ames, A., 3d (1976). Responses to acetylcholine of ganglion cells in an isolated mammalian retina. JNeurophysiol *39*, 1220-1235.

Masland, R. H., and Mills, J. W. (1979). Autoradiographic identification of acetylcholine in the rabbit retina. J Cell Biol *83*, 159-178.

Masland, R. H., Mills, J. W., and Cassidy, C. (1984a). The functions of acetylcholine in the rabbit retina. Proceedings of the Royal Society of London - Series B: Biological Sciences *223*, 121-139.

Masland, R. H., Mills, J. W., and Hayden, S. A. (1984b). Acetylcholine-synthesizing amacrine cells: identification and selective staining by using radioautography and fluorescent markers. Proc R Soc Lond B Biol Sci *223*, 79-100.

Masland, R. H., and Raviola, E. (2000). Confronting complexity: strategies for understanding the microcircuitry of the retina. Annu Rev Neurosci *23*, 249-284.

Massey, S. C., Linn, D. M., Kittila, C. A., and Mirza, W. (1997). Contributions of GABAA receptors and GABAC receptors to acetylcholine release and directional selectivity in the rabbit retina. Vis Neurosci *14*, 939-948.

Massey, S. C., and Neal, M. J. (1979). The light evoked release of acetylcholine from the rabbit retina iN vivo and its inhibition by gamma-aminobutyric acid. J Neurochem *32*, 1327-1329.

Massey, S. C., O'Brien, J. J., Trexler, E. B., Li, W., Keung, J. W., Mills, S. L., and O'Brien, J. (2003). Multiple neuronal connexins in the mammalian retina. Cell Commun Adhes *10*, 425-430.

Massey, S. C., and Redburn, D. A. (1982). A tonic gamma-aminobutyric acid-mediated inhibition of cholinergic amacrine cells in rabbit retina. J Neurosci *2*, 1633-1643.

Maturana HR, Lettvin JY, McCulloch WS, and WH, P. (1960). Anatomy and physiology of vision in the frog (Rana Pipiens). J Gen Physiol *43*, 129-175.

Merwine, D. K., Grzywacz, N. M., Tjepkes, D. S., and Amthor, F. R. (1998). Non-monotonic contrast behavior in directionally selective ganglion cells and evidence for its dependence on their GABAergic input. Vis Neurosci *15*, 1129-1136.

Meunier, C., and Segev, I. (2002). Playing the devil's advocate: is the Hodgkin-Huxley model useful? Trends Neurosci *25*, 558-563.

Meyer, T., and Stryer, L. (1991). Calcium spiking. Annu Rev Biophys Biophys Chem *20*, 153-174.

Migliore, M., and Shepherd, G. M. (2005). Opinion: an integrated approach to classifying neuronal phenotypes. Nat Rev Neurosci *6*, 810-818.

Millar, T. J., Ishimoto, I., Boelen, M., Epstein, M. L., Johnson, C. D., and Morgan, I. G. (1987). The toxic effects of ethylcholine mustard aziridinium ion on cholinergic cells in the chicken retina. J Neurosci *7*, 343-356.

Millar, T. J., and Morgan, I. G. (1987). Cholinergic amacrine cells in the rabbit retina synapse onto other cholinergic amacrine cells. Neurosci Lett *74*, 281-285.

Miller, R. F., and Bloomfield, S. A. (1983). Electroanatomy of a unique amacrine cell in the rabbit retina. Proc Natl Acad Sci U S A *80*, 3069-3073.

Mora-Ferrer, C., Hausselt, S., Schmidt Hoffmann, R., Ebisch, B., Schick, S., Wollenberg, K., Schneider, C., Teege, P., and Jurgens, K. (2005). Pharmacological properties of motion vision in goldfish measured with the optomotor response. Brain Res *1058*, 17-29.

Morgan, J., Huckfeldt, R., and Wong, R. O. (2005). Imaging techniques in retinal research. Exp Eye Res *80*, 297-306.

Mori, Y., Wakamori, M., Oda, S., Fletcher, C. F., Sekiguchi, N., Mori, E., Copeland, N. G., Jenkins, N. A., Matsushita, K., Matsuyama, Z., and Imoto, K. (2000). Reduced voltage sensitivity of activation of P/Q-type Ca2+ channels is associated with the ataxic mouse mutation rolling Nagoya (tg(rol)). J Neurosci *20*, 5654-5662.

Münch, T. A., and Werblin, F. S. (2006). Symmetric interactions within a homogeneous starburst cell network can lead to robust asymmetries in dendrites of starburst amacrine cells. J Neurophysiol *96*, 471-477.

Nathans, J. (1999). The evolution and physiology of human color vision: insights from molecular genetic studies of visual pigments. Neuron *24*, 299-312.

Neumeyer, C. (1998). Color vision in lower vertebrates. In Color Vision - Perspectives from different disciplines (Berlin-New York, Walter de Gruyter & Co.), pp. 149-162.

Numberger, M., and Draguhn, A. (1996). Patch-Clamp-Technik (Heidelberg; Berlin; Oxford, Spektrum Akademischer Verlag).

Oesch, N., Euler, T., and Taylor, W. R. (2005). Direction-selective dendritic action potentials in rabbit retina. Neuron *47*, 739-750.

O'Malley, D. M., and Masland, R. H. (1989). Co-release of acetylcholine and gamma-aminobutyric acid by a retinal neuron. Proceedings of the National Academy of Sciences *86*, 3414-3418.

O'Malley, D. M., Sandell, J. H., and Masland, R. H. (1992). Co-release of acetylcholine and GABA by the starburst amacrine cells. J Neurosci *12*, 1394-1408.

Oyster, C. W. (1968). The analysis of image motion by the rabbit retina. J Physiol *199*, 613-635.

Oyster, C. W., Amthor, F. R., and Takahashi, E. S. (1993). Dendritic architecture of ON-OFF direction-selective ganglion cells in the rabbit retina. Vision Res *33*, 579-608.

Oyster, C. W., and Barlow, H. B. (1967). Direction-selective units in rabbit retina: distribution of preferred directions. Science *155*, 841-842.

Oyster, C. W., Takahashi, E., and Collewijn, H. (1972). Direction-selective retinal ganglion cells and control of optokinetic nystagmus in the rabbit. Vision Res *12*, 183-193.

Oyster, C. W., Takahashi, E., and Levick, W. R. (1971). Information processing in the rabbit visual system. Doc Ophthalmol *30*, 161-204.

Ozaita, A., Petit-Jacques, J., Volgyi, B., Ho, C. S., Joho, R. H., Bloomfield, S. A., and Rudy, B. (2004). A unique role for Kv3 voltage-gated potassium channels in starburst amacrine cell signaling in mouse retina. J Neurosci *24*, 7335-7343.

Pannese, E. (1999). The Golgi Stain: Invention, Diffusion and Impact on Neurosciences. Journal of the History of the Neurosciences *8*, 132-140.

Perry, V. H., and Walker, M. (1980). Amacrine cells, displaced amacrine cells and interplexiform cells in the retina of the rat. ProcRSocLondB *208*, 415-431.

Peters, B. N., and Masland, R. H. (1996). Responses to light of starburst amacrine cells. J Neurophysiol *75*, 469-480.

Petersen, C. C., Grinvald, A., and Sakmann, B. (2003). Spatiotemporal dynamics of sensory responses in layer 2/3 of rat barrel cortex measured in vivo by voltage-sensitive dye imaging combined with whole-cell voltage recordings and neuron reconstructions. J Neurosci *23*, 1298-1309.

Poggio, T., and Reichardt, W. (1973). Considerations on models of movement detection. Kybernetik *13*, 223-227.

Polsky, A., Mel, B. W., and Schiller, J. (2004). Computational subunits in thin dendrites of pyramidal cells. Nat Neurosci *7*, 621-627.

Polyak, S. L. (1941). The retina. Chicago: University of Chicago Press.

Poznanski, R. R. (1992). Modelling the electrotonic structure of starburst amacrine cells in the rabbit retina: a functional interpretation of dendritic morphology. Bull Math Biol *54*, 905-928.

Priebe, N. J., and Ferster, D. (2005). Direction selectivity of excitation and inhibition in simple cells of the cat primary visual cortex. Neuron *45*, 133-145.

Pu, M. L., and Amthor, F. R. (1990). Dendritic morphologies of retinal ganglion cells projecting to the nucleus of the optic tract in the rabbit. J Comp Neurol *302*, 657-674.

Rall, W. (1964). Theoretical significance of dendritic trees for neuronal input–output relations (Stanford, Stanford University Press).

Ramón Y Cajal, S. (1893). La rétine des vertébrés. La Cellule *9*, 119-257.

Rodieck, R. W. (1998). The first steps in seeing (Sunderland, MA, U.S.A., Sinauer Associates, Inc.).

Roy, M. L., and Narahashi, T. (1992). Differential properties of tetrodotoxin-sensitive and tetrodotoxin-resistant sodium channels in rat dorsal root ganglion neurons. J Neurosci *12*, 2104-2111.

Sakmann, B., and Neher, E. (1984). Patch clamp techniques for studying ionic channels in excitable membranes. AnnRevPhysiol *46*, 455-472.

Sather, W. A. (2005). Selective Permeability of Voltage-Gated Calcium Channels. In Voltage-Gated Calcium Channels, G. W. Zamponi, ed. (New York, NY, Kluwer Academic).

Saxena, N. C., and Macdonald, R. L. (1994). Assembly of GABAA receptor subunits: role of the delta subunit. J Neurosci *14*, 7077-7086.

Scholze, A., Plant, T. D., Dolphin, A. C., and Nurnberg, B. (2001). Functional expression and characterization of a voltage-gated CaV1.3 (alpha1D) calcium channel subunit from an insulin-secreting cell line. Mol Endocrinol *15*, 1211-1221.

Schultze, M. (1866). Zur Anatomie und Physiologie der Retina. Archiv für mikroskopische Anatomie *2*, 175-286.

Söhl, G., Maxeiner, S., and Willecke, K. (2005). Expression and functions of neuronal gap junctions. Nat Rev Neurosci *6*, 191-200.

Stafford, D. K., and Dacey, D. M. (1997). Physiology of the A1 amacrine: a spiking, axon-bearing interneuron of the macaque monkey retina. Vis Neurosci *14*, 507-522.

Strichartz, G. R. (1973). The inhibition of sodium currents in myelinated nerve by quaternary derivatives of lidocaine. J Gen Physiol *62*, 37-57.

Tauchi, M., and Masland, R. H. (1984). The shape and arrangement of the cholinergic neurons in the rabbit retina. Proc R Soc Lond B Biol Sci *223*, 101-119.

Tauchi, M., and Masland, R. H. (1985). Local order among the dendrites of an amacrine cell population. J Neurosci *5*, 2494-2501.

Taylor, W. R. (1996). Response properties of long-range axon-bearing amacrine cells in the dark-adapted rabbit retina. Vis Neurosci *13*, 599-604.

Taylor, W. R., He, S., Levick, W. R., and Vaney, D. I. (2000). Dendritic computation of direction selectivity by retinal ganglion cells. Science *289*, 2347-2350.

Taylor, W. R., and Vaney, D. I. (2002). Diverse synaptic mechanisms generate direction selectivity in the rabbit retina. J Neurosci *22*, 7712-7720.

Taylor, W. R., and Vaney, D. I. (2003). New directions in retinal research. Trends Neurosci *26*, 379-385.

Taylor, W. R., and Wässle, H. (1995). Receptive field properties of starburst cholinergic amacrine cells in the rabbit retina. Europ J Neurosci *7*, 2308-2321.

Terlau, H., and Olivera, B. M. (2004). Conus venoms: a rich source of novel ion channel-targeted peptides. Physiol Rev *84*, 41-68.

Theer, P., Hasan, M. T., and Denk, W. (2003). Two-photon imaging to a depth of 1000 microm in living brains by use of a Ti:Al2O3 regenerative amplifier. Opt Lett *28*, 1022-1024.

Theer, P., Kuhn, B., Keusters, D., and Denk, W. (2005). Two-photon Microscopy and Imaging. In Encyclopedia of Molecular Cell Biology and Molecular Medicine, R. A. Meyers, ed. (Weinheim, Germany, Wiley-VCH Verlag GmbH & Co. KGaA,), pp. 676.

Torre, V., and Poggio, T. (1978). A synaptic mechanism possibly underlying directional selectivity to motion. Proc R Soc Lond B *202*, 409-416.

Treviranus, G. R. (1837). Resultate neuer Untersuchungen über die Theorie des Sehens und über den inneren Bau der Netzhaus des Auges, Vol 1 (Bremen, Heyse).

Tukker, J. J., Taylor, W. R., and Smith, R. G. (2004). Direction selectivity in a model of the starburst amacrine cell. Vis Neurosci *21*, 611-625.

Tumosa, N., Eckenstein, F., and Stell, W. K. (1984). Immunocytochemical localization of putative cholinergic neurons in the goldfish retina. Neurosci Lett *48*, 255-259.

Vaney, D. I. (1990). The mosaic of amacrine cells in the mammalian retina. ProgRetinal Res *9*, 49-100.

Vaney, D. I. (1994). Territorial organization of direction-selective ganglion cells in rabbit retina. J Neurosci *14*, 6301-6316.

Vaney, D. I., He, S., Taylor, W. R., and Levick, W. R. (2001). Direction-Selective Ganglion Cells in the Retina. In Motion Vision - Computational, Neural, and Ecological Constraints, J. M. Zanker, and J. Zeil, eds. (Berlin, Heidelberg, New York, Springer).

Vaney, D. I., Levick, W. R., and Thibos, L. N. (1981a). Rabbit retinal ganglion cells. Receptive field classification and axonal conduction properties. Exp Brain Res *44*, 27-33.

Vaney, D. I., Peichl, L., and Boycott, B. B. (1981b). Matching populations of amacrine cells in the inner nuclear and ganglion cell layers of the rabbit retina. J Comp Neurol *199*, 373-391.

Vaney, D. I., and Pow, D. V. (2000). The dendritic architecture of the cholinergic plexus in the rabbit retina: selective labeling by glycine accumulation in the presence of sarcosine. J Comp Neurol *421*, 1-13.

Vaney, D. I., and Weiler, R. (2000). Gap junctions in the eye: evidence for heteromeric, heterotypic and mixed-homotypic interactions. Brain Res Brain Res Rev *32*, 115-120.

Vaney, D. I., and Young, H. M. (1988). GABA-like immunoreactivity in cholinergic amacrine cells of the rabbit retina. Brain Res *438*, 369-373.

Velte, T. J., and Miller, R. F. (1997). Spiking and nonspiking models of starburst amacrine cells in the rabbit retina. Vis Neurosci *14*, 1073-1088.

Volgyi, B., Xin, D., Amarillo, Y., and Bloomfield, S. A. (2001). Morphology and physiology of the polyaxonal amacrine cells in the rabbit retina. J Comp Neurol *440*, 109-125.

Wade, N. (1999). A natural history of vision (Cambridge, MA, USA; London, England, A Bradord Book, The MIT Press).

Wang, P., and Slaughter, M. M. (2005). Effects of GABA receptor antagonists on retinal glycine receptors and on homomeric glycine receptor alpha subunits. J Neurophysiol *93*, 3120-3126.

Warrier, A., Borges, S., Dalcino, D., Walters, C., and Wilson, M. (2005). Calcium from internal stores triggers GABA release from retinal amacrine cells. J Neurophysiol *94*, 4196-4208.

Wässle, H. (2004). Parallel processing in the mammalian retina. Nat Rev Neurosci *5*, 747-757.

Wässle, H., and Boycott, B. B. (1991). Functional architecture of the mammalian retina. PhysRev *71*, 447-480.

Watanabe, S., Takagi, H., Miyasho, T., Inoue, M., Kirino, Y., Kudo, Y., and Miyakawa, H. (1998). Differential roles of two types of voltage-gated Ca2+ channels in the dendrites of rat cerebellar Purkinje neurons. Brain Res *791*, 43-55.

Wilcoxon, F. (1945). Individual Comparisons by Ranking Methods. Biometrics Bulletin *1*, 80-83.

Williams, S. R., and Stuart, G. J. (2002). Dependence of EPSP efficacy on synapse location in neocortical pyramidal neurons. Science *295*, 1907-1910.

Wyatt, H. J., and Daw, N. W. (1976). Specific effects of neurotransmitter antagonists on ganglion cells in rabbit retina. Science *191*, 204-205.

Wyatt, H. J. D., N. W (1975). Directionally Sensitive Ganglion Cells in the Rabbit Retina: Specificity for Stimulus Direction, Size and Speed. J Neurophysiol *38*, 613-626.

Xu, H. P., Zhao, J. W., and Yang, X. L. (2002). Expression of voltage-dependent calcium channel subunits in the rat retina. Neurosci Lett *329*, 297-300.

Xu, H. P., Zhao, J. W., and Yang, X. L. (2003). Cholinergic and dopaminergic amacrine cells differentially express calcium channel subunits in the rat retina. Neuroscience *118*, 763-768.

Yang, G., and Masland, R. H. (1994). Receptive fields and dendritic structure of diectionally selective retinal ganglion cells. JNeurosci *14*, 5267-5280.

Yoshida, K., Watanabe, D., Ishikane, H., Tachibana, M., Pastan, I., and Nakanishi, S. (2001). A key role of starburst amacrine cells in originating retinal directional selectivity and optokinetic eye movement. Neuron *30*, 771-780.

Zamponi, G. W. (2005). Voltage-Gated Calcium Channels (Georgetown and New York, Landes Bioscience/Eurekah.com and Kluwer Academic/Plenum Publishers).

Zhang, J. F., Randall, A. D., Ellinor, P. T., Horne, W. A., Sather, W. A., Tanabe, T., Schwarz, T. L., and Tsien, R. W. (1993). Distinctive pharmacology and kinetics of cloned neuronal Ca2+ channels and their possible counterparts in mammalian CNS neurons. Neuropharmacology *32*, 1075-1088.

Zheng, J. J., Lee, S., and Zhou, Z. J. (2004). A developmental switch in the excitability and function of the starburst network in the mammalian retina. Neuron *44*, 851-864.

Zhou, X., Dong, X. W., Crona, J., Maguire, M., and Priestley, T. (2003). Vinpocetine is a potent blocker of rat NaV1.8 tetrodotoxin-resistant sodium channels. J Pharmacol Exp Ther *306*, 498-504.

Zhou, Z. J., and Fain, G. L. (1995). Neurotransmitter receptors of starburst amacrine cells in rabbit retinal slices. J Neurosci *15*, 5334-5345.

Zhou, Z. J., and Zheng, J. (2006). Differential control of ACh and GABA release by N and P/Q type Ca channels in starburst amacrine cells. Paper presented at: ARVO #2673 (Ft.Lauderdale, FL).

Zipfel, W. R., Williams, R. M., and Webb, W. W. (2003). Nonlinear magic: multiphoton microscopy in the biosciences. Nat Biotechnol *21*, 1369-1377.

6 Appendix

A. Electrical responses to light: Values and significances

- **Components from spectral analysis (FFT) for all cells.**

	n	average	sem	p	sig	p	sig	p from zero	sig
tested populations				within group exp *vs* con		between groups Cs *vs* K			
test type				Wilcoxon signed ranks		Mann Whitney U		wilcoxon signed ranks	
K^+									
$V_{0,exp}$	58	0,663155	0,164832	0,00009538	**	0,9328	-	0,00003006	**
$V_{0,con}$	58	1,15019	0,170969					5,609E-08	**
Cs^+									
$V_{0,exp}$	25	0,78584	0,392402	0,5539	-	0,2317	-	0,01434	*
$V_{0,con}$	25	0,95668	0,42661					0,003989	**
Both									
$V_{0,exp}$	83	0,700108	0,16374	0,0002739	**			0,000001768	**
$V_{0,con}$	83	1,0919	0,174181					1,052E-09	**
K^+									
AI_1	58	0,157555	0,016885			0,6659	-	6,191E-10	**
AI_2	58	0,238984	0,041534			0,5749	-	0,000005021	**
AI_3	56	0,149132	0,019582			0,2717	-	0,003832	**
Cs^+									
AI_1	25	0,178886	0,031902					0,0001068	**
AI_2	25	0,201589	0,076735					0,01058	*(*)
AIT	25	0,260716	0,075548					0,003989	**
Both									
AI_1	83	0,16398	0,015145					2,318E-13	**
AI_2	83	0,22772	0,036887					1,917E-07	**
AI_3	81	0,183572	0,040792					0,00005801	**

Table 2. Averages and standard errors of the mean (sem) of V_0 and AI_1, AI_2 and AI_3 and significance tests (all cells)

- **Gaussian fit values for all cells with** $y_0 + A \cdot e^{-\frac{x-x_0}{width}}$

AI_1

$y_0 = 0.096111 \pm 0.331$
A $= 13.011 \pm 1.05$
$x_0 = 0.13356 \pm 0.011$
width $= 0.17162 \pm 0.0167$

AI₂

y0 = 0.35329 ± 0.421
A = 5.0317 ± 0.656
x0 = 0.24699 ± 0.0363
width = 0.3876 ± 0.0673

AI₃

y0 = 0.23416 ± 0.778
A = 4.097 ± 0.93
x0 = 0.22025 ± 0.0703
width = 0.50169 ± 0.155

- **Resting membrane potential.**

K^+: U_{mem} = -47.21 ± 1.33 mV
Cs^+: U_{mem} = -32.56 ± 1.19 mV

Difference between cells recorded with K^+ and Cs^+:
$p \leq 0.00001$, i.e. ** (highly significant)

- **Components from spectral analysis (FFT) for stimuli with different contrasts**

contrast	*AI₁*	sem	p against 0	sig	*AI₂*	sem	p against 0	sig
10%	0.205045	0.0499758	0.01562	*	0.0108277	0.196103	1	-
20%	0.183148	0.0543986	0.01562	*	0.197896	0.171181	0.4609	-
29%	0.186792	0.0446074	0.007812	**	0.380578	0.0925904	0.01562	*
46%	0.243717	0.0384783	0.007812	**	0.382315	0.0647947	0.007812	**
72%	0.281454	0.0444069	0.007812	**	0.251701	0.0837608	0.03906	*

Table 3. Averages and sem of *AI₁* and *AI₂* and significance tests (first set of cells, n=8, Fig. 20)

contrast	*AI₁*	sem	*AI₂*	sem
12%	0.0533514	0.0753672	0.266384	0.227161
23%	0.0651518	0.0618846	0.18033	0.29598
35%	0.0987251	0.0538698	0.265049	0.276849
57%	0.0846137	0.0523849	0.504764	0.0687942
73%	0.0476867	0.0614014	0.436172	0.0290611

Table 4. Averages and sem of *AI₁* and *AI₂* (second set of cells, n=3, Fig. 20)

- **Components from spectral analysis (FFT) for stimuli with different dendritic coverage.**

stimulus	AI_1	sem	AI_2	sem
Standard	0.268897	0.0871463	0.367686	0.0819029
Smaller from dist.	0.128071	0.0472696	0.387089	0.14311
Even smaller	0.0350554	0.0317196	0.0181705	0.0753039
Distal Ring	0.458875	0.0985392	0.459774	0.142143

Table 5. Averages and standard errors of the mean (sem) of AI_1 and AI_2 (Fig. 22, n=8)

AI	AI_1 vs. 0		AI_2 vs. 0		AI_1 *vs.* stand.		AI_2 *vs.* stand.	
stimulus	p	sig	p	sig	p	sig	p	sig
Standard	0.007812	**	0.01562	*				
Smaller	0.02344	*	0.05469	-	0.02344	*	0.7422	-
Smaller	0.25	-	1	-	0.007812	**	0.03906	*
Distal	0.007812	**	0.007812	**	0.1094	-	0.7422	-

Table 6. Significance tests of AI_1 and AI_2 (*vs*. 0 or standard stimulus, Fig. 22, n=8)

stimulus	AI_1	sem	AI_2	sem
Proximal ring	0.00615147	0.0240667	0.0341001	0.0606319
Standard	0.175828	0.0269418	0.408441	0.099765
Distal ring	0.187984	0.0477943	0.447021	0.143863
Surround ring	0.0890762	0.0521599	-0.124858	0.0959435

Table 7. Averages and standard errors of the mean (sem) of AI_1 and AI_2 (Fig. 23, n=3)

- **Components from spectral analysis (FFT) for pharmacological experiments.**

GABAzine

condition	AI_1	sem	p (vs. drug)	AI_2	sem	p (vs. drug)
pre	0.152374	0.0469896	0.4375	0.187453	0.1552	0.0625
Gabazine	0.16501	0.0507511	-	0.48635	0.0927986	-
washout	0.161144	0.0370997	0.8125	0.352497	0.109558	0.1875

Table 8. Averages, standard errors of the mean (sem) of AI_1 and AI_2 and p-values (Fig. 24, n=5)

TPMPA

condition	AI_1	sem	p (vs. drug)	AI_2	sem	p (vs. drug)
pre	0.2436	0.0578639	0.09375	0.450729	0.0827911	1
TPMPA	0.172744	0.0420026	-	0.450569	0.0800448	-
washout	0.180569	0.0603421	0.8125	0.356524	0.0839169	0.1875

Table 9. Averages, standard errors of the mean (sem) of AI_1 and AI_2 and p-values (Fig. 24, n=6, washout n=5)

PTX

condition	AI_1	sem	p (vs. drug)	AI_2	sem	p (vs. drug)
pre	0.141112	0.0415776	0.0625	0.266462	0.114416	0.4375
PTX	0.0524418	0.0465456	-	0.270818	0.0973709	-
washout	0.265288	0.154967	0.125	0.413163	0.154683	0.8125

Table 10. Averages, standard errors of the mean (sem) of AI_1 and AI_2 and p-values (Fig. 24, n=6)

Cd^{2+}

condition	AI_1	sem	p (vs. drug)	AI_2	sem	p (vs. drug)
pre	0.137995	0.0220865	0.4648	0.27395	0.103038	0.3203
Cd^{2+}	0.107941	0.0317609	-	0.20871	0.0736007	-
washout	0.137813	0.0244182	0.009766 **	0.422769	0.0845837	0.04883 *

Table 11. Averages, standard errors of the mean (sem) of AI_1 and AI_2 and p-values (Fig. R25, n=11, washout n=10)

B. Supporting calculations

- **Estimating the number of Ca^{2+} channels (n_{ch}) needed to generate the 2nd harmonic signals.**

For moderate voltage modulation amplitudes (V_A) the I-V curve, as any curve, can be expanded into a Taylor series about V_0,

$$I(V-V_0) = I_0 + n_{ch}\left[\left.\frac{\partial I_{sc}(V)}{\partial V}\right|_{V=V_0}(V-V_0) + \frac{1}{2}\left.\frac{\partial^2 I_{sc}(V)}{\partial V^2}\right|_{V=V_0}(V-V_0)^2 + O(V-V_0)^3\right] =$$
$$= I_0 + n_C\left[\alpha(V-V_0) + \beta(V-V_0)^2 + O(V-V_0)^3\right] \quad , \text{(i)}$$

where I_0 is the current when $V = V_0$. With sinusoidal voltage modulation, $V - V_0 = V_A \cos(\omega t)$, with V_A as the modulation amplitude, the current modulation is

$$I(t) - I_0 = n_{ch}\left\{\alpha V_A\cos(\omega t) + \beta\left[V_A\cos(\omega t)\right]^2 + O\left[V_A\cos(\omega t)\right]^3\right\} =$$
$$= n_{ch}\alpha V_A\cos(\omega t) + n_{ch}\beta V_A{}^2\left[\cos(2\omega t)/2 + 1/2\right] + \ldots = \quad , \text{(ii)}$$
$$= I_1\cos(\omega t) + I_2\cos(2\omega t) + \ldots$$

where "..." indicates frequency components at 3ω or higher. Solving for the number of channels yields:

$$n_{ch} = \frac{2I_2}{\beta V_A{}^2} \quad . \qquad \text{(iii)}$$

Using the I-V curve for P/Q-type channels (with E_{rev} = 46.8 mV, V_{50} = -10.9 mV, g_0 = 3 pS, and V_{Slope} = 4.56 mV) results in β = 687 pA/V^2 by calculating the magnitude of the second derivative (in the curve for P/Q-type in Fig. 29 this is at -18 mV, where the curvature becomes maximally negative) using eqn. v (see below). Neglecting

inactivation and kinetic aspects and using V_A = 5 mV (Fig. 17 A) with the channel parameters listed above ~930 channels are needed to get I_2 = 8 pA (Fig. 27 C).

- **Estimating the size of the slope conductance provided by the VGCCs known to be present in SACs.**

It can be assumed for the channel open probability (Eqn. 2.22 in Hille, 2001):

$$p_{open}(V) = \frac{1}{1 + e^{\frac{V_{50} - V}{V_{slope}}}}, \tag{iv}$$

where V_{50} is the voltage at which half the channels are open and V_{Slope} is the activation slope voltage. The total current is:

$$I(V) = n_{ch} g_0 p_{open}(V)(V - E_{rev}) = n_{ch} I_{sc}(V), \tag{v}$$

with the number of channels n_{ch}, the open-channel conductance g_0 (which can be assumed to be constant, however, only for voltages sufficiently far from E_{rev}), the reversal potential E_{rev}, and the single channel current I_{sc}. The slope conductance ($\alpha = \partial I / \partial V$) per channel amounts to:

$$\begin{aligned} \alpha(V) &= \frac{\partial\left[g_o p_{open}(V)(V - E_{rev}) \right]}{\partial V} = \\ &= \frac{g_0}{1 + \exp\left[(V_{50} - V)/V_{slope} \right]} + \frac{\exp\left[(V_{50} - V)/V_{slope} \right](V - E_{rev})}{\left\{ 1 + \exp\left[(V_{50} - V)/V_{slope} \right] \right\}^2 V_{slope}} \end{aligned} \tag{vi}$$

For E_{rev} = 46.8 mV, V_{50} = -10.9 mV, g_0 = 3 pS , and V_{slope} = 4.56 mV (g_0 from Guia et al. (2001), other numbers derived from fits to P/Q-type Ca^{2+}-channel data from Mori et al. (2000), see Table 1 and Fig. 29), $\alpha(V)$ can become as negative as -8.22 pS (at -12.2 mV), which for ~930 channels, as are needed to account for I_2 (see above), amounts to a negative slope conductance $n_{ch}\alpha$ = -930·8.22 pS ≈ 1/(-130 MΩ).

- **Calculations concerning the dendritic voltage divider**

Using the eqn. iv for the channel open probability of a voltage-gated channel (e.g. Hille, 2001) and

$$V_{DD} = E_{rev,leak} - \gamma\left(V_S + E_{rev,leak}\right) \tag{vii}$$

(with $\gamma = \frac{R_{Leak}}{R_{Leak} + R_{Long}}$), the equations

$$p_{open}\left(V_S\right) = \frac{1}{1 + e^{\frac{V_{50}' - V_S}{V_{slope}'}}} \tag{viii}$$

and

$$p_{open}\left(V_{DD}\right) = \frac{1}{1 + e^{\frac{V_{50} - V_{DD}}{V_{slope}}}} \tag{ix}$$

can be transformed to

$$\frac{\gamma \cdot \left(V_{50}' - V_S\right)}{V_{slope}} = \frac{\left(V_{50}' - V_S\right)}{V_{slope}'}. \tag{x}$$

Thus $$V_{slope}' \approx \frac{1}{\gamma} \cdot V_{slope}.$$

- **Volume of a starburst cell dendrite.**

The number of Ca2+ ions entering the SAC can be estimated using the equation:

$$n_{Ca^{2+}} = n_{ch} \cdot \Delta V \cdot \alpha \frac{\Delta t}{z}.$$

With n_{ch} the number of Ca^{2+} channels (500) ΔV the change in membrane potential (10 mV), α the single channel conductance (7.4 pS), Δt the time of opening (100 ms, the rising phase of the voltage response at 2.5 Hz) and z the valency of Ca^{2+} (2), the number of Ca^{2+} ions amounts to $32 \cdot 10^{-18}$ mol.

The amount of Ca^{2+} indicator (OGB-1) is calculated, assuming a volume of 3.2 pl (based on Famiglietti, 1991, Miller and Bloomfield, 1983 and own observations) for the dendritic arbor (see Table 13) and a concentration of 100 µM, to ~ $32 \cdot 10^{-17}$ mol.

section of dendritic sector	# 1	# 2	# 3	# 4	total
dendritic diameter [um]	1.3	0.3	0.3	0.4	
dendritic length [um]	30	55	35	30	150
# branches	1	3	7	20	
# varicosities per branch	0	0	2	9	194
diameter [um] of varicosities	0	0	1.7	1.7	

Table 12. Values underlying the calculation of dendritic volume; the SAC dendritic sectors were divided into four sections eact, with #1 the most proximal und #4 the most distal part.

volume of primary branch (dendritic sector)	639.5 µm^3	0.640 pl
volume of dendritic arbor	3197.7 µm^3	3.198 pl
volume of soma	523.6 µm^3	0.524 pl
total volume	3721.3 µm^3	3.721 pl
surface of dendrites	1236.7 µm^2	
surface of varicosities (minus "connecting" area)	92.4 µm^2	
surface of primary branch (dendritic sector)	1329.2 µm^2	

Table 13. Volume of SAC compartments and surface of the dendrites.

C. Dendritic two-compartmental model

To evaluate the influence of VGCs on direction discrimination a two-compartment model of a dendritic branch (Fig. 32, description in legend) was numerically analyzed. Both compartments contain the same type of active conductance, which is modeled as a Hodgkin-Huxley-type channel, containing one *m* and one *h* element (e.g. Hille, 2001). For the *m* element the activation probability follows as

$$m' = -mk_m + (1-m)k_m e^{\frac{V-V_{m50}}{V_{mSlope}}},$$

where m' denotes the time derivative of m and k_m the off-rate. Only the on-rate is assumed to be voltage (V) dependent, whereby V_{m50} and V_{mslope} are the half-activation and slope voltages, respectively. The equation for the *h* element is identical. The voltages in the two compartments (V_P and V_D) can be calculated by solving the following system of coupled differential equations:

$$V_P' = \left(-\left(V_P - E_{rev}\right) g_{open} n_{ch} m_P h_P - I_{P,zero} - \frac{V_P}{R} + I_{P,osc} + \frac{\left(V_D - V_P\right)}{R_{long}} \right) \Big/ C$$

$$V_D' = \left(-\left(V_D - E_{rev}\right) g_{open} n_{ch} m_D h_D - I_{D,zero} - \frac{V_D}{R} + I_{D,osc} + \frac{\left(V_P - V_{PD}\right)}{R_{long}} \right) \Big/ C$$

$$m_P' = -m_P k_m + \left(1 - m_P\right) k_m e^{\frac{V_P - V_{m50}}{V_{mSlope}}}$$

$$m_D' = -m_D k_m + \left(1 - m_D\right) k_m e^{\frac{V_D - V_{m50}}{V_{mSlope}}}$$

$$h_P' = -h_P k_h + \left(1 - h_P\right) k_h e^{\frac{V_P - V_{h50}}{V_{hSlope}}}$$

$$h_D' = -h_D k_h + \left(1 - h_D\right) k_h e^{\frac{V_D - V_{h50}}{V_{hSlope}}}$$

The direction discrimination of the model was analyzed using R_{long} = 1 GΩ, C = 183 pF, g_{open} n_{ch} = 5 nS, $1/g_{leak} = R$ = 160 MΩ, and a voltage-gated channel with E_{rev} = 50 mV, k_m = 1000/s, k_h = 7.25/s, V_{m50} = -15 mV, V_{h50} = -15mV, V_{mslope} = 4.5 mV, and V_{hSlope} = -4 mV. While the channel parameters do not apply to a specific type of

VGC they are in the range that is plausible for the types of Ca^{2+} channels found in SACs (see 4.2.2). To mimic a dendritic voltage gradient the resting potential of the two compartments were set to -19 and -16.5 mV, by setting $I_{P,zero}$ = 195 pA and $I_{D,zero}$ = 183 pA. This configuration is stable, i.e. in the absence of sinusoidal input currents the voltage remains steady, as shown by numerical simulation. Sinusoidal input currents injected into the two compartments had a frequency of 2.86 Hz and an amplitude of 1.25 pA. To simulate image motion the relative phase of the sinusoidal currents injected into the two compartments was set to either +90 or -90 degrees. Delaying the current injected into compartment D with respect to compartment P simulates 'out-going' motion (from P to D; first stimulation period in Fig. 32 B), reversing the timing simulates 'in-going' motion (from D to P, second stimulation period in Fig. 32 B).

The voltages in both compartments in response to the injection of oscillating currents (Fig. 32 C, D and other conditions) were further analyzed by Fourier decomposition, similar to the way the experimental data were analyzed (all amplitudes are given as root-mean-square at the fundamental frequency unless otherwise indicated). The results are summarized in Table 14.

Parameters			Results											
P,D	**P**	**D**	**P**						**D**					
I_{osc} [pA]	V_{rest} [mV]	V_{rest} [mV]	V_1 [mV]		V_2 [mV]		*AI_1 [-]*	*AI_2 [-]*	V_1 [mV]		V_2 [mV]		*AI_1 [-]*	*AI_2 [-]*
			P->D ('out-ward')	D->P ('in-ward')	P->D ('out-ward')	D->P ('in-ward')			P->D ('out-ward')	D->P ('in-ward')	P->D ('out-ward')	D->P ('in-ward')		
0.313	-19.00	-16.50	0.340	0.256	0.007	0.003	*0.141*	*0.350*	0.278	0.030	0.003	0.001	*0.806*	*0.550*
0.625	-19.00	-16.50	0.667	0.507	0.026	0.013	*0.137*	*0.343*	0.552	0.061	0.014	0.004	*0.802*	*0.556*
1.250	**-19.00**	**-16.50**	**1.258**	**0.982**	**0.092**	**0.047**	***0.123***	***0.321***	**1.086**	**0.128**	**0.053**	**0.014**	***0.789***	***0.576***
2.500	-19.00	-16.50	2.175	1.802	0.267	0.152	*0.094*	*0.275*	2.104	0.302	0.200	0.046	*0.749*	*0.626*
5.000	-19.00	-16.50	3.224	3.098	0.573	0.399	*0.020*	*0.179*	4.000	0.813	0.645	0.126	*0.662*	*0.674*
1.250	-16.50	-16.50	0.792	0.596	0.032	0.032	*0.141*	*-0.003*	0.596	0.792	0.032	0.032	*-0.141*	*0.003*
1.250	-17.75	-17.75	1.530	2.328	0.127	0.284	*-0.207*	*-0.383*	2.354	1.504	0.288	0.124	*0.220*	*0.398*
1.250	-19.00	-19.00	0.121	1.001	0.010	0.050	*-0.784*	*-0.667*	1.001	0.121	0.050	0.010	*0.784*	*0.667*

Table 14. Voltage 'responses' from the two compartments (P and D) in the model to different input currents and 'resting potentials'.

Generally, in both compartments the response is larger when the current in the compartment that has the more depolarized resting potential (-16.5 mV) is delayed, representing motion towards this compartment, e.g. compartment D. It is this compartment that shows a strong preference for one "motion direction" (D, blue trace in Fig. 32 C; 1.09 mV vs. 0.13 mV, i.e. ~8.5 fold larger). The other compartment has a much weaker preference but for the *same* direction (P, orange trace in Fig. 32 C; 1.26 *vs.* 0.98 mV, i.e. ~1.3 fold larger). For small currents, in the -19 mV/-16.5 mV state, the behavior is quasi linear (for 2.5, 1.25, and 0.625 pA the preferred direction voltages are 2.1, 1.09, and 0.55 mV and 7.0, 8.5, and 9.1 fold larger, respectively; see Table 14). The second harmonic in the P compartment, resting at -19 mV, is more strongly direction selective than the fundamental in this compartment – consistent with the experimental data – but not quite as strongly as the fundamental in the D compartment. Setting the injected DC current such that both compartments rest at the same potential, (e.g. at -16.5 mV, Fig. 32 D) results in different preferred directions for both compartments.

The two-compartment model shows that the inclusion of an active conductance can give rise to large DS, sufficient to explain the observation that in the distal dendrite (compartment D) the responses to out-going stimuli with weak contrasts (corresponding to small I_{osc}) are larger than responses to in-going stimuli with as much as 4 fold larger contrasts (Table 14). The model is stable, requires no regenerative, i.e. action potential-like, events and behaves largely linearly. It matches the experimental data insofar that both model compartments have the same preferred direction and thus explains why the somatic voltage and the dendritic Ca^{2+} both prefer out-going motion (Fig. 17). The necessary spatial asymmetry results from a mild voltage gradient, which shifts the voltage-gated channels in the two compartments into slightly different operating regimes. This suggests that the dendritic voltage gradient that is present in SACs may play this role in the cell's computation of DS. Finally, in further agreement with the SAC data (Fig. 27), directional discrimination in the model is voltage-dependent.

While this model explains qualitatively a number of the experimental observations it works only over a rather limited frequency range and requires somewhat unrealistically large capacitance and/or intra-dendritic resistance values. It is likely that it will be possible to overcome these shortcomings with the inclusion of a larger number of compartments and channel types.

Acknowledgements

> "I might have known," said Eeyore. "After all, one can't complain. I have my friends. Somebody spoke to me only yesterday. And was it last week or the week before that Rabbit bumped into me and said 'Bother!' The Social Round. Always something going on."
>
> **A. A. Milne, from 'Winnie-the-Pooh', 1926**

In the end, many people helped me to accomplish this thesis. I would like to thank my supervisors and colleagues, my friends and my family for their wonderful support.

> In the middle of difficulty lies opportunity.
>
> **Albert Einstein, (1879 - 1955)**